WASHINGTON UNIVERSITY
SERVER INSTITUTE OF TECHNOLOGY
DEPARTMENT OF CIVIL ENGINEERING

FAULT-TOLERANT CONTROL DESIGN FOR SMART DAMPING SYSTEMS

By

Steve Williams

Prepared under the direction of Professor Shirley J. Dyke

Thesis presented to the Sever Institute of
Washington University in partial fulfillment
of the requirements of the degree of

MASTER OF SCIENCE

May, 2004

Saint Louis, Missouri

WASHINGTON UNIVERSITY
SEVER INSTITUTE OF TECHNOLOGY
DEPARTMENT OF CIVIL ENGINEERING

ABSTRACT

FAULT-TOLERANT CONTROL FOR SMART DAMPING SYSTEMS
by Steven R. Williams

ADVISOR: Professor Shirley J. Dyke

May 2004
St. Louis, Missouri

This thesis contains a study of the effects of and develops a procedure for dealing with control component failure in smart damping systems. The procedure is developed by studying the effects of failure on a six story model building. Verification is achieved by applying the procedure to a full scale nine story plan-asymmetric building. This thesis also presents two additional studies. The first considers the applicability of a design procedure for passive systems modified to apply to MR dampers. The second compares the performance of a decentralized control system to that of the global controller used in this thesis in both functional controller conditions and in the presence of a failure.

This work is dedicated to my friends and family: the people who always believed in me.

Contents

Tables

Figures

Acknowledgments

I would like to thank my advisor Dr. Shirley Dyke for her continual support and help in the preparation of this study. My gratitude goes out to the guys in the lab for all the help they so readily provided me. I owe Obayashi Corporation and Dr Osamu Yoshida thanks as well. They graciously hosted me in Japan for two months during the summer of 2003. I would also like to thank Dr. Kevin Truman and Dr. Roger Chamberlain for taking the time out of their schedule to serve on my defense committee.

Chapter 1

Introduction

As the field of structural control advances, and control systems are beginning to be implemented on civil engineering structures, one must anticipate potential problems which might arise within the control system that might cause a loss of efficiency, or even instabilities in the control system, and the best way in which to respond to these problems [6]. Fault tolerance can be described as a system of safeguards against control system failures. Failures in the control system are referred to as faults, and these faults have the potential to have devastating impacts on the stability and performance of the system. The first chapter of this thesis is dedicated to a review of the technical literature dealing with various types of faults which may occur in a control system. This literature review will provide an overview of fault tolerance as a discipline, leading to an evaluation of the potential consequences of, and possible mitigation strategies for, faults in semiactive civil control systems. Most papers deal with the issue of fault detection and identification, and as this thesis focuses on fault accommodation, the review will be helpful in learning what kind of faults to anticipate and the means by which they may be detected.

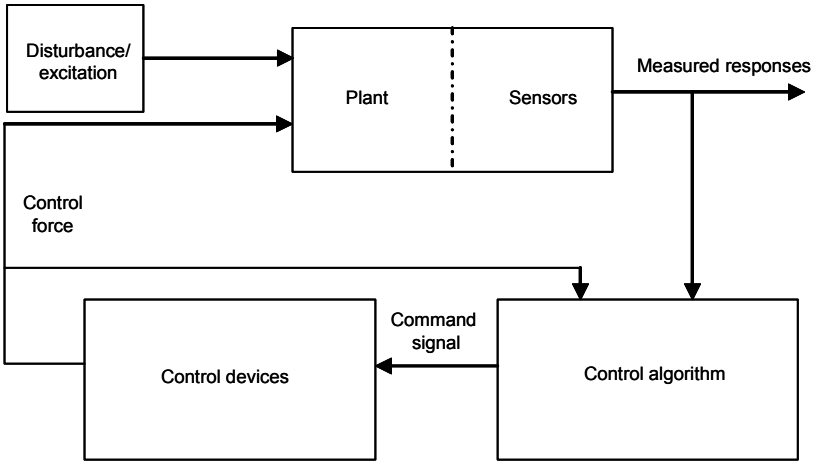

FIGURE 1-1. Block diagram of general control system.

In general, a control system utilizes sensors and control devices to control a plant. Figure 1-1 shows a simple block diagram demonstrating the function of a control algorithm.The plant is the system which is to be controlled. It is outfitted with sensors which measure the responses of the system to the disturbance or excitation. The signals output from the sensors are sent to the control algorithm. This computes the command signal to be sent to the control devices. Located within the plant, the devices output a force which is input back into the plant with the purpose of minimizing the response.

The control components discussed previously are critical to the functioning of the system, and their failures may have serious consequences. The sensors and control devices are designed to be quite reliable. Thus, although the probably of a failure occurring in such a system is very small, it is not equal to zero. Therefore, it is necessary to anticipate the types of failures that are possible, and implement strategies to mitigate the consequences of these failures. All control system applications (e.g. aircraft, vehicles, machinery, etc) are prone to such failures, and should have fault-tolerant strategies built into their designs. This thesis will examine specific issues in the fault-tolerant design of semiactive control systems for civil engineering structures.

To deal with these types of failure issues, a fault tolerant system (FTS) would be introduced to the control scheme. In general, a FTS consists of two steps: fault detection and identification (FDI), and fault accommodation (FA). The first portion consists of the part of the system which will analyze the system responses, feedback signals, and control performance to determine if the system is acting as it is expected. When the system is not behaving as expected, a fault has occurred, and the FDI system recognizes this and enters the identification portion of the algorithm.

Identification is, in general, a much more complicated process than detection. There are a variety of methods, depending on the method used for detection, and they all have advantages and disadvantages which will be discussed later. For purposes of this thesis, it is assumed that the fault can be properly detected and identified, and so focus on the FA step. This is the step in which a decision is made as to how to proceed with control in the presence of a fault. This decision will chose, by the nature of the fault, the best path for the situation: this might include switching to a redundant sensor, switching control algorithms to one designed around the fault, reverting to a fail-safe passive mode, etc.

Such systems may be classified as fail-operational, fail-safe, or fault tolerant [7]. A *fail-operational* control system is one which is able to, without changing control objectives, operate without losing performance despite the occurrence of a failure. A control system which is *fail-safe* will, when a failure occurs, fail to a state which is classified as safe in the particular context. *Fault-tolerance* is defined as the ability of a control system, in the presence of a fault, to maintain control objectives, though performance may suffer slightly. It is the goal of this thesis to study the performance of MR dampers in a fault-tolerant system. While the research discussed in this thesis focuses on the FA portion of the fault-tolerant system, this chapter surveys various types of failures and means of detecting these failures. Subsequently, it is assumed that failures have already been detected, and the results of a fault-tolerant approach are examined.

One common field of engineering in which faults are designed for to a large extent is aerospace engineering. Control systems are abundant in modern aeroplanes, making them safer and giving them greater longevity. Because the consequences of control system failure can be catastrophic, the robustness of the controller is similarly important.

Control systems in aerospace engineering are generally active in nature. An active control system is one which is capable of adding mechanical energy into the system. The control devices of such a system are actually able to impart forces on the plant, i.e. they are capable of forcing the system into action. Devices used in active systems are called actuators. Semiactive systems, on the other hand, are not capable of introducing mechanical energy to the system. Rather, these systems are only capable of dissipating energy in a very efficient manner. Semiactive devices are referred to as smart dampers or simply devices.

This thesis focuses on civil engineering applications of semiactive control systems. Because semiactive systems are relatively new, a large part of this introduction focuses on the discussion of fault-tolerance in active systems. Semi-active as well as active control strategies attempt to impart, to the best of the system's ability, the optimum force to minimize unwanted responses in the plant. Additionally, due to the risk-mitigating nature of aerospace designs, most of the research in fault-tolerance focuses on aerospace systems.The first consideration for failure is device failure, and as the systems considered in this section are generally active, the focus is actuator failure.

1.1 Actuator Failure

Actuator failure in control systems may cause severe system performance deterioration [13], and as such these failures have been researched extensively, especially in the fields of aerospace and automotive engineering. In these cases, aerospace in particular, actuators are used to direct the motion of the plant to avoid hitting objects such as other planes, mountains, or the ground in general. As such, control systems are extremely

important in these applications, and a failure could lead to the loss of lives. It is therefore a very good place to look for fault-tolerant design schemes dealing with failed actuators.

One approach to detection of actuator failures is residual generation, which involves analyzing errors between an analytical model and the responses of the actual structure. Residuals are generally observer-based, meaning that they are produced from a state space model of the plant into which the excitations and forces are fed. Fault detection and identification methods using observers or Kalman filters have been studied extensively, and in recent years considerable attention has been devoted to the study of observer design for the unknown input [33]. The residual is essentially the difference between the observer output and the responses of the plant as measured. When the observer signal is zero the structure is healthy, acting as it is expected. When the observer signal diverges from zero by more than the margin of error allowed, it is determined that a fault has occurred in the system, and the proper action is taken.

One example of fault detection and identification is discussed for a 6-DOF model of an aircraft [21]. In the detection scheme, computation is kept to a minimum when possible by using lower level computation to monitor the aircraft for the possibility of faults; when one is detected, higher levels of computation are entered such that a hierarchy exists. The first level, model based detection, is based on the measured responses and the observers predictions. In its operation, it is essentially the observer based residual generator described previously. The residuals for the actuators are compared for three modes, and if none produce a small residual, a fault is detected. When the fault detection algorithm registers a fault, then the state derivatives of the detection model are compared with the derivatives of the measured states. Sensor noise presents a problem which is avoided by careful filtering the signal to eliminate noise without altering the actual signal. In the steady state (trim), fault detection is achieved by utilizing the redundancy of the control surfaces: a test signal is sent to one of the actuators and the inverse signal to the others to cancel the effects of the test signal on the plant, while obtaining valuable information about the state of the system. In the case where no redundancy in control

surfaces exists, small signals must be exerted on the system for a brief period so as not to disturb the state too much. In both cases, the residuals are recorded and used for system identification, and also to possibly identify the fault. When differences in parameters are detected, the controller is updated. Updating the controller is achieved by changing the system variables in the aerodynamic tables, which control the dynamics of the system. This type controller is adaptive, as it is continuously updated with the values of the current estimates of the parameters of the system obtained in the fault identification section of the system.

Another adaptive approach to detecting faults in aircraft control devices considers an online approach to FDI using an adaptive interacting multiple observers (AIMO) method with a modification that cuts back on the computational burden of the system [10]. The basic AIMO scheme simultaneously uses different observers to monitor the system. These observers are constructed for different system models reflecting the conditions due to faults which might arise. When a fault occurs, and is recognized by an observer, all the observer signals are compared. When the error of any observer falls within a tolerance range, more specifically the observer with the smallest performance index, the other observers are reset to reflect the new nominal control. This method is computationally taxing, and a method which offers the benefits, but not the drawbacks of the AIMO FDI can be developed. The authors edited the monitoring system so that one main observer monitors the system until a fault is detected, which constitutes the nominal index exceeding its threshold. Once this occurs, a fault subsystem is entered in which the appropriate observer is chosen in the same manner as before, and the corresponding controller is implemented. Once it is verified that this is the correct controller/observer set by residual analysis, the other observers are reset and the new nominal regime takes over control.

Actuator failure can also be treated as an uncertainty in the aerodynamics of a plane. An adaptive approach, which is capable of handling system uncertainties, is desirable and useful in the event of actuator failure compensation because it is often uncertain how

many actuators fail, when an actuator fails and how large the failure is [13]. An approach for detecting and dealing with control surfaces on an airplane which may become frozen at some unknown fixed value, utilizes two control schemes: one for state tracking and one for output tracking, both based on pole placement design. To simplify design, the aircraft dynamics have been assumed to be linear. The first case under consideration is the failure of the spoiler, which is decoupled such that left and right spoilers are controlled separately and therefore independent left and right spoiler controller may be designed. Likewise, for the case of elevator failure, the elevator has been segmented into four distinct pieces. These divisions and separations give some redundancy to the control system: the failure of one part as opposed to the entire control surface. In the FT controller, matching conditions are constructed so that error is minimized. These matching conditions are then used to choose the parameters which will accommodate failures and match the desired output or state vector. As these parameters are piecewise continuous, the solution is not continuous. Yet the actuator failure pattern is fixed so that the plant is stable. Both state tracking and output tracking schemes use a matching algorithm to modify the controller. This approach can be described generally as an adaptive pole placement approach for both the state tracking and output tracking cases. Matching parameters are chosen in the control law such that they lead the closed-loop system to one that matches the reference system exactly (ideally) via the pole placement parameters. These parameters are determined as described above.

Adaptive control has also been used to deal with actuators stuck at unknown values, as well as dynamic values varying at an unknown rate with respect to the control signal about an unknown constant value [39]. In this study, the key issue is the parameterization of failure compensation in order to achieve the control objective while at the same time using fewer and simpler plant conditions. It is necessary to design the state feedback for output tracking such that the use of feedback control for the plant with actuator failures ensures that all signals for the closed-loop system remain bounded and that the plant output asymptotically tracks the output generated by the reference system. The compensation conditions for a fault tolerant system dictate that a feedback control

should be designed such that signals remain bounded even in the presence of errors. In order to stabilize the system, and ensure that all responses are bounded in the closed loop system, the adaptive scheme attempts pole-zero cancellation online by using the matching conditions discussed above.

An innovative approach to dealing with the constant and persistent disturbances caused by actuators which may become frozen in a constant position due to loss of hydraulic power, malfunctions of the servo loop, or stuck levers utilizes an observer to generate a residual, and identify the faulty actuator [3]. Having been identified, the frozen control surface is decoupled from the system and the controller adjusted to account for the change in dynamics. In this case, a stuck actuator is in effect a persistent disturbance in the system, and as such it is constant (its rate of change is zero). When possible, the controller uses a measurement of the point of failure of the actuator, or if that fails an estimate is used. Because the failures considered are a constant disturbance, they can be subtracted from the control vector. The results show that for simultaneous failures in two control surfaces the control system will bring the error down to zero, whereas the nominal control scheme can hover around a fairly large error. A persistent failure such as this could also be considered a parametric change. This type of failure is discussed in the following section.

1.2 Parametric Changes

Parametric changes can be caused by many different types of faults. Anything which may change the dynamic, or static properties of a plant is considered a parametric change. For instance, a change in damping or structural damage seen in a change in stiffness are both faults which would change the dynamic properties of the plant [14]. Actuator failure and loss of effectiveness may, under certain conditions, be modeled as parametric failures as well. Just as there were many approaches to detecting and dealing with actuator failures, there are also many methods by which parametric faults may be detected.

One such approach for detection of faults/structural damage employs a wavelet approach. Essentially the fault/damage is a change in stiffness of the system [14]. The wavelet approach basically employs the forward and inverse Fourier Transforms of the measured signals times a wave function Ψ. This function has two parameters that may be adjusted for best performance: the first controls the translation of the window along the time axis, and the second changes the size of the window of data used. These are chosen so that the Ψ's are orthonormal, lending ease to expansion of the wavelets. The aforementioned parameters are generally taken as powers of 2, dyads. The signal can be broken down for different dyadic scales from a mother wavelet. Sudden changes in the wavelet signal identify changes in structural stiffness, indicating a parametric fault in the system. Benefits of using this detection method include the fact that only a small portion of data is necessary for this approach, making it fast and more robust; and because just the accelerations are needed, calculation is less complicated.

Another approach to detection of these types of faults is found in a neural network scheme [14]. This scheme implements the displacement and velocity estimate errors to detect the faults. This approach does need a large amount of information to work properly, and is very model-dependent. This scheme utilizes a residual signal, generated from the displacement and velocity estimates compared to the measured values, which is analyzed and subjected to the following criteria for detection: i) prior to failure, the state position and velocity errors are zero ii) when a failure occurs then the errors attain a non-zero value, and then converge back to zero. For MDOF systems, the detection is based on the position and velocity vectors maintaining a zero value prior to failure. If these vectors are initially non-zero, there will be a problem with false detections: a dead-zone is implemented. In their case studies, they use a sine input with some small percentage of white noise. The level one details of the accelerations give the criteria for the wavelet analysis. Jumps in the estimate errors provide the neural network criteria. The signals are fed into the neural network which compares them to the learned nominal values. This network can accurately predict the new value of the stiffness, but it is model-dependent and needs a large amount of information.

Fault detection is a complicated process, and sometimes one method may work well for a particular type of fault, but not another. In the event of two types of faults occurring, a more robust system should be considered. The idea of a hybrid system is not new, but many new and innovative ideas build on that concept. By combining the ideas of two fault detection systems and creating a hybrid control model, a fault detection system is created that is robust and has the ability to calculate the size of the fault [16]. The two systems which are combined include a residual analysis and a parametric approach to fault detection. The combined approach uses a detection filter for residual generation congruently with a methodology to isolate parametric faults. Residuals are generated via the parity equation whose coefficient matrices are the nominal values of the system parameters. By taking the parity vector far enough back in time so that the noise is attenuated, the residual vector is obtained. This constitutes the observer-based portion. The parametric approach utilizes a feature vector which is computed on-line via a recursive least squares identification. As a function of the diagnostic parameter vector which varies with time, the feature vector changes as the parameters of the plant change. To isolate faults, the maximum correlation between the residual and the estimated residuals is located. The estimated residuals are generated by a number of failure hypotheses. Parameters subject to failure in the study are dubbed diagnostic parameters. It is concluded that the scheme eliminates the need for on-line parameter identification techniques for the purpose of isolating parametric failures. This decreases the computational burden on the computer, and allows for faster analysis and identification.

1.3 Sensor Failures

The final section of this literature review will focus on the effects of a sensor failure in a controlled system. Sensors are critical to effective control, and as such failure of a critical sensor can degrade performance and possibly lead to instabilities. Many of the same strategies discussed in the previous two sections are available for the detection of sensor failure, and a few techniques are discussed for dealing with these failures as well.

One approach to detection of sensor failures employs neural networks to both detect and also to accommodate sensor faults in structural systems [2]. Widrow-Hoff learning rules are utilized to teach the neural network what constitutes nominal response for the structure. Detection is achieved by performing frequency analysis on all signals. The nominal system is subjected to excitations and an FFT is taken of every sensor signal to analyze the nominal frequency content. When implemented, a certain tolerance is accepted, but when the frequency content leaves the tolerated deviance, a fault is detected. The accommodation network learns the nominal system as well, but uses one sensor signal to predict what is happening, or should be happening, at the other sensor site. When the FDI network finds sensor failure, the accommodation network kicks in and overrides the faulted sensor signal with its own estimation.

The majority of studies considered the detection of faults, and a fair number considered fault accommodation. For civil structures, however, the answers to the accommodation may not always be the same. Much depends on cost and efficacy of the measures to be taken. The object of the last study reviewed is to experimentally consider the effects of sensor failures in an H_2/LQG active mass driver control system [6]. Four options for control once an error has been detected (assumed prior to excitation) are suggested: 1) shut off control, 2) switching to duplicate sensor, 3) continuing normal operation, and 4) switching to an alternate control algorithm which takes into account the failed sensor. Two of these strategies are explored experimentally: disconnecting the sensor and continuing normal control, and implementing an alternative algorithm which is designed around the healthy sensors. In the study, a few main results surfaced. The first is that for the three story structure, sensors on the third and second floors were critical to the performance of the control system. The nominal controller could function adequately as long as the second and third floor sensors were intact. In the case of the alternative algorithm, the same general results were realized, but better performance was achieved than in the previous study. As long as sensors on the floors two and three were available for measurement the structure was stable and adequately controlled. The main conclusion is

that an alternative algorithm will return better results in the absence of a sensor failure for all cases considered (comparing the same sensor failures).

1.4 Failure Accommodation

Most of the literature reviewed, up to this point, has dealt with faults in active control systems. It is clear that little work in the fields of fault detection, identification and accommodation has been done regarding the specific issues related to civil engineering structures. As demonstrated by Battaini and Dyke (1997), a failure in an active control system can lead to significant loss of performance during seismic excitation, depending on the type and degree of failure, and the implementation of an appropriate mitigation strategy. An improperly designed active system, or an active control system with a fault, has the potential to even introduce instabilities into the system.

The focus of this thesis is fault accommodation in civil engineering applications of semi-active control. Semiactive devices are inherently stable because they cannot introduce mechanical energy into the structural system (including the structure and the devices). Thus, dealing with failures in a semiactive control system is less complicated than in an active system. In fact, because of the nature of many semi-active devices, they revert to passive energy dissipation devices when there is no power supplied to change the device properties in response to the feedback measurements.

One means of dealing with failures in semiactive systems is to introduce a fail-safe backup system. Kurata and Kobori (2003) investigate the reliability of a semiactive control system with a fail-safe passive mode as a backup in case of failure. The authors utilize a velocity feedback law based on a linear quadratic regulator to achieve semiactive control. The devices used are semiactive hydraulic dampers (SHD). Monitoring of the control system is carried out by a system of checks within the control computer system. Depending on the failure which occurs, the system reverts to the passive fail-safe for the devices which are malfunctioning. In the case of a system malfunction, all devices operate in the passive mode. The results for the fail-safe passive system using a sinusoidal

input show that the building can be controlled, though not optimally. Tests were run on one SHD, subjecting it to a sinusoidal input as well as the 1940 El Centro earthquake input. When the device fails to its passive state, the orifice goes to its minimum opening size, and the damping force increases. The authors indicate that these results are achieved in the El Centro excitation as well. The building is also subjected to a sinusoidal input, and the devices fail to the passive state described before. The authors indicate that the building's responses remain controlled, though not as effectively as with the semiactive control.

Observing this work by Kurata and Kobori (2003), it is apparent that a passive fail-safe system can be utilized in the case of system failures. It is the goal of this thesis to expand upon this idea of the passive fail-safe to account for more variables. These include the time of failure and its effects on the system, as well as the passive setting used. To ensure the best performance possible in the case of a fault in the control system, the passive fail-safe should be designed to minimize building response when the nominal controller is not functioning properly.

1.5 Overview of Thesis

Control systems which are subject to failure can be diagnosed by a variety of methods, depending on the plant, control system, type of fault, and measurements available. The description of many types of detection, and monitoring systems was the purpose of the first chapter of this thesis. To follow, a description of a civil engineering application of fault tolerance is developed. Therefore Chapter Two is devoted to the background information necessary to introduce the structures, MR models, and control strategy. Chapter Three discusses the simulations and results for a simple, planar six story model structure, and Chapter Four presents the results of a nine-story plan-irregular building. In Chapter Five a method for design of the fail-safe system is presented, and Chapter Six compares the clipped-optimal controller with a decentralized control scheme in both nominal control and in the presence of failures.

Chapter 2

Background

Issues concerning the test structures, devices, control methodology, and evaluation criteria will be discussed in this chapter. These issues are important to the problem formulation and also to the results of the simulations. Section 2.1 will discuss magnetorheological (MR) dampers and provide a model that has been shown to reproduce their nonlinear characteristics. The parameters for each device model will also be presented. Semi-active control algorithms will be discussed in Section 2.3, along with the specific class of semi-active controller used in this study: clipped-optimal control. The coefficients by which performance is measured, the evaluation criteria, are presented in Section 2.4. The faults considered in this thesis are in Section 2.5.

2.1 MR Dampers

Control schemes in civil structures are very much based on the devices used to implement the controller. The choice of semiactive control for this thesis is based on the attractive qualities of utilizing a semiactive device, or smart damper. Recently, these devices have attracted a great deal of attention due to the following facts: i) they provide controllable characteristics; ii) stability is an inherent quality; iii) and they require little power [43,36,20]. Magnetorheological (MR) dampers are classified as controllable fluid devices and have been demonstrated to be superior to comparable passive systems in both experimental and analytical studies. In addition, testing of full scale devices has

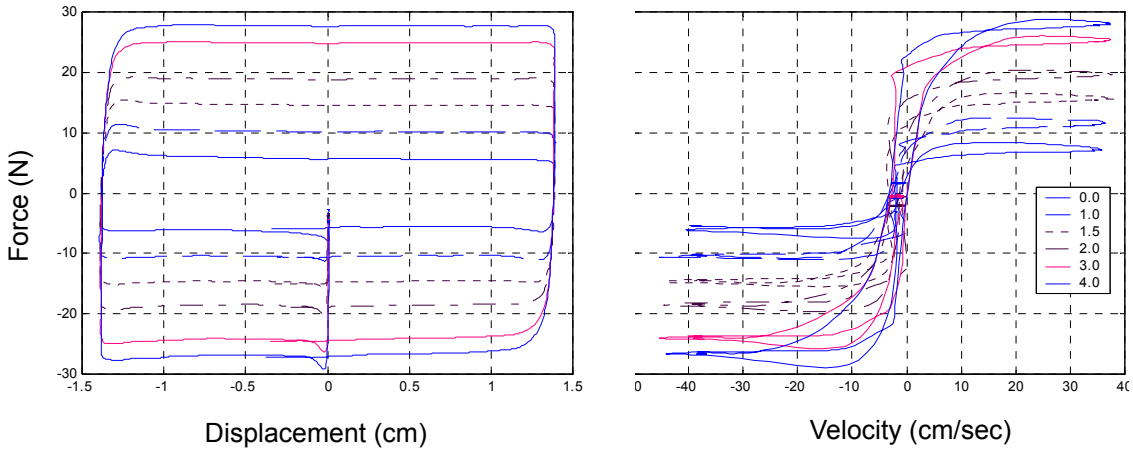

FIGURE 2-1. Force displacement and velocity displacement loops for the shear-mode MR dampers

shown that MR dampers can deliver the magnitude of forces required for full-scale structural implementation [37].

The forces developed in MR dampers are dependent on the relative velocities between the floors at which the devices are located as well as the relative displacements between the floors. The devices have memory, meaning that the past responses impact the response of the device. This hysteretic behavior results in force-displacement and force-velocity loops, such as those shown in Figure 2-1.

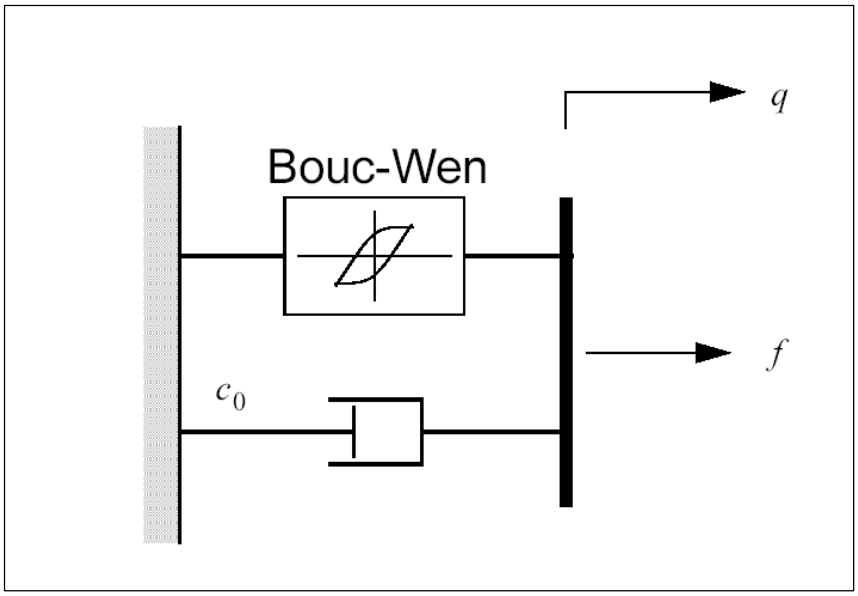

FIGURE 2-2. Simple mechanical model of MR dampers

Based on experimental data, models were developed for these devices [36,43,20,17]. The behavior of these devices can be modeled by a Bouc-Wen element in parallel with a viscous dashpot, as shown in Figure 2-2.

With few moving parts, MR dampers are reliable, and, combined with the low power requirements and inherent stability due to their inability to introduce energy to the system, an attractive solution for control of civil structures [20,43]. The nonlinearity of the devices requires the development of a nonlinear semi-active control scheme. Several authors have developed such algorithms for semi-active devices, and those selected for this study will be discussed in Section 2.3 which concerns clipped-optimal control.

Two MR damper models are utilized in this study: one for a small scale device and one for a large scale device. Figure 2-3 presents a schematic of a prototype shear mode MR damper. This shear-mode prototype damper was constructed by the Lord Corporation, Cary, N.C. for experimental testing [43]. The magnetic field is generated by passing current through the coil shown in the bottom of the device shown in Figure 2-3. The current is regulated by controlling the voltage which is sent to the coil, ranging from 0-5V in

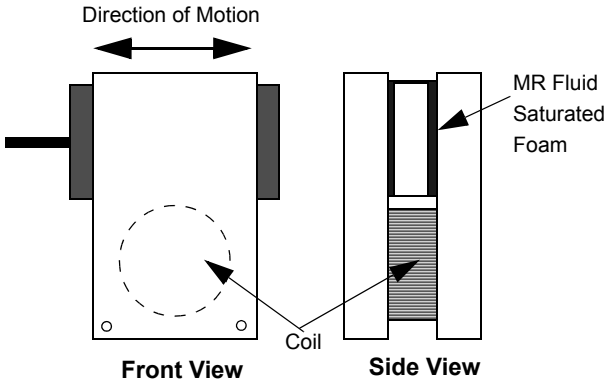

FIGURE 2-3. Model of shear mode MR damper

this particular device. The equations describing the mechanics of this shear-mode damper are developed below. Through experimentation, the behavior of the shear mode damper has been shown to be effective in modeling the large scale devices as well [44]. The force is given by

$$\boldsymbol{f} = c_0\dot{\boldsymbol{x}} + \alpha \boldsymbol{z} \tag{2-1}$$

where

$$\dot{\boldsymbol{z}} = -\gamma|\dot{\boldsymbol{x}}|\boldsymbol{z}|\boldsymbol{z}|^{n-1} - \beta\dot{\boldsymbol{x}}|\boldsymbol{z}|^{n} + A\dot{\boldsymbol{x}} \tag{2-2}$$

and $\boldsymbol{z}$ is an evolutionary variable accounting for the history dependence of the response. The voltage dependence of the device is described by the variables

$$\alpha = \alpha_a + \alpha_b \boldsymbol{u}\text{, and } c_0 = c_{0a} + c_{0b}\boldsymbol{u}\,. \tag{2-3}$$

Due to the resistance and inductance in the circuit dynamics are introduced into the electrical system [43]. These dynamics are observed as a first-order time lag represented by the first-order filter of Equation (2-4)

$$\dot{\boldsymbol{u}} = -\eta(\boldsymbol{u} - v)\,. \tag{2-4}$$

The parameters used to model the shear mode device are presented in Table 2-1 [26,43]. The parameters used to model the large scale device are given in Table 2-2 [44].

TABLE 2-1. Shear mode MR damper parameters

MR Parameter	Value	
c_{0a}	0.0064	N s/cm
c_{0b}	0.0052	N s/(cm V)
α_a	8.66	N/cm
α_b	8.86	N/(cm V)
A	120	
β	300	1/cm/cm
γ	300	1/cm/cm
η	80	Hz

TABLE 2-2. Large scale MR damper parameters

MR Parameter	Value	
c_{Oa}	4.4	N s/cm
c_{Ob}	44	N s/(cm V)
α_a	1.09E+05	N/cm
α_b	4.96E+05	N/(cm V)
A	0.12	
β	0.3	1/cm/cm
γ	0.3	1/cm/cm
η	50	Hz

2.2 Clipped-Optimal Control

As mentioned previously, MR devices are highly nonlinear. Often the most effective nonlinear control algorithm is dependent on the specific device which is to be implemented, and the measurements available. For civil structures these measurements are typically absolute accelerations, as well as device displacement and force applied by the device [19]. The clipped-optimal method is very well adapted to these conditions, and is

therefore a good choice for semiactive control of a civil structure [20,26,43]. In essence, it is an attempt to mimic optimal active control with semiactive devices.

The control strategy based on absolute acceleration feedback for controlling a single MR damper was proposed [20]. The control algorithm was extended to control multiple MR devices [17], and experimentally verified the performance of this algorithm [43].

For a system with n MR dampers, the approach utilized in the clipped-optimal control algorithm is to maintain n force feedback loops that induce each MR damper to produce approximately the desired control force. The desired control force of the ith MR damper is denoted f_{ci} . A linear optimal controller $\mathbf{K}_c(s)$ is designed that calculates a vector containing the desired control forces, $\mathbf{f}_c = \left[f_{c1}\, f_{c2}\, \ldots\, f_{cn}\right]^T$, based on the measured structural response vector $\mathbf{y}_m$ and the measured control force vector $\mathbf{f}_m$, *i.e.*,

$$\mathbf{f}_c = L^{-1}\left\{-\mathbf{K}_c(s)L\left\{\begin{matrix}\mathbf{y}_m\\ \mathbf{f}_m\end{matrix}\right\}\right\} \tag{2-5}$$

where $L\{\cdot\}$ is the Laplace transform [44]. Although the controller $\mathbf{K}_c(s)$ can be synthesized by a variety of methods, H_2/LQG (Linear Quadratic Gaussian) strategies are advocated herein because of the stochastic nature of earthquake ground motions and because of the successful application of these algorithms in other civil engineering structural control applications [18,19,20].

Due to the fact that the forces generated in the MR dampers are dependent on the local responses of the structural system, the desired optimal control force f_{ci} cannot always be developed in the MR damper. The control voltage v_i is the only variable which can be directly controlled to increase or decrease the force produced by the device. There-

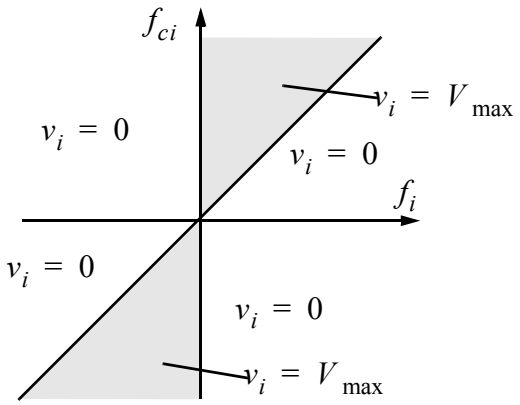

FIGURE 2-4. Graphical Representation of Clipped-Optimal Control Algorithm.

fore, a force feedback loop is introduced such that the forces produced by the MR damper will be approximately equal to the desired optimal control force f_{ci} [44,17,19].

The approximation of the desired optimal force is achieved in the following manner. The algorithm compares the magnitude and direction of the measured forces in the MR devices and the optimal forces output by the LQG controller. This results in three classifications: i) the force commanded is larger in magnitude than the force applied; ii) the commanded force is smaller in magnitude than the applied force; iii) and the forces are of opposite sign. The first category results in the command of maximum voltage, whereas categories two and three result in the command of minimum voltage. The algorithm for selecting the command signal for the *i*th MR damper is graphically represented in Figure 2-4 and can be stated as

$$v_i = V_{\max} H(\{f_{ci} - f_i\} f_i) \tag{2-6}$$

where $V_{\max}$ is the maximum voltage to the current driver, and $H(\cdot)$ is the Heavyside step function [17,20,26,43]. This cycle of maximum and minimum voltages commanded results in the force applied by the MR damper mimicking as best as possible the optimal force dictated by the H_2/LQG controller.

2.3 Evaluation Criteria

Evaluation criteria are used to analyze and classify the performance of a structural control system. For structures, damage is generally a result of excessive deformation which is related to the interstory drift. This damage is indicated by the peak value of drift. Fatigue is also of concern when considering a structure subjected to excitations of this type. RMS values indicate the magnitude of the cyclic loading which would cause fatigue. Also important for occupied buildings are the accelerations during excitation. Buildings such as hospitals with delicate equipment and patients must not only be guarded against structural damage, but the contents of the building must also be protected from inertial forces. Non-structural damage, which can be caused by either accelerations or interstory drifts, presents life-safety issues along with potentially expensive damage to the interior of the building. Therefore, evaluation criteria based on both interstory drifts and absolute accelerations are considered for the evaluation criteria used in this study. There are two criteria based on the peak responses and two based on the RMS values. All of these measures are compared to the appropriate values of the uncontrolled structure.

$$J_1 = \frac{max_{i,t}(d_i)}{d_u} \tag{2-7}$$

$$J_2 = \frac{max_{i,t}(a_i)}{a_u} \tag{2-8}$$

$$J_3 = \frac{max_i \| d_{i,t} \|}{\| d_u(t) \|} \tag{2-9}$$

$$J_4 = \frac{max_i \| a_{i,t} \|}{\| a_u(t) \|} \tag{2-10}$$

Where $max_{i,t}(\ _i)$ indicates the maximum value of drift or acceleration over all *i* floors of the controlled (semiactive or passive) case for all times within the excitation record, $max_i \| \ _{i,t} \|$ indicates the maximum of the rms values of drift or acceleration over all

floors at all times throughout the duration excitation. Also, d_u indicates the maximum drift of the uncontrolled case over all time and all floors, and $\|d_u(t)\|$ represents the maximum RMS value for the drifts in the uncontrolled structure over all time and all floors [44].

2.4 Faults Considered

The occurrence of a fault in a semi-active control system is highly improbable. As MR dampers are very reliable and composed of few moving parts, it is reasonable to assume that the most likely cause of a system malfunction would be the loss of controllability of the device. This event might be caused by disconnected control signal wires, power loss, or battery failure, losing the ability to control the voltage sent to the devices. This constitutes the fault under consideration for this thesis.

To simulate a failure of this kind, a decision block is entered into the model in which a failure time is defined. When the simulation clock passes this designated failure time, the command signal is switched from the output of the control algorithm to a specific constant voltage is applied to the MR damper model. If the clock has not surpassed the failure time then the control signal commanded from the clipped-optimal block passes through unchanged. Thus, simulation of a failure at specific times can be achieved, and different voltage levels can be commanded for the fail-safe passive mode. This approach, using constant voltages, represents the presence of a permanent magnet designed such that the MR dampers produce the optimal damping properties for the structure under consideration. This type of decision block and fail-safe passive system could also be applied in the case of any type of fault provided that it can be detected. In the unlikely event a device failure, switching to the passive fail-safe mode will be shown to be an effective means of limiting the loss of control efficacy in this study.

2.5 Summary

Information essential to the understanding of the studies in this thesis has been provided in this chapter. Models of MR dampers have been introduced for small and large scale devices, and their properties found useful to structural damping explained. The control algorithm found to be effective for these devices has been summarized. Device parameters used in the building of MR damper models for simulation were presented. Subsequently, the evaluation criteria used to judge the performance of a given controller were presented and discussed. Finally, the types of faults accounted for in this study are discussed, providing an idea of the situation under which this fail-safe passive system will be useful.

Chapter 3

Numerical Example: Fault Tolerant Design in a Six Story Model Structure

The six story structure discussed within this chapter is used as an example of the effects of device failure in the clipped-optimal control system, and to develop a procedure by which failures may be accommodated in a more complex system. Because the six story model is a simple MDOF system, different types of failures can more easily be investigated in detail, providing a bed of knowledge from which an investigation of a more complex system can be formulated. Effects such as failure time and passive fail-safe voltages can be explored much easier in this system than in one of higher complexity. Therefore this structure is used to determine what considerations must be taken in more complicated structures and develop a procedure for dealing with failures.

This chapter will first present the building model in section 3.1, followed by the uncontrolled, clipped-optimal, passive-off, and passive-on responses of the structure to the scaled El Centro earthquake excitation in section 3.2. This section presents the data which is used for comparison of the performance of the structure with faults occurring in the control system. The optimal design for this example is taken from Jansen and Dyke [26]. Section 3.3 discusses the performance of the system in the presence of these faults, and section 3.4 considers the effects of changing the passive voltage in the purely passive system.

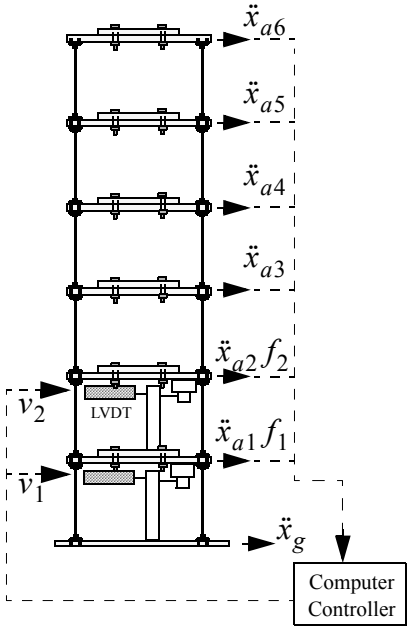

FIGURE 3-1. Six story model building.

3.1 Numerical Model of the Building

The structure under consideration is model of a six story scale test building (see Figure 3-1). MR devices are placed on the first and second floors, two on each floor, but assumed to fail simultaneously for this study. Vertical loads are supported by four columns between each floor arranged for a straight vertical load path. Each MR damper is capable of producing a force equal to 1.3% of the weight of the entire structure. The mass of each floor, $m_{i,}$ is defined as 0.227 N/(cm/sec^2), the stiffness of each floor, k_i, as 297 N/cm, and the damping ratio for each mode is considered to be 0.5%. This system is a simple model of a scaled, six-story, test structure that has been used in previous control studies at the Washington University Structural Control and Earthquake Engineering Laboratory [43].

As illustrated in Figure 3-1, the available measurements include the absolute accelerations from all six floors, as well as the forces generated by the MR dampers measured by

force transducers i.e., $y = (\ddot{x}_a^1, \ddot{x}_a^2, \ddot{x}_a^3, \ddot{x}_a^4, \ddot{x}_a^5, \ddot{x}_a^6, f_1, f_2)$. Written in the state space form, the equations of motion become

$$\dot{x} = \mathbf{A}x + \mathbf{B}u\,,\; y = \mathbf{C}x + \mathbf{D}u \tag{3-1}$$

where x is the state vector, y is the measurement vector, and

$$\mathbf{A} = \begin{bmatrix} \mathbf{0} & \mathbf{I} \\ -\mathbf{M}^{-1}\mathbf{K} & -\mathbf{M}^{-1}\mathbf{C}_\mathrm{d} \end{bmatrix},\; \mathbf{B} = \begin{bmatrix} \mathbf{0} \\ \mathbf{M}^{-1}\lambda \end{bmatrix},\; \mathrm{C} = \begin{bmatrix} \mathbf{I} \\ \mathbf{M}^{-1}\mathbf{K} - \mathbf{M}^{-1}\mathbf{C}_\mathrm{d} \end{bmatrix},\; \mathbf{D} = \begin{bmatrix} \mathbf{0} \\ \Lambda \end{bmatrix} \tag{3-2}$$

given **M** is the diagonal mass matrix whose values are the masses of each respective floor, **K** is the full stiffness matrix with values corresponding to the stiffnesses between the floors, and $\mathbf{C}_\mathrm{d}$ is the damping matrix whose values correspond to the damping characteristics of the structure. Also, λ is a square matrix of ones, and

$$\Lambda = \mathbf{M}^{-1}\left(\mathbf{I} - \begin{bmatrix} 0 & 1 & 0 \\ 0 & 0 & 1 \\ 0 & 0 & 0 \end{bmatrix}\right). \tag{3-3}$$

3.2 Uncontrolled, Passive, and Clipped-Optimal Responses

To obtain a basis for comparison of the performance of the control system in the presence of a fault, data on the responses in the uncontrolled and controlled cases is necessary. Because the structure under consideration is a scaled model, the full scale El Centro earthquake excitation record is scaled to 10% of its original magnitude [26]. When subjected to the scaled excitation, the responses are simulated for the uncontrolled state with no dampers whatsoever, as well as in the passive and clipped-optimal semi-active control states. The passive cases consist of passive-off (0V applied to dampers) and passive-on (maximum voltage applied to dampers). These four cases are used here

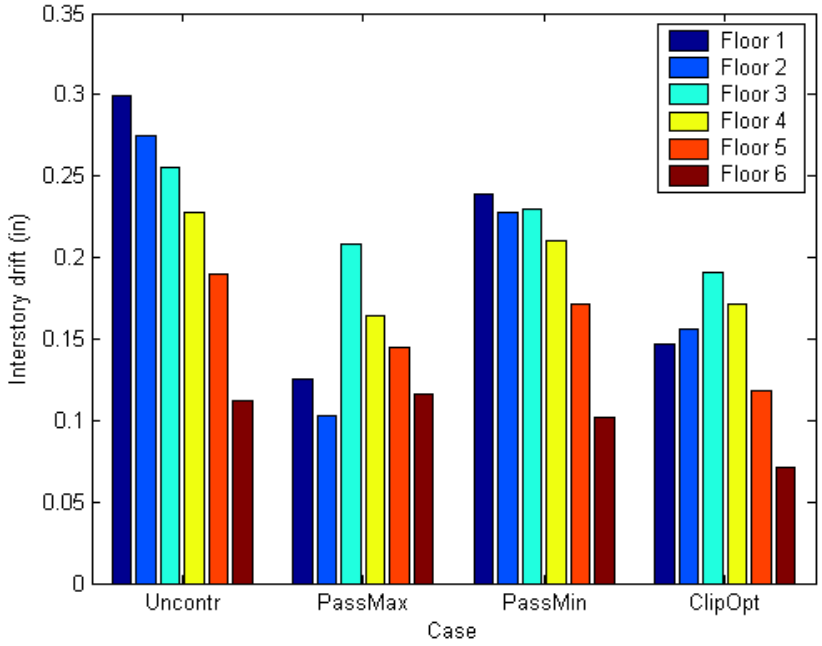

FIGURE 3-2. Interstory drifts of the uncontrolled, clipped-optimal, passive-off, and passive-on passive-off cases for the scaled El Centro excitation for all six floors.

as references for analysis of the performance of the system in the presence of faults. The results are shown graphically in Figure 3-2, and numerically in Table 3-1.

Considering the values obtained from the four cases presented, it becomes clear that each of the efforts to control the motion of the building was successful in lessening the drifts. The passive-on case actually achieves the greatest reduction in drift for three of

TABLE 3-1. Interstory drifts of the uncontrolled, pass max, pass min, and clipped-optimal for the El Centro excitation.

Maximum Drifts				
Floor	Uncontrolled	Clipped-optimal	Passive-off	Passive-on
1	0.299	0.147	0.239	0.125
2	0.275	0.156	0.228	0.102
3	0.255	0.191	0.230	0.208
4	0.227	0.172	0.211	0.164
5	0.190	0.118	0.172	0.145
6	0.112	0.071	0.101	0.116

the six floors, while the passive-off case is least effective in the reduction of drift. For the overall case, clipped-optimal control has the lowest maximum drift. There is more to evaluating the responses though: while these drifts give an idea of the maximum deformation on each floor, the overall performance of the building is more complex. Therefore, the evaluation criteria discussed in chapter 2 are presented for each of these cases in Figure 3-3.

It is apparent that the clipped-optimal configuration results in the best overall performance when all of the evaluation criteria are considered. By using this scheme, the absolute accelerations are reduced along with drifts. The peak values, corresponding to J_1 and J_2, are reduced by nearly 40% from the uncontrolled case. Also, this semi-active scheme achieves greater than 50% reduction of the RMS values corresponding to J_3 and

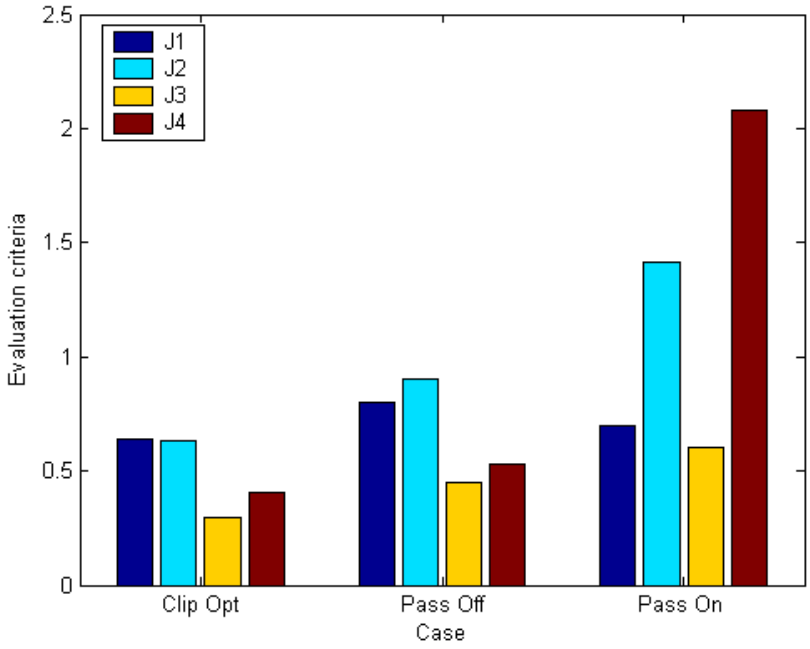

FIGURE 3-3. Evaluation criteria of the passive max, passive min, and clipped-optimal cases for the El Centro excitation.

TABLE 3-2. Evaluation criteria of the passive max, passive min, and clipped-optimal cases for the El Centro excitation.

Evaluation Criteria				
Case	J1	J2	J3	J4
Clipped-optimal	0.6396	0.636	0.295	0.4067
Passive-off	0.8007	0.9038	0.4511	0.5285
Passive-on	0.6956	1.4119	0.6054	2.0794

J_4. Overall, clipped-optimal control delivers good performance in drifts and accelerations, surpassing the performance of the passive schemes.

3.3 Voltage Dependence of Simulation Results

From the passive cases run previously, it is apparent that different voltages generate different performance. Passive-on control limits drifts well, but the accelerations exceed the maximum uncontrolled value. Passive-off control keeps accelerations below the uncontrolled case, but is not as effective in limiting drift. It is possible that there is a voltage between the passive-off and passive-on cases for which the passive responses are both very reasonable. However, the particular value that performs best will vary with the excitation, which is the reason a semiactive control algorithm is used. In the case of a failure, though, a passive design voltage can be selected for the device which will result in reasonable performance for a range of earthquakes.

To examine the relationship between voltage and the structures response, the voltage is increased over the range of 0V to 5V by increments of 0.5V. Results are compared by considering the evaluation criteria, and looking for the responses resulting in the best

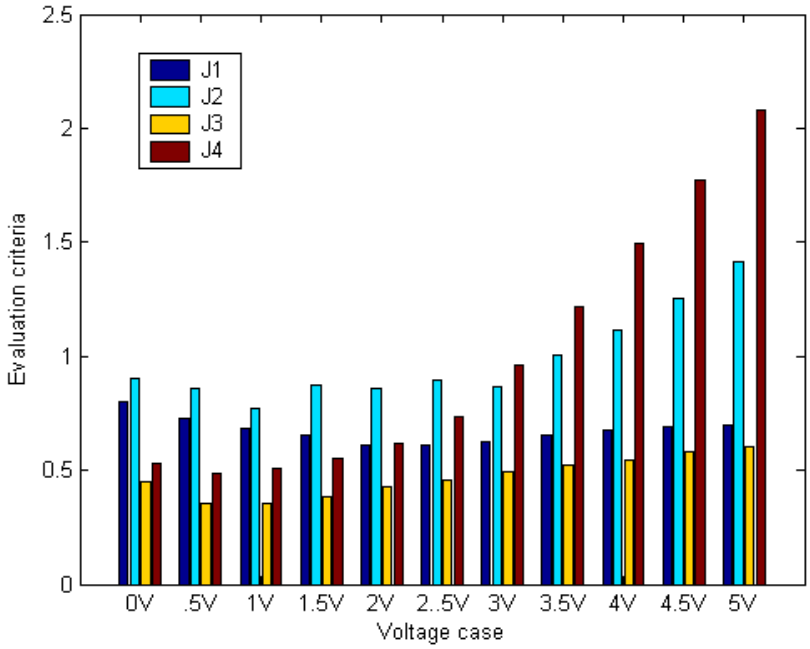

FIGURE 3-4. Evaluation criteria versus passive voltage level.

overall performance. In Figures 3-4 and 3-5, the effects of varying the passive voltage level are plotted for all four evaluation criteria.

Both of these graphs depict the same information by different means. The bar graph gives a clear picture of the overall performance while the line plot shows the trend in

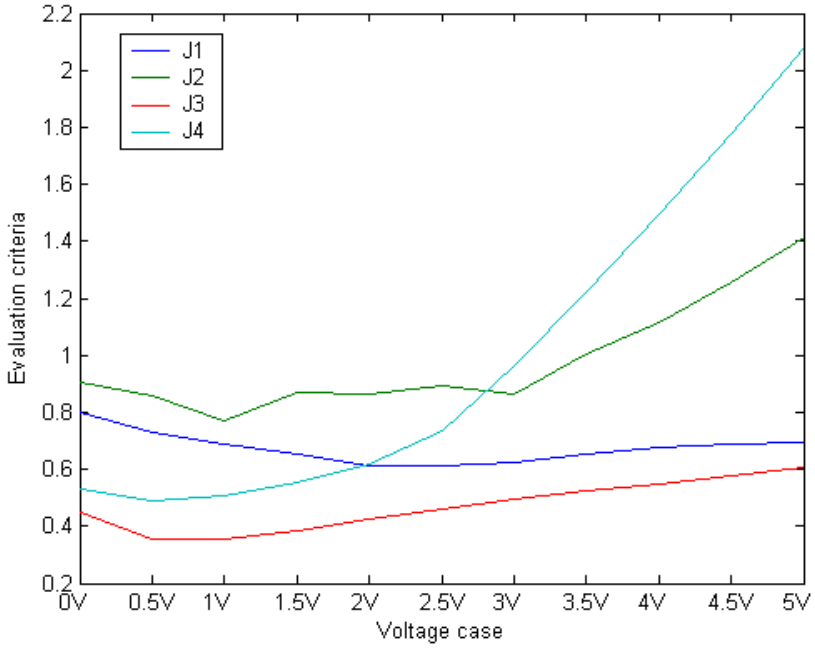

FIGURE 3-5. Evaluation criteria versus passive voltage level.

each of the performance criteria very clearly. The peak drifts decrease as the voltage increases from 0V to 2.5V, and then begin increasing slowly thereafter. The peak accelerations reach a minimum near 1.0V, and the general trend thereafter is to increase with increasing passive voltage. The RMS drifts and accelerations follow a similar trend of decreasing at first and then leveling out between 0.5V and 1V before increasing again as the voltage increases. The RMS accelerations increase much more rapidly than the RMS drifts with increasing voltage. Considering the bar graph in Figure 3-4, it appears that to take advantage of each trend and achieve the best overall passive performance for the El Centro earthquake, the 1.0V level should be chosen as the optimal passive voltage. This voltage level takes advantage of decreasing peak drifts, the lower ranges of RMS drifts and accelerations, as well as the dip in the peak accelerations. This voltage delivers reasonable performance, but it should be noted that it is not good enough to replace clipped-optimal control. The semiactive system still returns much better accelerations than the passive case, and as such it is still advocated for control.

3.4 Effects of Failure Time

As earthquakes are random events, it is impossible to predict the excitation that the structure will experience. The ground motion may, however, have a peak after which the severity of the accelerations drops dramatically. In this section the effects of the time of device failure are explored for two purposes. The first is to ascertain whether the time of failure will impact the performance of the structure. It is important to consider all conditions of failure for the faults considered to be sure that the passive fail-safe system will work under the worst case scenario of failure. The second purpose is to determine the time after which a failure is no longer detrimental to the structure. This second outcome is useful because it will reduce the computation time required for simulations.

3.4.1 Simulating Failures

Simulation of a failure at a specific time requires that a decision block be added to the Simulink model. This block switches the signal from the clipped-optimal control to the passive state at a designated failure time. The passive fail-safe system is chosen to be a constant voltage which simulates the constant magnetic field that is achieved by placing

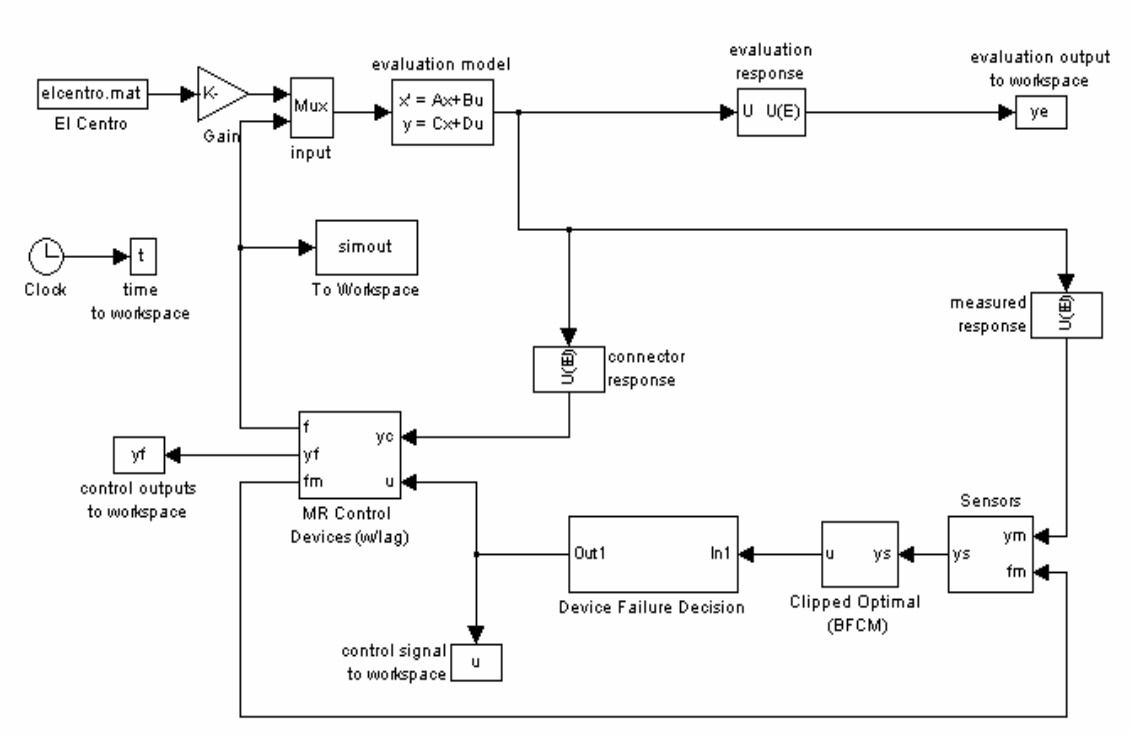

FIGURE 3-6. Simulink model for the clipped-optimal control with the device failure decision block inserted.

a permanent magnet in the MR device. As shown in Figure 3-6, the clipped-optimal control is monitored at the transition between the control signal coming out of the clipped-optimal block and the MR control devices block. It is here that the signal is interrupted to decide whether the device has failed or if it will still receive the clipped-optimal signal. Figure 3-7 depicts the layout of the device failure decision block, though it appears more complicated than it is. To overview the function of this block, the clock indicates simulation time. That time signal is fed into the *if* blocks for floors one and two, where it

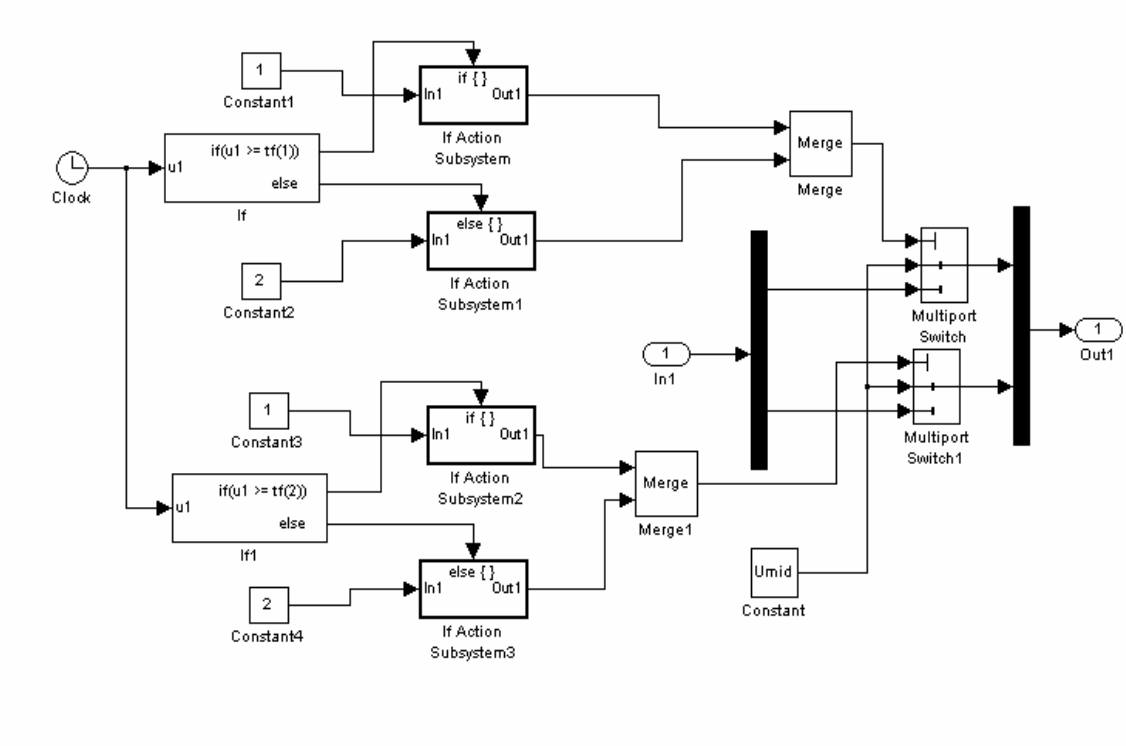

FIGURE 3-7. Device failure decision block from Simulink model.

compares the current time with that of the designated failure time for each floor. If the current time is greater than the failure time, the *if action* subsystem is activated and the switch for that floor is commanded to change to the constant voltage. If, however the time is less than the failure time, the *else action* subsystem is activated and the switch for that floor continues to use the clipped-optimal signal.

3.4.2 Preliminary Evaluation of the Effects of Failure Time

Large increases in peak drift and acceleration draw the most attention here because the purpose of this particular analysis is to identify a critical time period for a failure in the control system. This step is achieved by simulating failures at regular intervals throughout the excitation. If the peak responses of the building do not change after a certain failure time, that will be considered the last time necessary for this comprehensive study. Maximum and minimum voltages are used to compare the effects of failure time. Figure 3-8 shows the evaluation criteria for the clipped-optimal case as

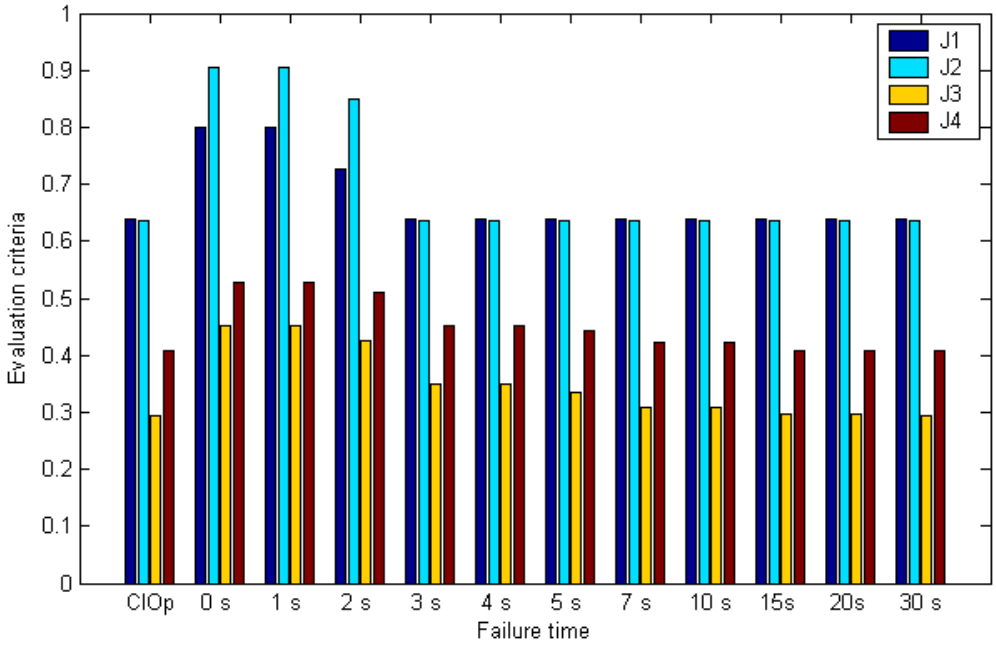

FIGURE 3-8. Evaluation criteria versus failure time (failing to 0V) for the El Centro earthquake excitation.

well as a range of failure time cases for a passive fail-safe voltage of 0V, or passive-off. It is noted that the peak drift and accelerations undergo large increases for failures occurring between 0 and 2 seconds for the El Centro earthquake, and return to the clipped-optimal values if the failure occurs after this time period. The RMS values, though, remain higher than the clipped-optimal values up until nearly 20 sec.

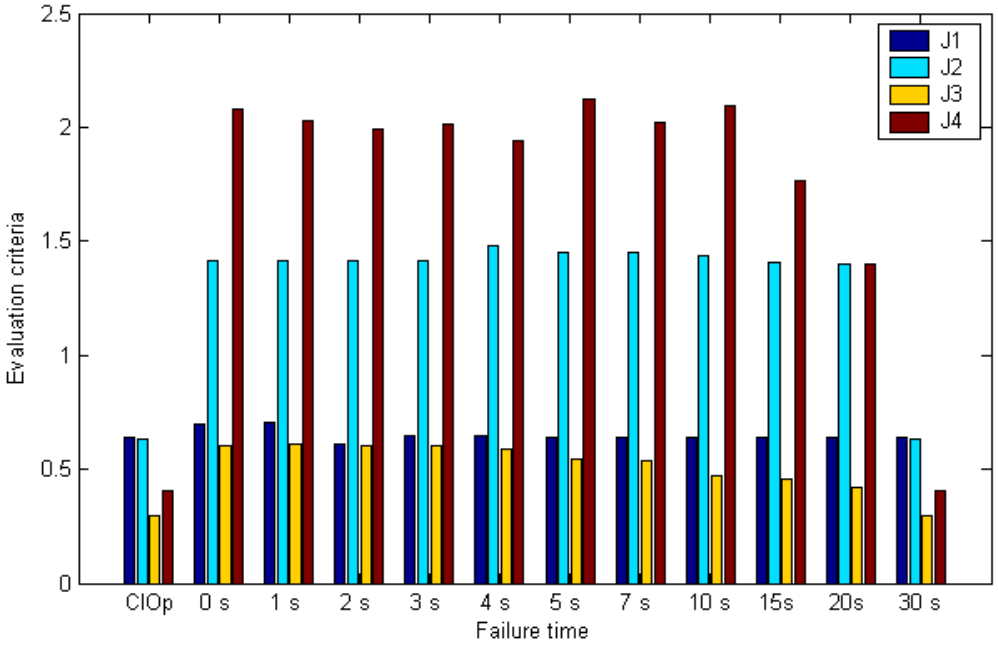

FIGURE 3-9. Evaluation criteria versus failure time (failing to 5V) for the El Centro earthquake excitation.

Figure 3-9 shows the evaluation criteria for both devices failing to 5V at various times. In this case, the peak interstory drifts (J_1) do not fluctuate much with respect to failure time, and both peak and RMS accelerations (J_2 and J_4) remain well above those of the uncontrolled case. Comparing Figures 3-8 and 3-9, the effects of failure time may be characterized for the scaled El Centro earthquake. Note that after about three seconds, the peak drifts due to failure return to values close to those of the clipped-optimal scheme for both scenarios. The RMS values for the passive-off case converge to the clipped-optimal value long before those of the passive-on failure state. In the passive-on case, RMS values remain high for failure times up to 2/3 of the earthquake record time.

The peak accelerations in the passive-on case remain high, but do not fluctuate much with failure time. Such large accelerations throughout the excitation can be attributed to the first two floors of the structure becoming ‘locked’ due to high forces in the devices

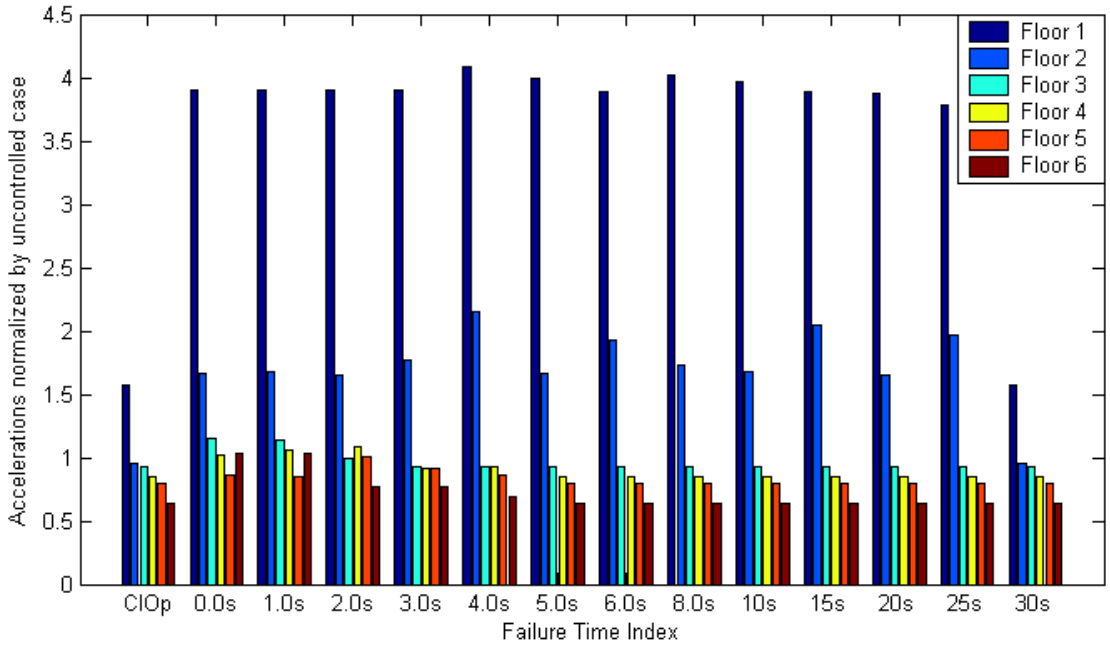

FIGURE 3-10. Acceleration by floor versus failure time (failing to 5V) for the scaled El Centro earthquake excitation.

[18,43]. This locking effect is demonstrated in Figure 3-10. The accelerations for each floor in the failure cases are normalized by the corresponding floor accelerations in the uncontrolled case. Notice that floors one and two (the floors with devices) demonstrate the largest accelerations for the failure cases.

Considering the information above, it seems that the accelerations that accompany large voltage are not a function of failure time. Figure 3-8 is therefore used to determine the time for which failures should be considered in this study. As the responses return to clipped-optimal for failure times after two seconds, three seconds is chosen as the latest time necessary for consideration with the scaled El Centro excitation. This result is not important for design, but for analysis. It is important to understand how the building will respond in the worst case scenarios.

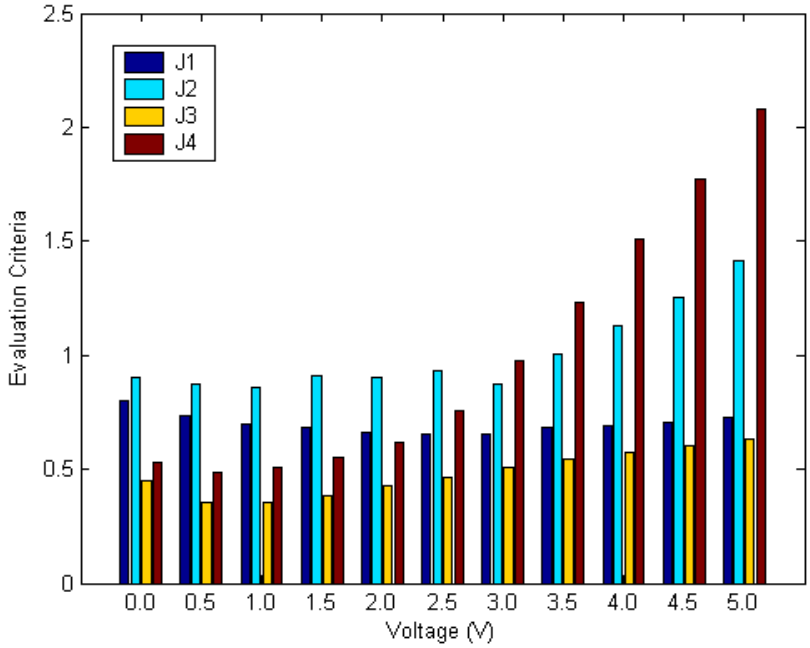

FIGURE 3-11. Worst case evaluation criteria over all considered failure times between 0 and 3s organized by voltage for the El Centro earthquake excitation.

3.4.3 Designing the Fault Tolerant System

Previously, in section 3.3, the passive case was run for voltages between 0V and 5V to find the optimum passive voltage. This section considers, once again, voltages between 0V and 5V to find the best value of the passive fail-safe voltage. This time though, failure time is added to the simulation to verify the results of the passive run. The voltages considered range from zero to five in increments of 0.5V.

Figure 3-11 shows highlights of the values presented in Tables 3-4 and 3-5. These are the worst case criteria over all failure times at each voltage level. As before, the passive-off case has the largest peak drifts. The passive-on case has a low peak drift, but that low drift is accompanied by accelerations near 1.5 times the uncontrolled case. A voltage of 2.5V achieves the lowest peak drift, but the other criteria for it are high. The 1.0V level

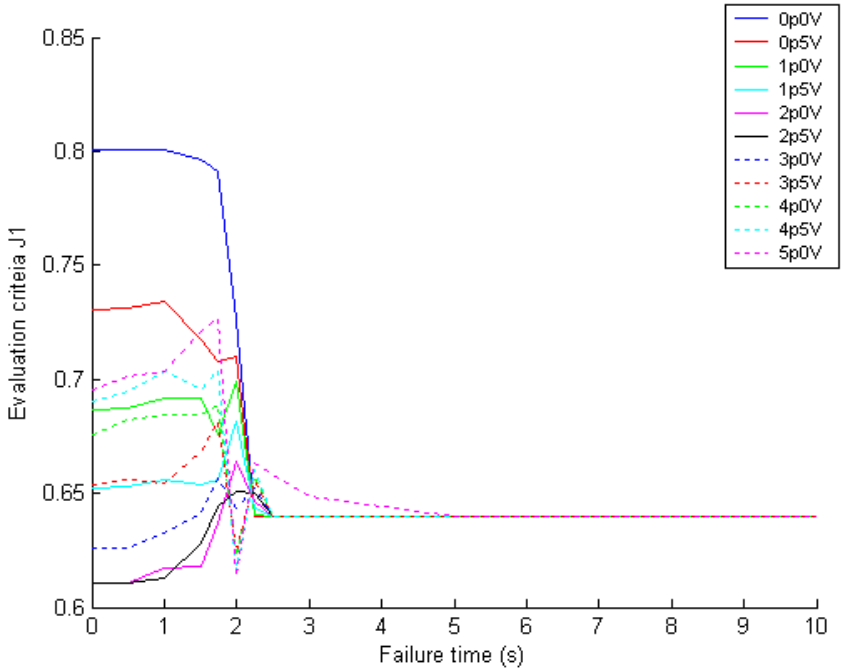

FIGURE 3-12. Trend for evaluation criteria J_1 versus failure time for all voltage cases.

achieves a balance between the assets of high and low voltages with the best overall evaluation criteria.

3.4.4 Analysis Focusing on the Responses Before the Peak Excitation

In the scaled El Centro earthquake used for excitation input in this chapter, there is a time at which the failure of the system does not increase the peak response evaluation criteria. From Figure 3-8 it is apparent that a peak in the excitation exists, and it was decided in section 3.4.2 that if the devices fail after 3 seconds, the responses are affected minimally. To take advantage of this, a more detailed investigation of the response dependence on failure time before the peak excitation time is conducted. Simulations are run for all the considered voltages at failure times between 0 and 3 seconds by steps of 0.5s as well as for voltages between 0V and 5V by steps of 0.5V. Numerical values detailing this are found in Tables 3-4 and 3-5.

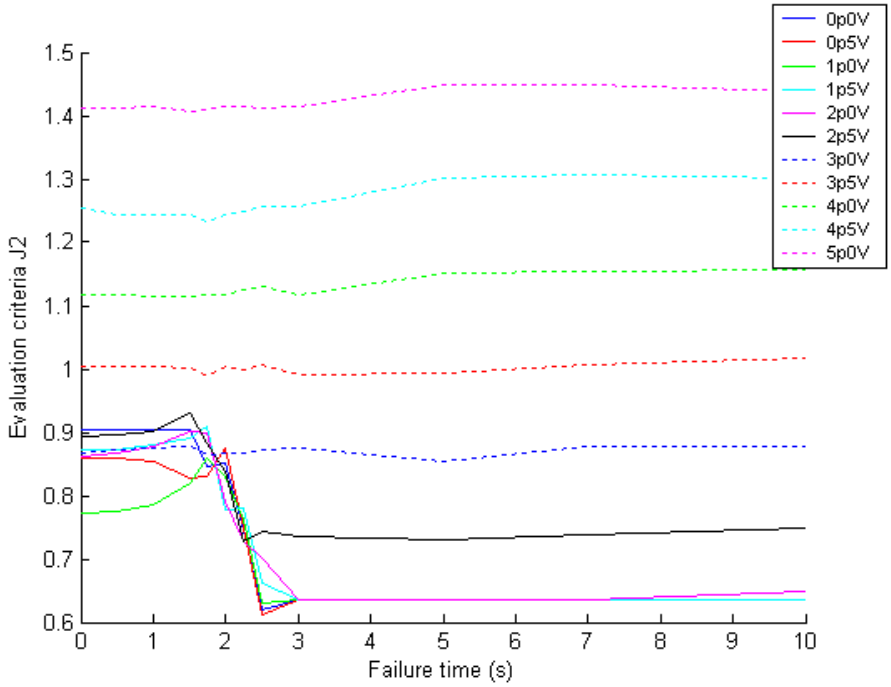

FIGURE 3-13. Trend for evaluation criteria J_2 versus failure time for all voltage cases.

The trend for J_1 versus failure time is plotted for each voltage case in Figure 3-12. Failure times are extended to 10s here to verify that the worst case scenario occurs before 3s through the trend for each voltage. The maximum drifts converge to the clipped-optimal value for all voltages at 2.5s in all cases except the 5V trial which converges at 5s. In all cases, the worst case scenario occurs before 3s, verifying that the time chosen in the passive-off study was correct. Figure 3-13 shows the trend for each voltage versus failure time of J_2. For voltages below 3V the worst case scenario occurs before 3s. Voltages above 3V, however start out with a J_2 greater than 1.0 and remain that way for all failure times. Recalling the passive-on case from section 3.4.2, the accelerations remain high for all failure times. That phenomenon is linked to the locking of the floors, and so the trends of the voltages shown in Figure 3-13 may be linked to locking as well. As the criteria for these are above 1.0, they should be disregarded as possible fail-safe voltages regardless.

TABLE 3-3. Numerical values of the maximum of each evaluation criteria over failure times between 0 and 3 seconds for voltages between 0 and 5V (minimum values bolded)

Voltage (V)	J_1	FT (s)	J_2	FT (s)	J_3	FT (s)	J_4	FT (s)
0	0.8007	0	0.9042	0.5	0.4511	0	0.5286	1
0.5	0.7345	0.5	0.8757	C.O.	0.3551	0	**0.4884**	0.5
1	0.6987	1.75	**0.8593**	1.5	**0.3548**	0.5	0.5094	0.5
1.5	0.6814	1.75	0.908	1.5	0.3863	0.5	0.5531	0.5
2	0.6638	1.75	0.9009	1	0.4283	0.5	0.6158	0.5
2.5	**0.651**	1.75	0.9316	1	0.4654	2.5	0.7553	3
3	0.657	1.5	0.8769	1	0.507	2.5	0.9784	0
3.5	0.6812	1.5	1.0074	2.5	0.5446	2.5	1.2326	0
4	0.6885	1.5	1.13	2.5	0.5752	2.5	1.5104	0
4.5	0.7038	1.5	1.2572	3	0.6021	2.5	1.7741	C.O.
5	0.7267	1.5	1.4147	3	0.6306	2.5	2.0794	C.O.

Depending on which evaluation criteria is considered, a different voltage delivers the best performance. For J_1 the best voltage is 2.5V, while for J_2 and J_3 the best voltage is 1V, and for J_4 the best voltage is 0.5V. Overall, 1V delivers the best performance with lowest values for both J_2 and J_3. Concerning peak drifts (J_1) the 1V fail-safe is 0.0477 above the minimum value, which indicates a loss in performance of 4.8%. Looking at the other criteria, the difference is made up. The 1V fail-safe performance in criteria J_2, J_3, and J_4 compared to the 2.5V performance are better by 0.0723, 0.1106, and 0.2459, respectively. That is to say, using 1.0V instead of 2.5V which returns the best peak drift performance, results in an improvement of 7.23% in peak acceleration, 11.1% in RMS drift, and 24.6% in RMS acceleration. This information is readily drawn from Table 3-3.

If a failure occurs, and the system fails to a fail-safe voltage of 1.0V, the RMS values do not increase dramatically and the peak responses also remain well controlled. The trend for the failures is presented for 1.0V in Figure 3-14. Complete results for 0V through 5V

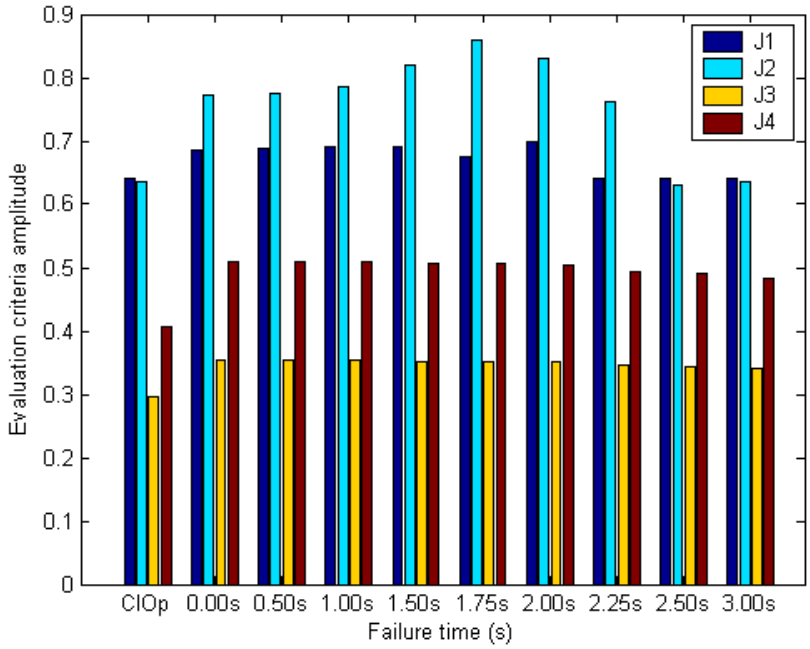

FIGURE 3-14. Evaluation criteria for failure times between 0 and 3 seconds failing to 1V for the El Centro earthquake excitation.

can be found in Tables 3-4 and 3-5. Note that the peak drifts (J_1) remain under 0.7 and the RMS values, J_3 and J_4, remain under 0.36 and 0.51, respectively for the 1.0V case.

TABLE 3-4. Evaluation criteria all voltages and failure times for the El Centro earthquake excitation.

V	Failure Time	J_1	J_2	J_3	J_4	V	Failure Time	J_1	J_2	J_3	J_4
0 V	Clip Opt	0.6396	0.636	0.295	0.4067	0.5 V	Clip Opt	0.6396	0.636	0.295	0.4067
	0 s	**0.8007**	0.9038	**0.4511**	0.5285		0 s	0.7311	0.8592	**0.3551**	0.4883
	0.5 s	0.8003	**0.9042**	0.451	0.5284		0.5 s	**0.7345**	0.8552	0.355	**0.4884**
	1 s	0.796	0.9035	0.4498	**0.5286**		1 s	0.7175	0.8275	0.3507	0.4837
	1.5 s	0.7911	0.8459	0.4462	0.524		1.5 s	0.7082	0.8296	0.3498	0.4819
	1.75 s	0.7261	0.8503	0.4247	0.5096		1.75 s	0.7098	**0.8757**	0.3437	0.4745
	2 s	0.6396	0.7458	0.3754	0.4713		2 s	0.6399	0.7479	0.3281	0.4567
	2.5 s	0.6396	0.619	0.3655	0.4588		2.5 s	0.6396	0.612	0.3233	0.4521
	3 s	0.6396	0.636	0.3493	0.453		3 s	0.6396	0.636	0.3204	0.4495
V	Failure Time	J_1	J_2	J_3	J_4	V	Failure Time	J_1	J_2	J_3	J_4
1 V	Clip Opt	0.6396	0.636	0.295	0.4067	1.5 V	Clip Opt	0.6396	0.636	0.295	0.4067
	0 s	0.6877	0.7746	0.354	0.5089		0 s	0.653	0.8722	0.3852	0.5528
	0.5 s	0.6919	0.7854	**0.3548**	**0.5094**		0.5 s	0.656	0.8812	**0.3863**	**0.5531**
	1 s	0.692	0.819	0.3526	0.5075		1 s	0.6537	0.8918	0.3856	0.5521
	1.5 s	0.6758	**0.8593**	0.3518	0.506		1.5 s	0.656	**0.908**	0.3821	0.5503
	1.75 s	**0.6987**	0.8292	0.3506	0.5047		1.75 s	**0.6814**	0.7774	0.3826	0.5446
	2 s	0.6407	0.762	0.3455	0.4927		2 s	0.6435	0.7795	0.3833	0.5419
	2.5 s	0.6396	0.6309	0.3428	0.4909		2.5 s	0.6396	0.6619	0.382	0.5387
	3 s	0.6396	0.636	0.3401	0.4842		3 s	0.6396	0.636	0.3792	0.5298
V	Failure Time	J_1	J_2	J_3	J_4	V	Failure Time	J_1	J_2	J_3	J_4
2 V	Clip Opt	0.6396	0.636	0.295	0.4067	2.5 V	Clip Opt	0.6396	0.636	0.295	0.4067
	0 s	0.6108	0.8664	0.4274	0.6152		0 s	0.6108	0.8949	0.4599	0.744
	0.5 s	0.6174	0.8777	**0.4283**	**0.6158**		0.5 s	0.6126	0.9014	0.4612	0.7398
	1 s	0.6181	**0.9009**	0.4271	0.6149		1 s	0.6283	**0.9316**	0.4605	0.7293
	1.5 s	0.637	0.8997	0.4228	0.6085		1.5 s	0.6443	0.8834	0.4529	0.7409
	1.75 s	**0.6638**	0.7904	0.4235	0.6081		1.75 s	**0.651**	0.8387	0.4549	0.7545
	2 s	0.6468	0.7264	0.4267	0.6051		2 s	0.6498	0.7266	0.4616	0.7398
	2.5 s	0.6396	0.7006	0.4266	0.6043		2.5 s	0.6396	0.7442	**0.4654**	0.7461
	3 s	0.6396	0.636	0.423	0.5921		3 s	0.6396	0.7355	0.4591	**0.7553**
V	Failure Time	J_1	J_2	J_3	J_4	V	Failure Time	J_1	J_2	J_3	J_4
3 V	Clip Opt	0.6396	0.636	0.295	0.4067	3.5 V	Clip Opt	0.6396	0.636	0.295	0.4067
	0 s	0.6261	0.8718	0.4949	**0.9784**		0 s	0.6558	1.0048	0.5241	**1.2326**
	0.5 s	0.6329	0.8746	0.4964	0.9658		0.5 s	0.6545	1.0034	0.5248	1.2162
	1 s	0.6415	**0.8769**	0.4943	0.958		1 s	0.6683	1.001	0.5237	1.2047
	1.5 s	**0.657**	0.8649	0.4883	0.9695		1.5 s	**0.6812**	0.9892	0.5202	1.2014
	1.75 s	0.6435	0.8662	0.4903	0.9689		1.75 s	0.6245	1.004	0.5228	1.1925
	2 s	0.6526	0.8661	0.4991	0.9638		2 s	0.6551	0.9985	0.5345	1.1719
	2.5 s	0.6396	0.8712	**0.507**	0.9543		2.5 s	0.6396	**1.0074**	**0.5446**	1.163
	3 s	0.6396	0.8744	0.497	0.9483		3 s	0.6396	0.9917	0.5334	1.1458

TABLE 3-5. Evaluation criteria all voltages and failure times for the El Centro earthquake excitation (cont'd)

V	Failure Time	J_1	J_2	J_3	J_4
4 V	Clip Opt	0.6396	0.636	0.295	0.4067
	0 s	0.6822	1.1168	0.5477	**1.5104**
	0.5 s	0.6844	1.1145	0.5492	1.479
	1 s	0.6846	1.1143	0.548	1.4659
	1.5 s	**0.6885**	1.1165	0.5457	1.4513
	1.75 s	0.6222	1.1168	0.5489	1.4378
	2 s	0.6577	1.1253	0.561	1.4114
	2.5 s	0.6396	**1.13**	**0.5752**	1.4045
	3 s	0.6396	1.1172	0.5602	1.4204

V	Failure Time	J_1	J_2	J_3	J_4
4.5 V	Clip Opt	0.6396	0.636	0.295	0.4067
	0 s	0.6946	1.2442	0.5785	**1.7737**
	0.5 s	0.7034	1.2431	0.582	1.7256
	1 s	0.6952	1.2442	0.5792	1.7082
	1.5 s	**0.7038**	1.2331	0.5736	1.7099
	1.75 s	0.6158	1.2426	0.5754	1.706
	2 s	0.6606	1.2496	0.5893	1.6762
	2.5 s	0.6396	1.2559	**0.6021**	1.6686
	3 s	0.6396	**1.2572**	0.5857	1.6984

V	Failure Time	J_1	J_2	J_3	J_4
5 V	Clip Opt	0.6396	0.636	0.295	0.4067
	0 s	0.7014	1.4131	0.6055	**2.0717**
	0.5 s	0.7035	1.4136	0.607	2.0321
	1 s	0.721	1.4066	0.6058	2.0095
	1.5 s	**0.7267**	1.4102	0.6062	1.9731
	1.75 s	0.6132	1.4133	0.6	1.9924
	2 s	0.6636	1.4142	0.613	1.9857
	2.5 s	0.6583	1.4116	**0.6306**	1.9371
	3 s	0.6487	**1.4147**	0.605	2.0118

Looking at the maximum values for each voltage level, the minimum of these maximum values shown in bold is shown below. The corresponding voltage is given for each evaluation criteria.

Evaluation Criteria	Min J_1	Min J_2	Min J_3	Min J_4
	0.651	0.8593	0.3511	0.4884
Corresp. Voltage	2.5 V	1 V	0.5 V	0.5 V

3.4.5 Effects of the Devices Failing Separately by Floor

The effects of failure time on the system will be expanded to cover separate failures of the control devices by floor. Figure 3-15 is a graph of the effects of separate failures. This figure shows the evaluation criteria for devices of floor 1 failing at the first mentioned time, and devices of floor 2 failing at the second. All devices failed to a passive

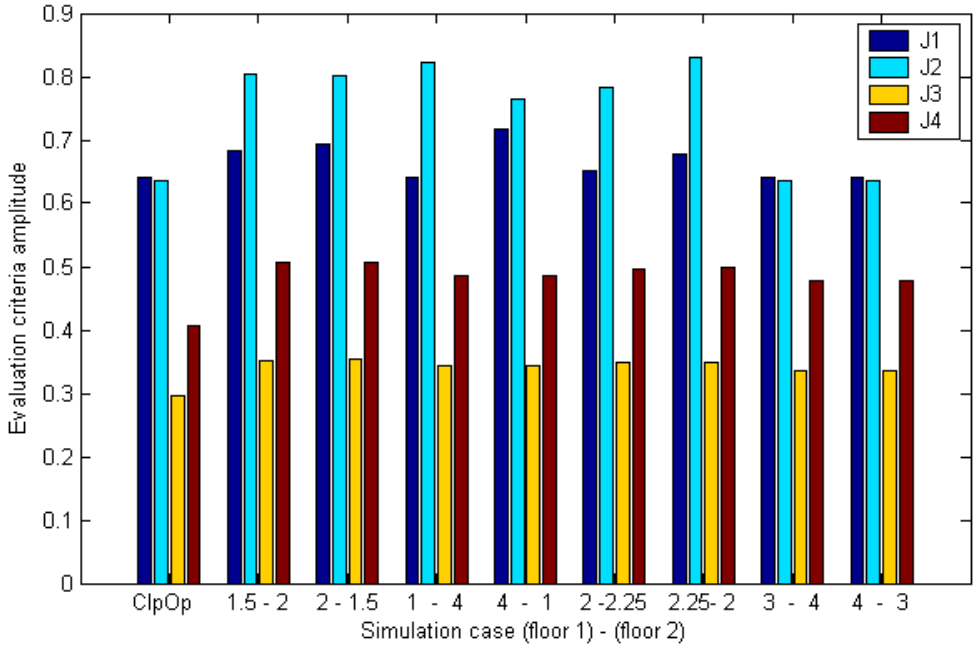

FIGURE 3-15. Evaluation criteria for separate failure times by floor for the El Centro earthquake excitation (1V).

fail-safe state of 1V, as that is the voltage designed for in this case. The results are shown in Figure 3-15.

The cases are organized in four trials, such that i) each floor failed before the peak earthquake excitation, ii) one floor before the peak, iii) one floor after, iv) and both floors failing after the peak. For the cases in which at least one device fails before the peak, the maximum values (J_1 and J_2) differ depending on which device fails first. In all cases except clipped-optimal and the case with failures at 3 and 4 seconds, it is apparent that the second floor failing first causes larger peak drifts. Once again, all failure cases result in larger RMS values. As the peak was determined to be around 3 seconds, two cases were run when the devices fail at 2 and 2.25 seconds. This returns similar results to the rest of the cases run. Comparing Figure 3-15 with Figure 3-14, it is evident that in the case of device 2 failing at 1s and device 1 failing at 4s the maximum drifts can increase over the case in which both devices fail together though accelerations remain lower than the worst case of both devices failing simultaneously to 1V. An important conclusion

which can be drawn from this graph that if one of the devices fails before the peak has passed, performance will degrade. It is therefore important that the fail-safe system be developed. The fact that drifts have the possibility to increase for a single device failure serves as further impetus to revert to the entirely passive fail-safe mode for any failure in the control system.

3.5 Summary

This chapter considered a fault tolerant analysis and design procedure for the six-story model structure. This structure was chosen for this initial study because of its relative simplicity and the ability to utilize the simulation results to identify points of focus in subsequent studies. The responses of the uncontrolled structure as well as passive and clipped-optimal control were used in evaluating the effects of failure. In addition, the effects of the time of failure changing the passive voltage level were discussed. Failures which occurred in the first three seconds of the excitation record proved the worst case response of the structure. This result is important because it lightens the computational burden of failure time investigation, as well as the design procedure in general. A fail-safe voltage was designed based on the passive responses of the structure to different constant voltage signals.

The following conclusions have been drawn from this chapter regarding the performance of the structure with device failure.

- The structure's responses were never greater than those of the uncontrolled case. This outcome is important because if the responses had surpassed the uncontrolled case, then the control system in the fail-safe mode might actually have been harming the structure instead of protecting it.
- The time of failure is important. If the failure occurs after the peak excitation has passed, then performance does not deteriorate as the largest responses have occurred in clipped-optimal mode. This can be exploited to lessen the computational burden.

- The effect of changing the passive parameters (via voltage in this case) affects the results. The passive fail-safe system should be designed for the building and damper type. In this case the best scenario occurred when the passive fail-safe voltage was set at 1.0V. This system achieves reasonable control gains, though not good enough to replace clipped-optimal control. The passive system is best used as the fail-safe backup.
- The optimal voltage found with a the strictly passive case was corroborated by time failure simulations. Both studies found that 1.0V is the best passive fail-safe voltage.
- Device failure in 1 device can cause a worse response than for all devices failing together. Any failure detected should shut the control system down completely and revert to the passive fail-safe design.
- A procedure has been developed through which failures may be dealt with. First, the optimal passive voltage is found without considering time failures. Then, the peak excitation time is located and the optimal passive voltage is verified with the worst case time failures.

Chapter 4

Numerical Model: Nine Story Irregular Building

After developing a procedure to handle failures in the control system with the simpler six story model building, this method is implemented on a more complex structure for verification. Simulating failures on a full scale building provides a more realistic insight to the effects of these failures in the real world. The full scale model considered in this chapter is a nine story plan asymmetric building which has been designed and constructed in Japan. Failures will be implemented in the same manner as in the six story model building, with a decision block in Simulink.

The numerical model will be presented in section 4.1, followed by the uncontrolled, passive, and clipped-optimal responses in section 4.2. Section 4.3 covers the effects of device failures, and section 4.4 covers the effects of considering a voltage distribution in a passive fail-safe system.

4.1 Numerical Model

This section will present the numerical model of the nine story plan irregular building which is located in Japan [44].

4.1.1 Building Plan and Device Placement

The full scale asymmetric building considered in this section is a nine-story (9-story) building measuring 34.4 m by 25.6 m in plan and 40.25 m in elevation. The main structural system of this building is constituted by steel reinforced concrete (SRC); the plan of this structure is shown in Figure 4-1. There are five bays in the x-direction and four bays in the y-direction; the important feature of this building, though, is the unequal distribution of shear walls which gives this structure an asymmetric stiffness for motion in the x-direction.

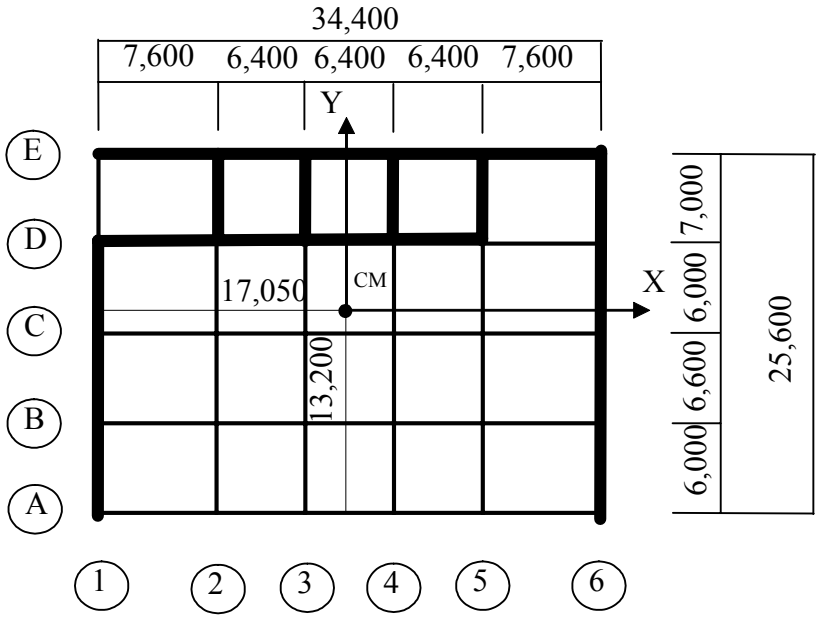

FIGURE 4-1. Plan of 9-Story asymmetric building (dimensions in mm).

Figure 4-2 depicts the device placement used in these simulations. This placement was chosen via genetic algorithm in order to obtain the optimal damping characteristics [44].

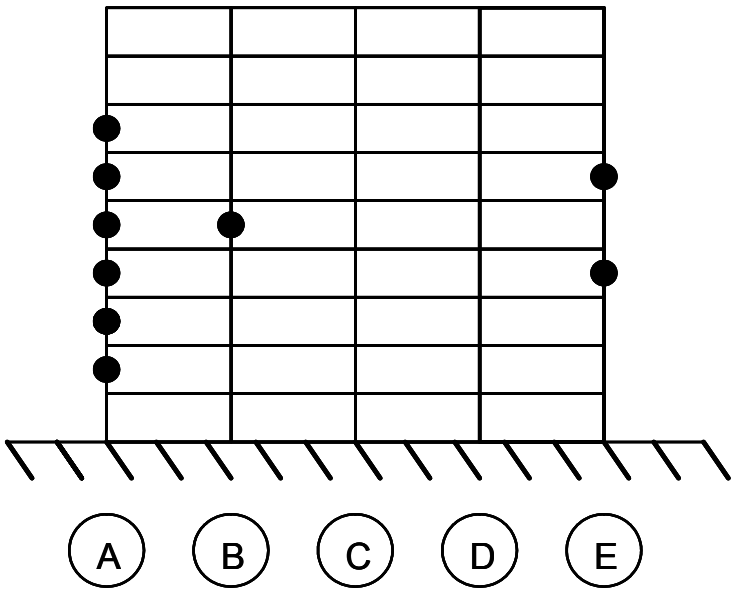

FIGURE 4-2. Device placement of MR dampers.

As with the previous six-story building discussed in Chapter 3, the measurements available for control input are the absolute accelerations of each floor, along with the forces exerted by the devices. These are fed to the clipped-optimal control algorithm developed by Yoshida [44]. This clipped-optimal algorithm is very similar to the one used in the six story model building, but the system is more complicated due to the torsional mode.

A linear, lumped-parameter model of this building has been developed [44]. In the numerical model of this 9 story irregular building, the columns and beams are considered to be reinforced concrete (RC), for which the contribution of the steel members is taken into account as equivalent steel bars. Each shear wall is divided into three RC columns. In this scheme, the center column resists moments and shear forces and the two side columns, assuming pin connections at the ends, resist only the vertical loads. A nonlinear analysis of this structure was performed by Obayashi Corporation, Technical

Research Institute [44], in which a bilinear hysteresis model is used for the RC members and the shear force-story drift diagrams for each frame are obtained via static pushover analysis. The three-dimensional model of this structure is shown in Figure 4-3. From the

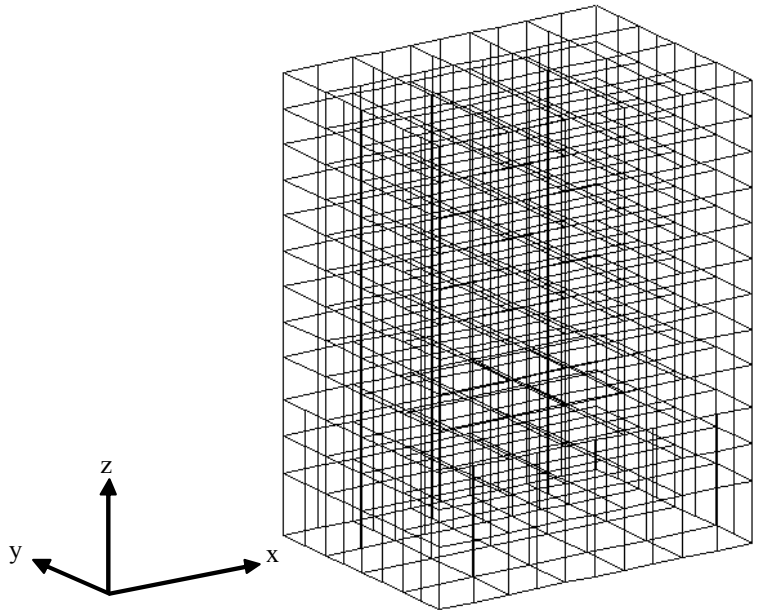

FIGURE 4-3. Three-Dimensional Model of the 9-Story Asymmetric Building.

results of that analysis, a linear stiffness coefficient of each frame is estimated assuming linearity between the origin and the yielding point. Tables 4-1 and 4-2 present the stiffness of each frame obtained using this approach along with the mass and moment of inertia of each floor. Using these values, the first and second calculated natural frequencies are 0.83 Hz (translation), and 1.29 Hz (torsion). The damping is assumed to be 2% for all modes of the structural model.

TABLE 4-1. Structural Parameters (x-direction).

Story i	Weight W_i (kN)	Inertia I_i (kNcm^2)	Radius of Gyration r_i (cm)	Initial Stiffness k_{xij} (kN/cm)				
				Frame A	B	C	D	E
				Coordinate L_y = -1320(cm)	-720	-60	540	1240
9	15556	2.50E+10	1268.1	833.3	783.8	677.0	3163	3749
8	10198	1.64E+10	1268.1	863.3	859.6	807.5	3794	5192
7	10118	1.63E+10	1268.1	901.2	802.6	750.1	3527	5428
6	10205	1.64E+10	1268.1	976.9	932.7	905.1	3530	5387
5	10295	1.66E+10	1268.1	1053	1021	984.9	3677	5521
4	10294	1.66E+10	1268.1	1208	1122	1092	3895	5866
3	10382	1.67E+10	1268.1	1208	1257	1255	4028	7425
2	10470	1.68E+10	1268.1	1485	1478	1443	4240	7655
1	10983	1.77E+10	1268.1	1852	1886	1792	4651	8128

Story i	Total Stiffness k_{xi} (kN/cm)	Torsional Stiffness $k_{\theta i}$ (kNcm/rad)	Natural Frequency Ratio $\omega_{\theta i}/\omega_{xi}$	Eccentricity e_{yi} (cm)	Eccentricity ratio e_{yi}/r_i	Eccentricity ratio e_{yi}/L
9	9206	2.65E+10	1.337	505.3	0.398	0.197
8	11516	3.07E+10	1.288	580.0	0.457	0.227
7	11408	3.25E+10	1.333	598.0	0.472	0.234
6	11731	3.32E+10	1.328	560.0	0.442	0.219
5	12257	3.48E+10	1.329	542.3	0.428	0.212
4	13182	3.83E+10	1.344	524.1	0.413	0.205
3	15172	4.35E+10	1.335	580.6	0.458	0.227
2	16301	4.63E+10	1.328	531.9	0.419	0.208
1	18309	5.34E+10	1.347	474.1	0.374	0.185

TABLE 4-2. Structural Parameters (y-direction).

Story i	Weight W_i (kN)	Inertia I_i (kNcm^2)	Radius of Gyration r_i (cm)	Initial Stiffness k_{yij} (kN/cm)					
				Frame 1	2	3	4	5	6
				Coordinate L_x = -1705 (cm)	-945	-305	335	975	1735
9	15556	2.50E+10	1268.1	2768	1308	1233	1129	905.9	2520
8	10198	1.64E+10	1268.1	2370	1327	1278	1185	1137	3408
7	10118	1.63E+10	1268.1	2554	1305	1268	1211	1097	3770
6	10205	1.64E+10	1268.1	2622	1313	1281	1242	1157	3859
5	10295	1.66E+10	1268.1	2784	1358	1337	1296	1230	4036
4	10294	1.66E+10	1268.1	3127	1444	1420	1390	1332	4481
3	10382	1.67E+10	1268.1	3428	1650	1631	1604	1539	4949
2	10470	1.68E+10	1268.1	3662	1857	1799	1773	1716	5179
1	10983	1.77E+10	1268.1	4899	2107	2071	2404	2324	5495

Story i	Total Stiffness k_{yi} (kN/cm)	Torsional Stiffness $k_{\theta i}$ (kNcm/rad)	Natural Frequency Ratio $\omega_{\theta i}/\omega_{yi}$	Eccentricity e_{xi} (cm)	Eccentricity ratio e_{xi}/r_i	Eccentricity ratio e_{xi}/L
9	9863	2.65E+10	1.291	-70.73	-0.056	-0.0206
8	10706	3.07E+10	1.336	161.9	0.128	0.0471
7	11205	3.25E+10	1.345	182.2	0.144	0.0530
6	11473	3.32E+10	1.343	186.2	0.147	0.0541
5	12041	3.48E+10	1.341	182.6	0.144	0.0531
4	13193	3.83E+10	1.343	182.6	0.144	0.0531
3	14801	4.35E+10	1.352	184.0	0.145	0.0535
2	15985	4.63E+10	1.341	169.3	0.134	0.0492
1	19299	5.34E+10	1.312	84.41	0.067	0.0245

4.1.2 Equations of Motion

In general, the equation of motion for an *n*-story, asymmetric building is written

$$\mathbf{M}_s\ddot{\mathbf{x}} + \mathbf{C}_s\dot{\mathbf{x}} + \mathbf{K}_s\mathbf{x} = -\mathbf{M}_s\Gamma\ddot{X}_g + \Lambda\mathbf{f} \tag{4-1}$$

where $\mathbf{x} = \begin{bmatrix} X\ Y\ \Theta \end{bmatrix}^T$. The terms $X = \begin{bmatrix} x_1 \ \ldots \ x_n \end{bmatrix}$ and $Y = \begin{bmatrix} y_1 \ \ldots \ y_n \end{bmatrix}$ are row vectors of the relative displacements of the center of mass of each floor in the x- and y-directions, respectively, and $\Theta = \begin{bmatrix} \theta_1 \ \ldots \ \theta_n \end{bmatrix}$ is the vector of the rotations of each floor about the vertical axis. The disturbance, $\ddot{X}_g = \begin{bmatrix} \ddot{x}_g\ \ddot{y}_g \end{bmatrix}^T$, is a vector of the ground accelerations, and the coefficient matrix is

$$\Gamma = \begin{bmatrix} -1_{n\times 1} & 0_{n\times 1} \\ 0_n & -1_{n\times 1} \\ 0_{n\times 1} & 0_{n\times 1} \end{bmatrix}. \tag{4-2}$$

Also, $\mathbf{f}$ is the vector of control forces, where its coefficient matrix, Λ, is the matrix determined due to the location of control devices.

The mass matrix takes the form

$$\mathbf{M}_s = \begin{bmatrix} \mathbf{M} & 0 & \mathbf{M}_{x\theta} \\ 0 & \mathbf{M} & \mathbf{M}_{y\theta} \\ \mathbf{M}_{x\theta} & \mathbf{M}_{y\theta} & I \end{bmatrix}, \tag{4-3}$$

where $\mathbf{M} = diag\left(\begin{bmatrix} m_1 \ \ldots \ m_n \end{bmatrix}\right)$ is the diagonal $n \times n$ matrix of the masses of each floor, and

$$I = diag\left(\left[I_1 + m_1(L_{CMx1}^2 + L_{CMy1}^2) \ \ldots \ I_n + m_n(L_{CMxn}^2 + L_{CMyn}^2)\right]\right), \tag{4-4}$$

where I_i is the moment of inertia of the *i*th floor, and (L_{CMxi}, L_{CMyi}) are the coordinates of the center of the mass of *i*th floor. The coupling terms in the mass matrix are given by

$$\mathbf{M}_{x\theta} = diag\left(\left[-m_1 L_{CMy1} \ \ldots \ -m_n L_{CMyn}\right]\right), \tag{4-5}$$

$$\mathbf{M}_{y\theta} = diag\left(\left[m_1 L_{CMx1} \ \ldots \ m_n L_{CMxn}\right]\right). \tag{4-6}$$

The stiffness matrix takes the form

$$\mathbf{K}_s = \begin{bmatrix} \mathbf{K}_x & 0 & \mathbf{K}_{x\theta} \\ 0 & \mathbf{K}_y & \mathbf{K}_{y\theta} \\ \mathbf{K}_{x\theta} & \mathbf{K}_{y\theta} & \mathbf{K}_{\theta} \end{bmatrix}, \tag{4-7}$$

where

$$\mathbf{K}_x = \begin{bmatrix} k_{x1} + k_{x2} & -k_{x2} & 0 & 0 \\ -k_{x2} & \ldots & \ldots & 0 \\ 0 & \ldots & \ldots & -k_{xn} \\ 0 & 0 & -k_{xn} & k_{xn} \end{bmatrix}, \tag{4-8}$$

$$\mathbf{K}_y = \begin{bmatrix} k_{y1}+k_{y2} & -k_{y2} & 0 & 0 \\ -k_{y2} & \cdots & \cdots & 0 \\ 0 & \cdots & \cdots & -k_{yn} \\ 0 & 0 & -k_{yn} & k_{yn} \end{bmatrix}, \tag{4-9}$$

and

$$\mathbf{K}_\theta = \begin{bmatrix} k_{\theta 1}+k_{\theta 2} & -k_{\theta 2} & 0 & 0 \\ -k_{\theta 2} & \cdots & \cdots & 0 \\ 0 & \cdots & \cdots & -k_{\theta n} \\ 0 & 0 & -k_{\theta n} & k_{\theta n} \end{bmatrix}. \tag{4-10}$$

Here k_{xi}, k_{yi}, and $k_{\theta i}$ correspond to the stiffnesses of the *i*th floor in the x-, y-, and θ-directions, respectively. The coupling terms in the stiffness matrices are written

$$\mathbf{K}_{x\theta} = \begin{bmatrix} k_{x\theta 1}+k_{x\theta 2} & -k_{x\theta 2} & 0 & 0 \\ -k_{x\theta 2} & \cdots & \cdots & 0 \\ 0 & \cdots & \cdots & -k_{x\theta n} \\ 0 & 0 & -k_{x\theta n} & k_{x\theta n} \end{bmatrix} \tag{4-11}$$

and

$$\mathbf{K}_{y\theta} = \begin{bmatrix} k_{y\theta 1}+k_{y\theta 2} & -k_{y\theta 2} & 0 & 0 \\ -k_{y\theta 2} & \cdots & \cdots & 0 \\ 0 & \cdots & \cdots & -k_{y\theta n} \\ 0 & 0 & -k_{y\theta n} & k_{y\theta n} \end{bmatrix} \tag{4-12}$$

where $k_{x\theta i} = -k_{xi}L_{yi}$, $k_{y\theta i} = k_{yi}L_{xi}$, where (L_{xi} , L_{yi}) are the coordinates of the center of rigidity in the *i*th floor [44].

4.2 Uncontrolled, Passive and Clipped-optimal Responses

The clipped-optimal controller used in these simulations was developed by Yoshida [44]. As with the simulations for the six story model, the uncontrolled responses of the structure are obtained for a reference of the efficacy of the control scheme applied. Passive-off and passive-on cases are also simulated to obtain the range of responses in a passive state; the clipped-optimal control is simulated as the nominal case, the case with best performance.

It should be noted that, in this model, the evaluation criteria are slightly different. Because the structure has a weak side and a strong side, performance of the control system should consider both sides. The effects of failures may become more pronounced in the case of torsion. The evaluation criteria in this section look at the weak side and strong side separately as follows:

$$J_{1w} = \frac{max_{t,i}(d_{iw})}{\mathrm{d}_u}, J_{1s} = \frac{max_{t,i}(d_{is})}{\mathrm{d}_u} \tag{4-13}$$

$$J_{2w} = \frac{max_{t,i}(a_{iw})}{\mathrm{a}_u}, J_{2s} = \frac{max_{t,i}(a_{is})}{\mathrm{a}_u} \tag{4-14}$$

$$J_{3w} = \frac{max_i\|d_{iw}\|}{\|d_u\|}, J_{3s} = \frac{max_i\|d_{is}\|}{\|d_u\|} \tag{4-15}$$

$$J_{4w} = \frac{max_i\|a_{iw}\|}{\|a_u\|}, J_{4s} = \frac{max_i\|a_{is}\|}{\|a_u\|} \tag{4-16}$$

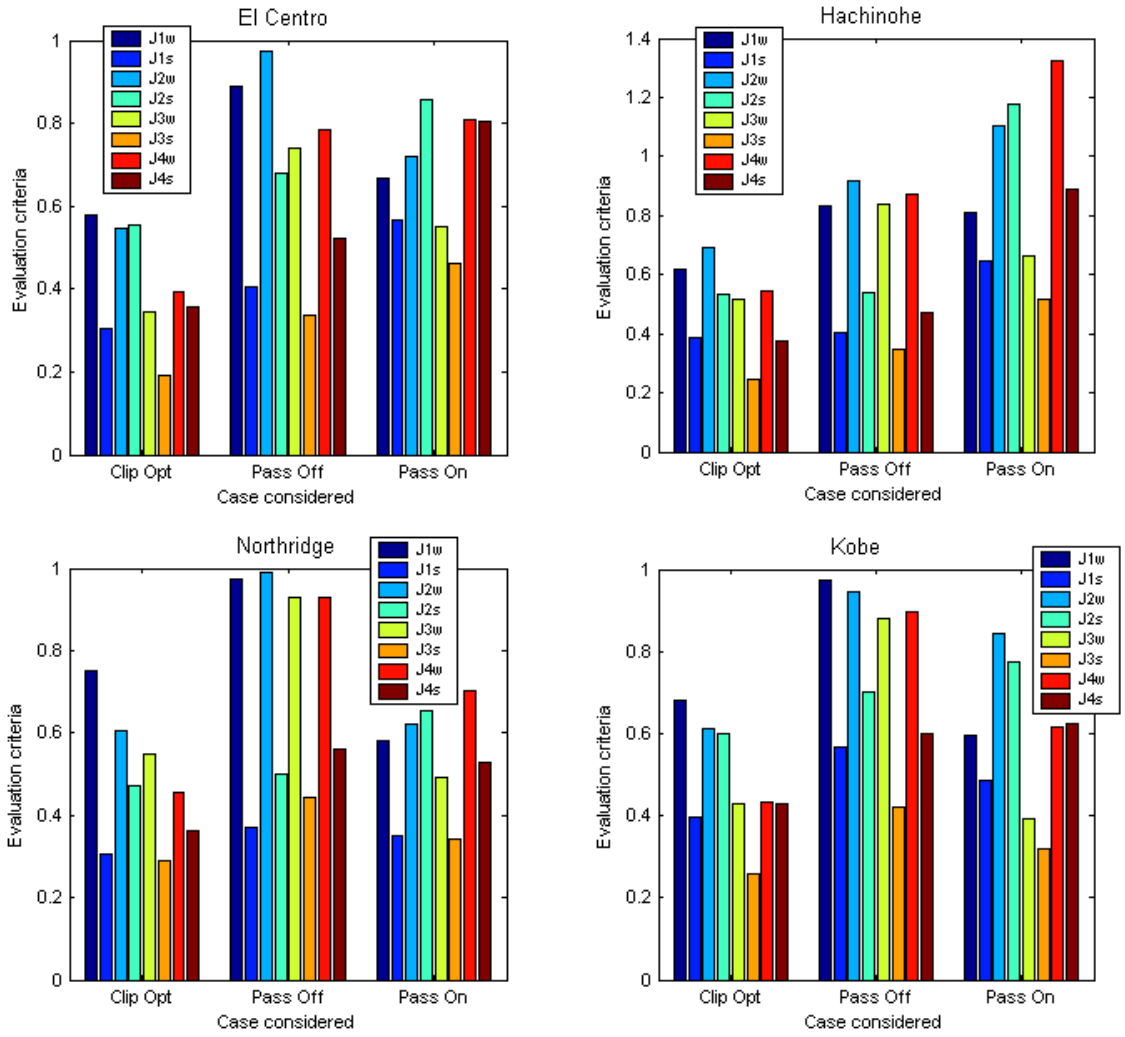

FIGURE 4-4. Evaluation criteria for the four considered earthquakes in the clipped-optimal, passive-off, passive-on, and passive-on cases.

where the subscripts $(\,)_w$ and $(\,)_s$ indicate weak and strong side, respectively. The values d_u and a_u represent the maximum values of the interstory drifts d_u and the accelerations a_u. All maximum values are taken over the entire excitation period and all floors for each side, weak and strong. Also note that the denominator in each pair is the same. The strong and weak response in the case considered are each compared to the worst response over all time and floors in the uncontrolled structure. This approach will help

to identify how effective the control system under consideration is in mitigating the torsional effects created by plan asymmetry.

Simulation results for the four different earthquakes are presented in Figure 4-4. Notice that the weak side drifts are consistently the worst. This is the effect of the asymmetric lateral load resistance in the structure. The goal of the passive fail-safe system should be to limit the responses of the weak side while not degrading those of the strong side. Looking at the results, it is apparent that the weak side generally performs better in the passive-on, clipped-optimal case. The function voltage plays in the response of the passive system will be explored later in this chapter.

4.3 Effects of Device Failure

As shown in the previous section, the passive systems are much less effective in mitigating the effects of the seismic excitations than the clipped-optimal controller is. It is worthwhile to look more closely at the effects of when the devices fail, and the voltage values to which they are set to in the fail-safe system.

4.3.1 Effects of failure time

As in the six story model, the effect of the time at which a device fails must be considered. This departs slightly from the procedure set out in chapter 3 because a failure time simulation is done before the voltage dependence is investigated. This is due to the complexity of the full scale structure and the greater possibility for only some devices to fail. The worst case scenario must be found in regards to which devices fail. The time of failure may be a critical factor when searching for a worst-case scenario. A device failure while the building is in motion could possibly cause conditions worse than the uncontrolled case. The most likely cause of device failure is loss of power. Therefore, simulations are run in which the devices are switched to the passive-off value after the designated failure time. Four failure cases are considered: all devices fail, weak side

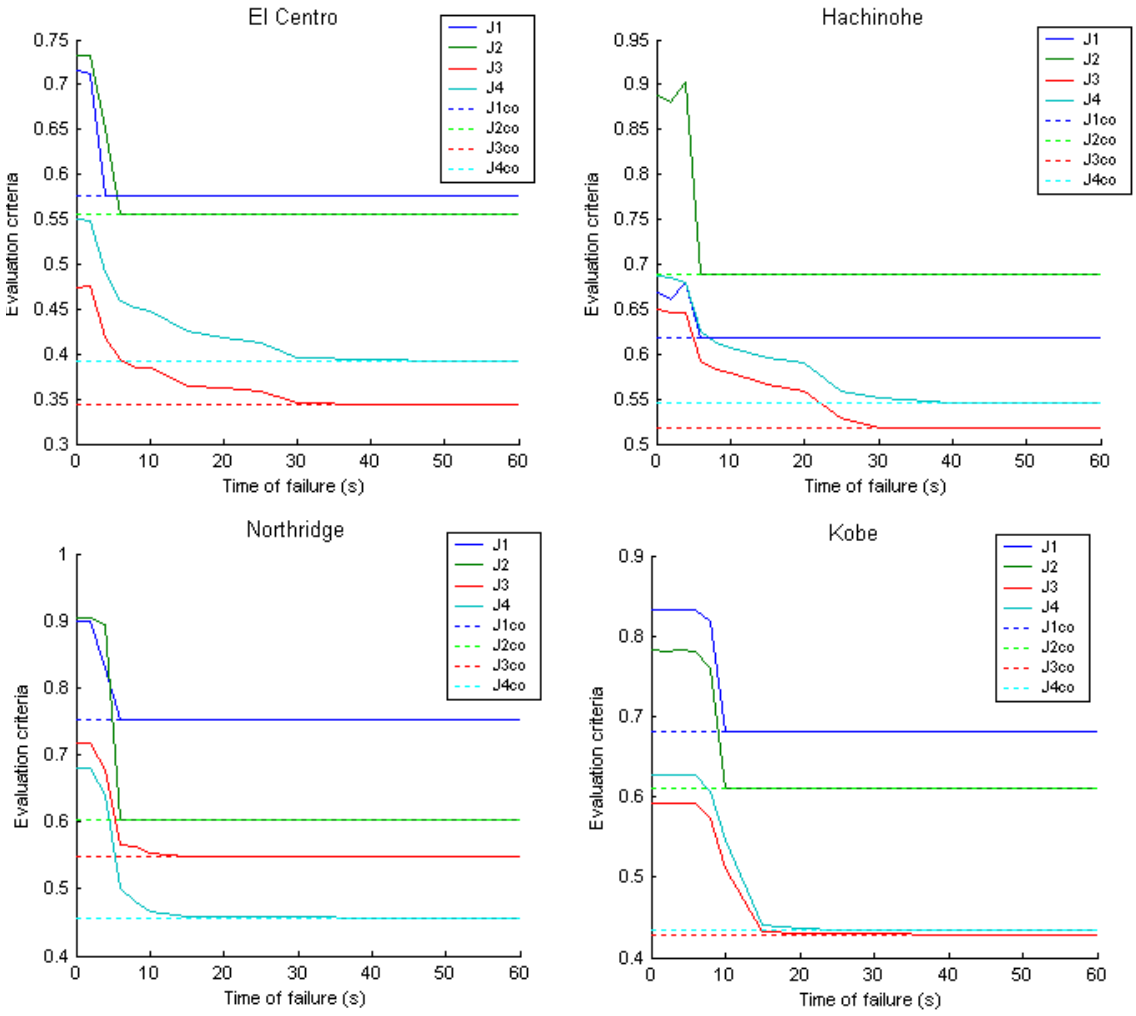

FIGURE 4-5. Evaluation criteria for the four considered earthquakes subjected to different failure times throughout the simulation (dashed lines are clipped-optimal values).

devices fail, strong side devices fail, and devices on floors two and three fail. Figure 4-5 shows the response of the structure to all considered earthquakes for failure times up to 60 seconds. It is shown that the latest time value which causes the peak performance to degrade is below 10 seconds in all cases.

The first case involves all devices failing to the passive-off case. Figure 4-6 presents the results of simulated failures in all devices at times between 1 and 16 seconds in intervals of 1sec. The choice of 16 seconds as the maximum failure time is based upon the

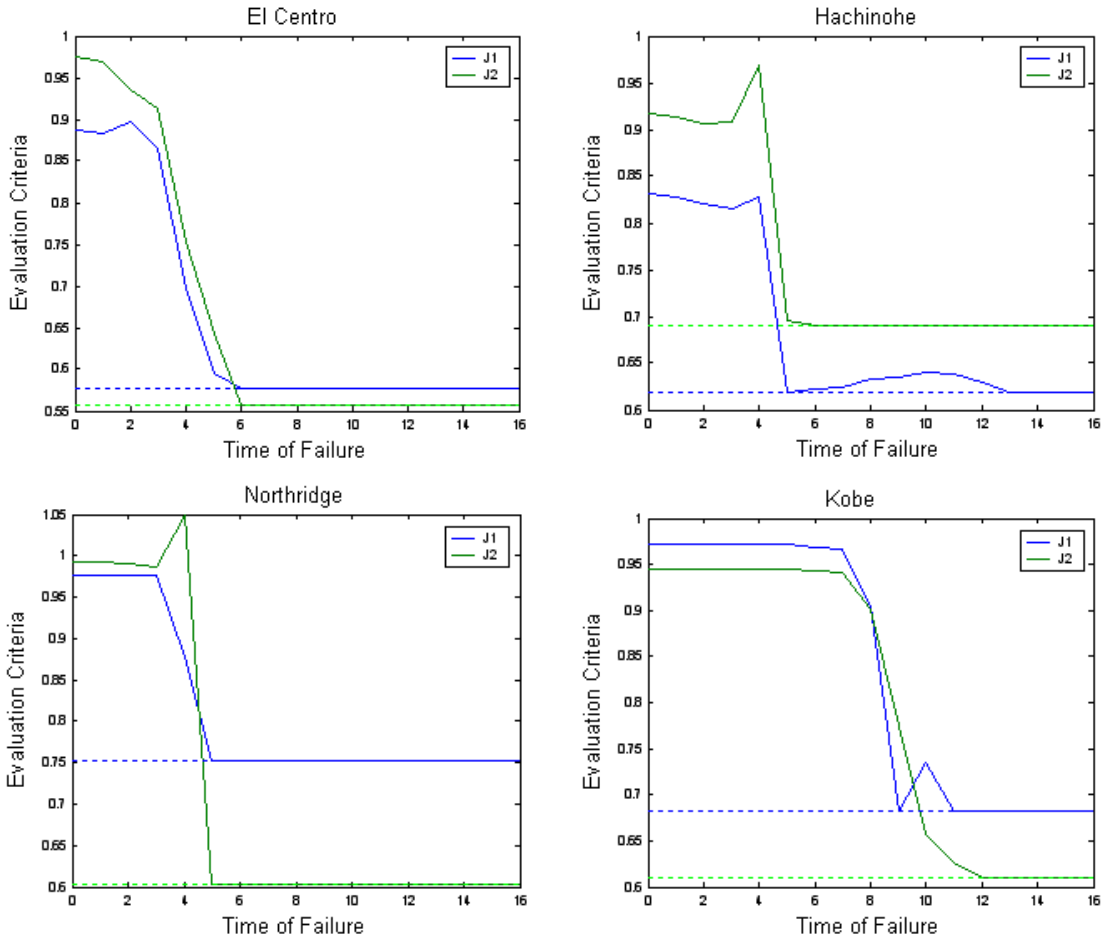

FIGURE 4-6. Time failure results for all devices failing at the specified time of failure, dashed lines are clipped-optimal values.

information presented in Figure 4-5. This choice is corroborated by the trends shown in Figures 4-6 through 4-9. Because the goal of this section is to determine the worst case scenario, only the peak drifts and peak accelerations are being considered as these are the leading indicators of damage. In general, both drift and acceleration in the presence of a failure in the control system increase substantially. Only in one case does an evaluation criteria exceed 1.0, indicating a performance worse than uncontrolled, and that is a peak acceleration in the Northridge earthquake for a failure time of 4s. Looking at the J_2 criteria in particular, it is apparent that the accelerations of the building are more susceptible to bad performance with respect to the time of failure of the device in all cases. Drifts, indicated by J_1, never cross the 1.0 barrier, meaning that the most critical

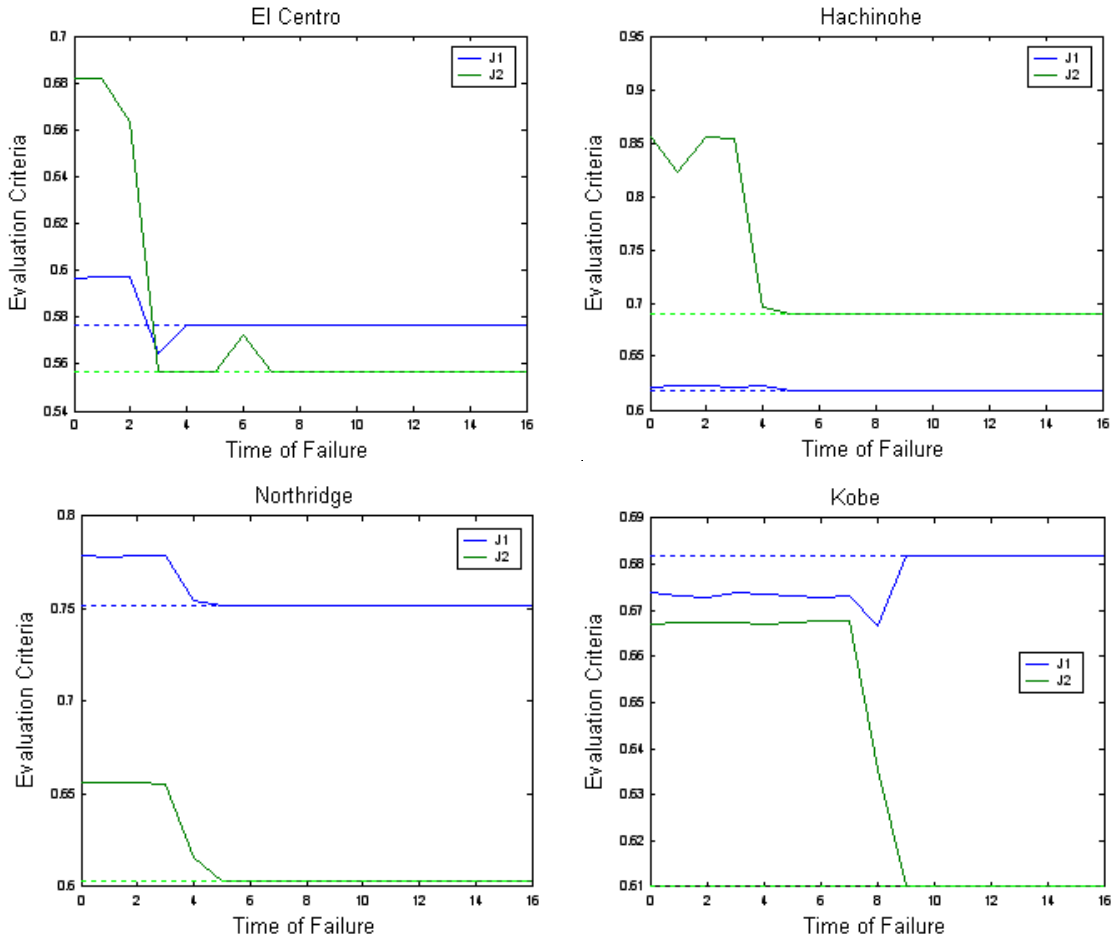

FIGURE 4-7. Time failure results for devices on the strong side of the structure failing at the specified time of failure, dashed lines are clipped-optimal values.

indication of possible structural damage remains below the uncontrolled case, meaning that the building will remain in better condition than if uncontrolled. To better determine what the worst case scenario might be, more failure situations are considered.

The first additional scenario considered involves only the devices on the strong side of the building failing. When the devices on the strong side of the structure fail it is apparent that the peak accelerations are increased dramatically, yet the peak drifts can actually be decreased below clipped-optimal as seen in the Kobe simulation. Additionally, no criteria exceed the 1.0 threshold, hence device failure in the strong side of the building does

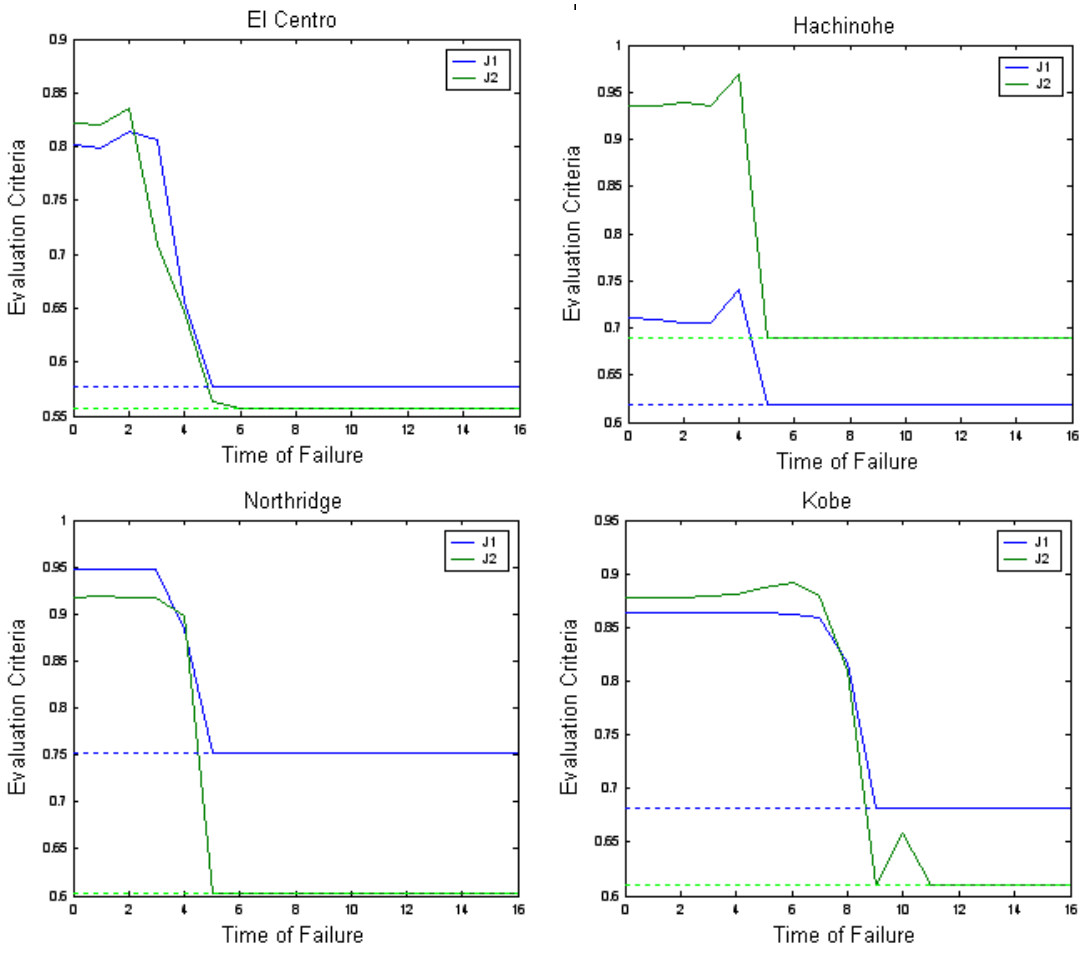

FIGURE 4-8. Time failure results for devices on the weak side of the structure failing at the specified time of failure, dashed lines are clipped-optimal values.

not degrade performance to a state worse than uncontrolled. The results for this scenario are presented in Figure 4-7 The next case considered is not considerably different in outcome than the case in which all devices fail. When devices on the weak side of the asymmetric building fail, both peak drift and peak acceleration increase. In this case, though, no evaluation criteria exceeds 1.0, and the controlled situation remains better than the uncontrolled case in the presence of device failure. Figure 4-8 depicts the results for this case with devices on the weak side of the structure experiencing failure to the passive-off mode.

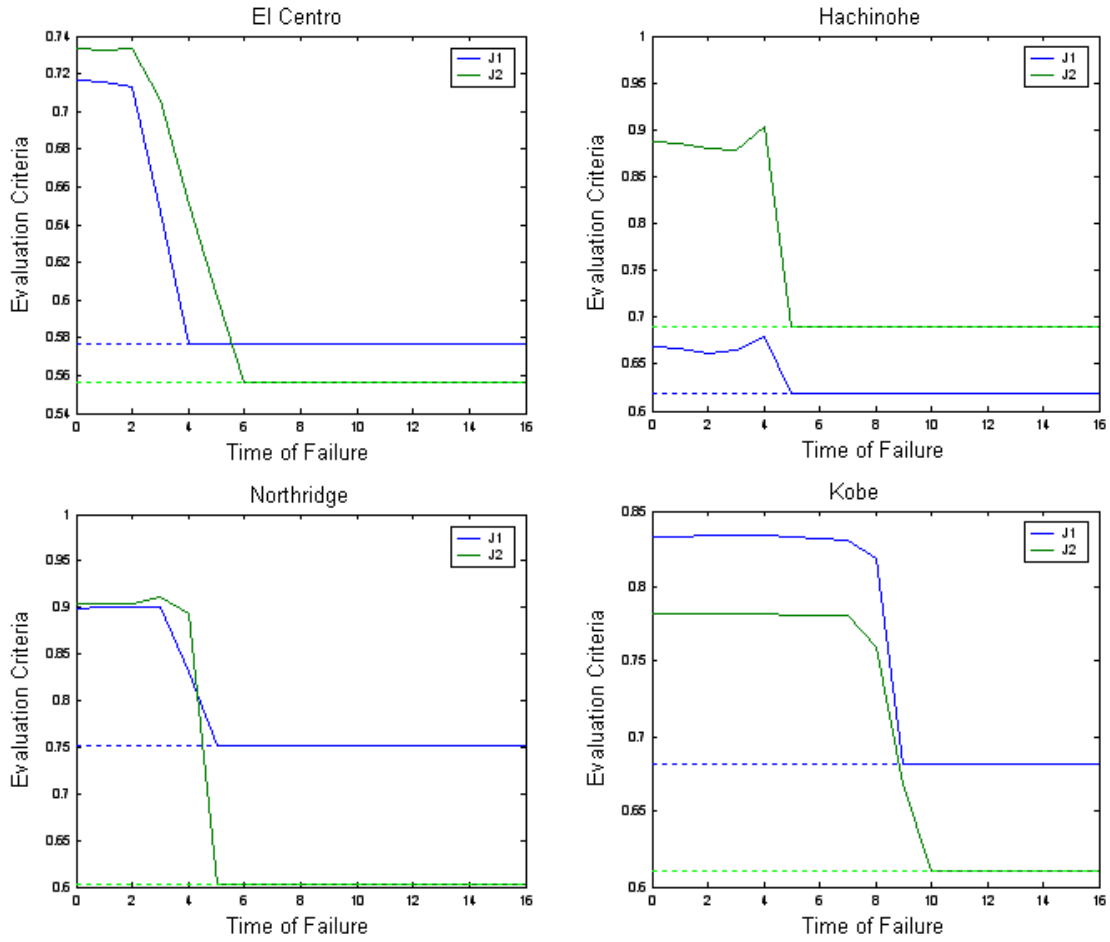

FIGURE 4-9. Time failure results for devices on floors two and three failing at the specified time of failure, dashed lines are clipped-optimal values.

One last case is considered in which the devices on floors two and three, the bottom two devices, are considered to fail at the specified time. The results procured from this simulation indicate similar responses to the weak side and all devices failing, as peak drifts are high as well as peak accelerations. Results for this simulation are found in Figure 4-9. Comparing all of the failure scenarios over all of the failure times and earthquake excitation simulations, it is apparent that failure of all devices induces the least favorable responses. Figure 4-10 shows the bar graph of the worst case evaluation criteria J_1 and J_2 for each failure case in each earthquake. Numerical values of these worst case scenarios

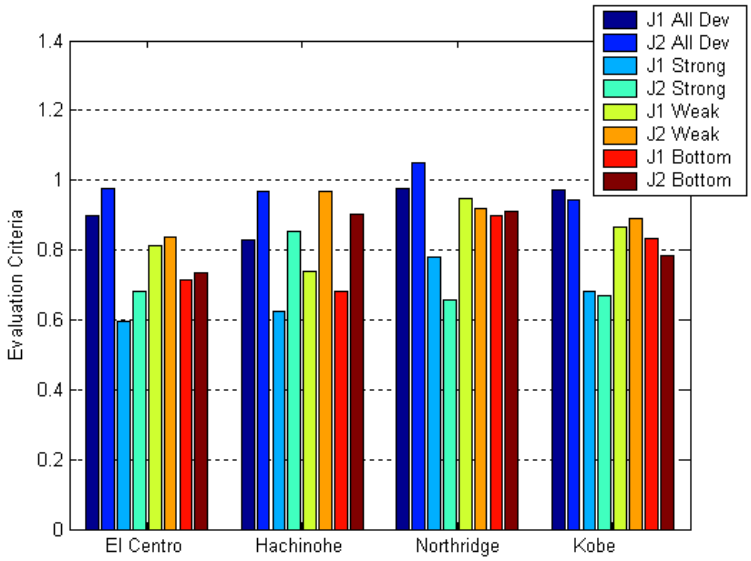

FIGURE 4-10. The worst case scenarios for all earthquakes, failure times, and failure patterns.

TABLE 4-3. The worst case scenario evaluation criteria for all earthquakes, failure times, and failure patterns.

		El Centro	Hachinohe	Northridge	Kobe
All Devices	J1	**0.8975**	**0.8305**	**0.977**	**0.9719**
	J2	**0.9753**	0.968	**1.0492**	**0.9445**
Strong Side Failure	J1	0.5976	0.6226	0.7789	0.6818
	J2	0.6821	0.8555	0.6561	0.6678
Weak Side Failure	J1	0.8134	0.7409	0.9482	0.8642
	J2	0.8357	**0.9693**	0.9184	0.891
Bottom 2 Devices	J1	0.7162	0.68	0.9001	0.8334
	J2	0.7331	0.9027	0.9104	0.7819

are found in Table 4-3. All but one of the maximum evaluation criteria are found in the case for which all devices fail. The one maximum criteria that does not fall in this category was the maximum acceleration for the Hachinohe earthquake, but it is only a maximum by 0.0013. It is reasonable to conclude that the worst case scenario is failure of all devices to passive-off.

TABLE 4-4. Failure times for the worst case drift (top row) and worst case acceleration (bottom row)

	El Centro	Hachinohe	Northridge	Kobe
Failure Time	0 2	0 4	3 4	0 6

The times at which the worst case failures occur depend on the earthquake. Considering the graphs of Figure 4-6, the failure times for El Centro should be 0s and 2 sec, for Hachinohe 0s and 4s, for Northridge, 3 sec and 4 sec, and for Kobe 0 sec and 6 sec. These values are presented in Table 4-4. From this point, it is necessary to find a voltage for which the performance is optimized for all devices failing to a passive fail-safe value.

4.3.2 Voltage Dependence of the Simulation Results

The voltage applied to the MR damper, as in the last chapter, affects the results of the simulation. In this instance, however, two patterns appear. Because we are considering four different earthquakes, two of small maximum acceleration magnitude and two of large acceleration magnitude, the results of changing the voltage depend upon the type of earthquake considered. Graphs depicting the worst of the two sides (strong and weak) in performance criteria evidence these patterns. For the earthquake excitations with the smaller maximum ground acceleration, the criteria appear in a pattern which dips in a voltage of 2V to 3V, whereas the large maximum ground acceleration excitations result in evaluation criteria that generally decrease with increasing voltage. These patterns are shown in Figure 4-11. From the El Centro and Hachinohe earthquake excitations, one would conclude that the best passive voltage is somewhere between 2 and 3 Volts. Looking at the Northridge and Kobe earthquake excitations, it appears that the maximum drifts drop considerably as the passive voltage increases, and the best performance

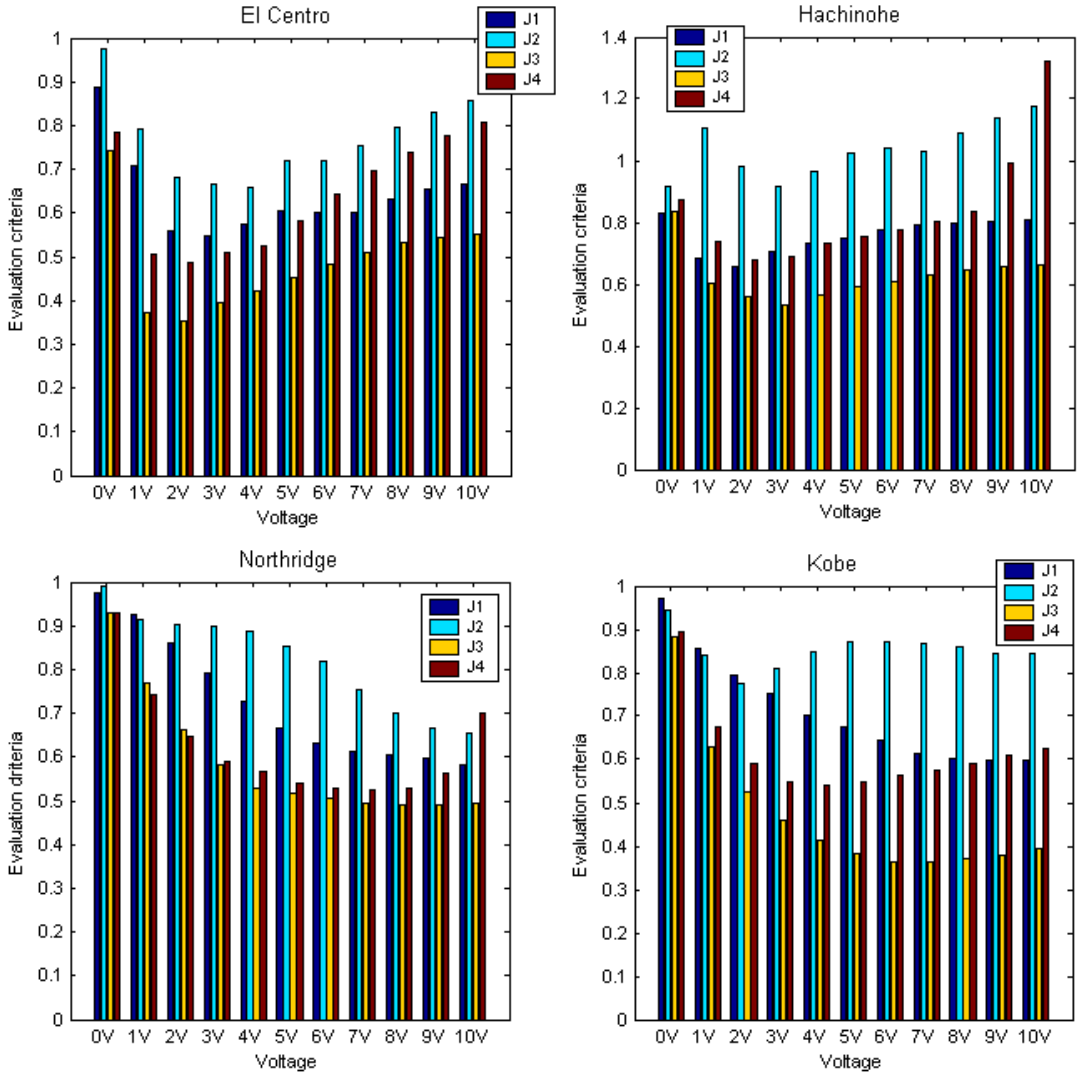

FIGURE 4-11. Evaluation criteria for the four earthquakes considered with various passive voltage levels (failure at 0 sec).

could be achieved by using 9V or even 10V as the passive voltage level. These results are quite different, which leads to the conclusion that the seismic properties at the construction site must be considered when designing the passive fail-safe level. A building which is to be constructed in an area of high seismicity with a significant possibility of large accelerations should be designed with a high passive fail-safe voltage. A building to be constructed in an area with a likelihood of more moderate accelerations should

consider a lower passive fail-safe voltage. Design considerations of this nature will be discussed in chapter 5.

4.3.3 Verification of Optimal Voltage

As discussed in the previous section, the time of failure can impact the response of the structure during a seismic excitation. Looking at the graphs for the passive-off failure case, the failure times for the largest peak drift and largest peak acceleration are recorded in Table 4-4. These values are used to verify that the voltages found in the strictly passive case are still optimal at these worst-case failure times. To do this, a range of voltages near the optimal voltage found in the passive case are selected and run at 0.25V intervals. For the El Centro and Hachinohe earthquake records, the voltage range is from 1 to 4 V, while values for the Northridge and Kobe records range from 6 to 10 V.

First, the values for the El Centro excitation record are presented in Figure 4-12. For both the 0 sec and 2 sec time failure cases, the best voltage remains around 2.25 V. The trend for the drifts shows a local minima at 2.75V for the 0V case and at 2.5V for the 2 sec case. The accelerations in that vicinity are level in the 0 sec case, and at a minimum at 2.25V for the 2 sec case. A voltage of 2.5V returns the best overall evaluation criteria between the two worst case scenarios, and should therefore be chosen as the design voltage.

For the Hachinohe earthquake, the drift trend in the 0 sec case shows a minimum at 2.25V, as shown in Figure 4-13. In the 4 sec failure case, the drifts are level up until the 3V level, and then decrease as the voltage moves towards 4V. The accelerations, however, are very high in this 4 sec failure case and the minimum is at 2V. This value is only slightly over 1.0, while as the voltage increases past 2V the J_2 value climbs towards 1.5. In the end, taking 2V is the most reasonable choice for this earthquake as it has the lowest drifts in the 0 sec case, and in the 4 sec case it returns the best acceleration.

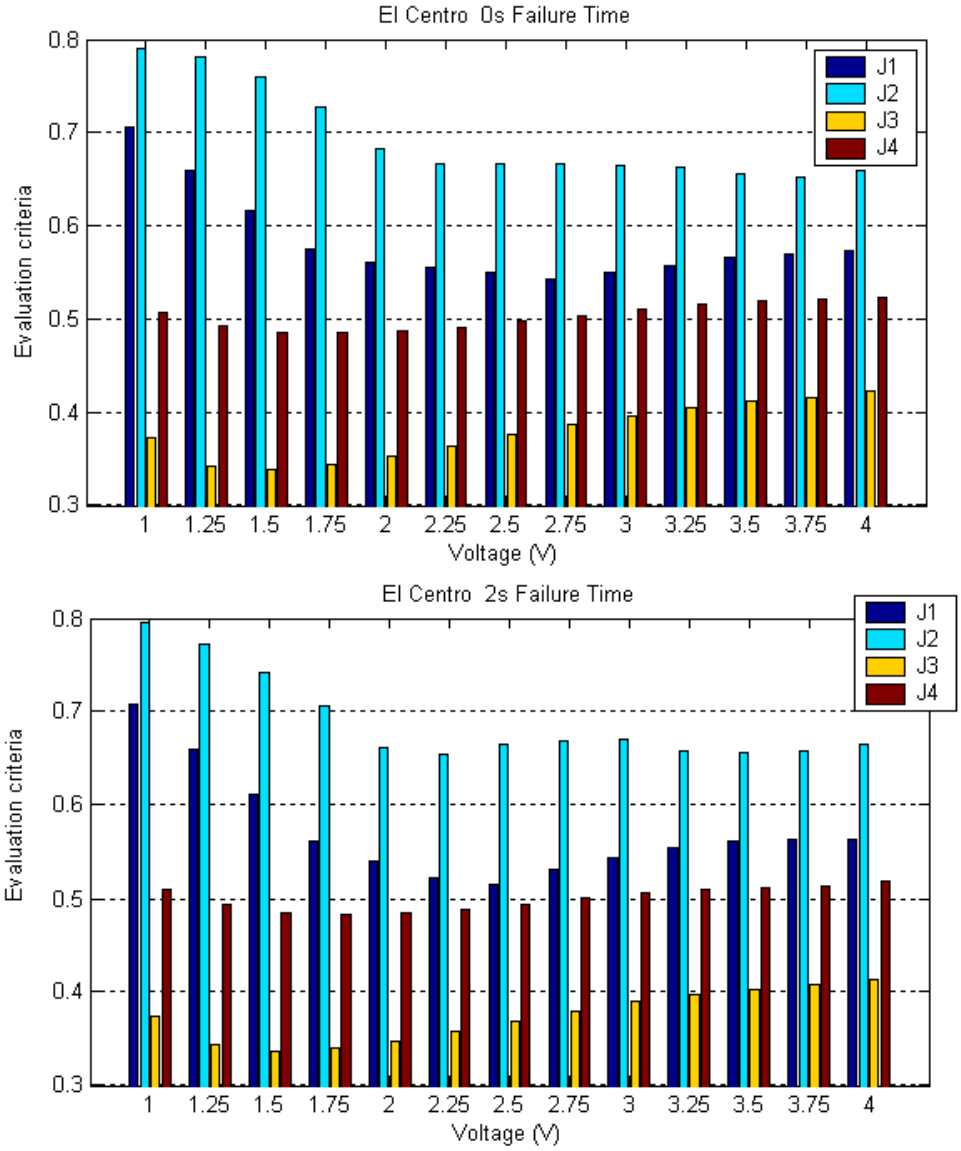

FIGURE 4-12. Evaluation criteria for the worst case time failures (0 sec and 2 sec) for the El Centro excitation at a voltage range near the optimal

In the Northridge simulation, the results of which are shown in Figure 4-14, evaluation criteria J4 in both the 3 sec and 4 sec failure cases show the trend to be the same as in the passive simulations. A downward trend in the peak acceleration values is prominent as the voltage approaches 10V in the 3 sec time failure case, and less pronounced but still visible in the 4 sec failure case. Peak accelerations are highest at the 6V level, but drop as the voltage increases and then begin to level out near 9V. Even though the RMS

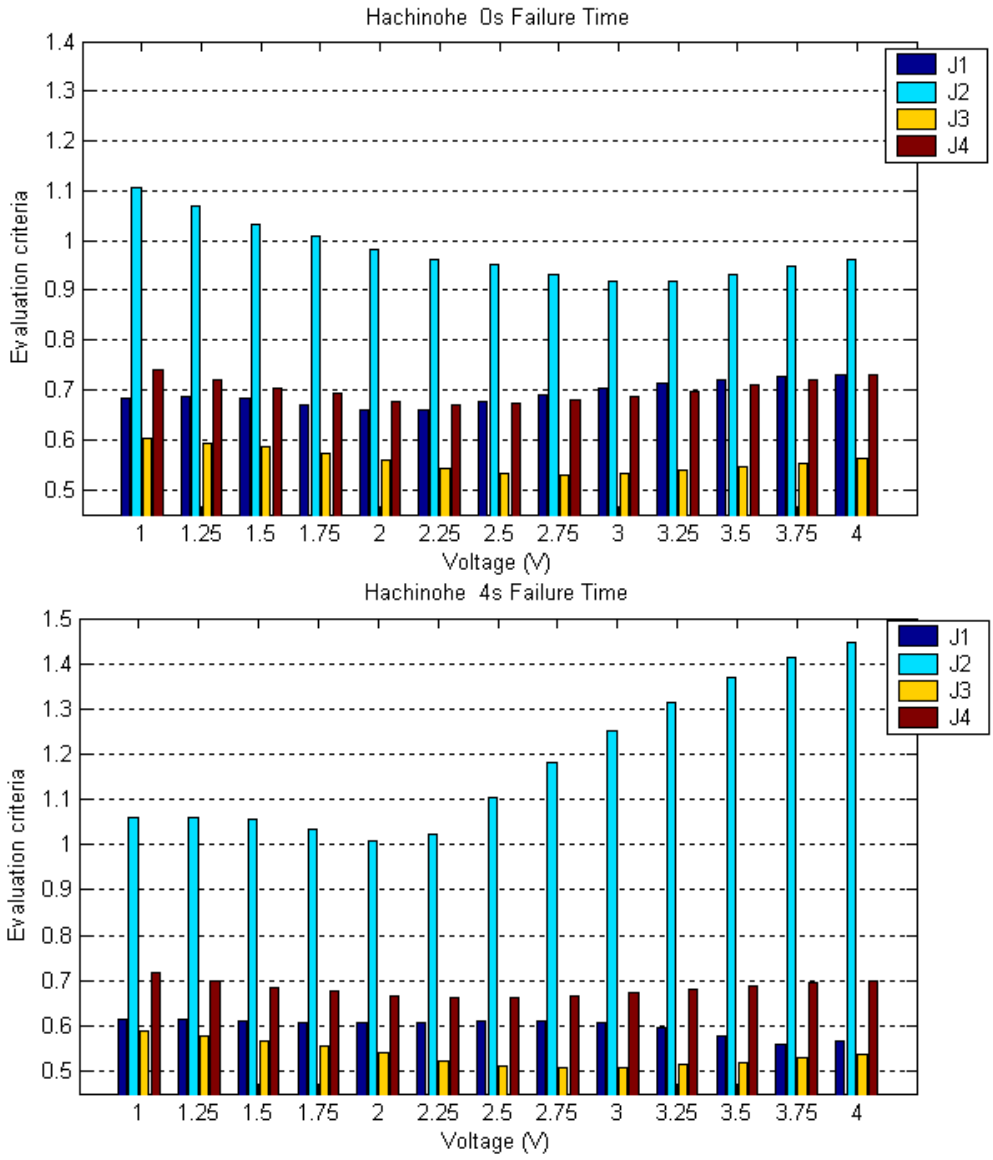

FIGURE 4-13. Evaluation criteria for the worst case time failures (0 sec and 4 sec) for the Hachinohe excitation at a voltage range near the optimal

accelerations increase as the voltage climbs past 9V, the peak drifts and accelerations continue to drop up to the maximum 10V. This voltage, then, should be the design voltage as the RMS accelerations in both cases remain under 1.0 and are the least important consideration for structural damage. Low peak interstory drifts and peak accelerations are the design criteria in this case.

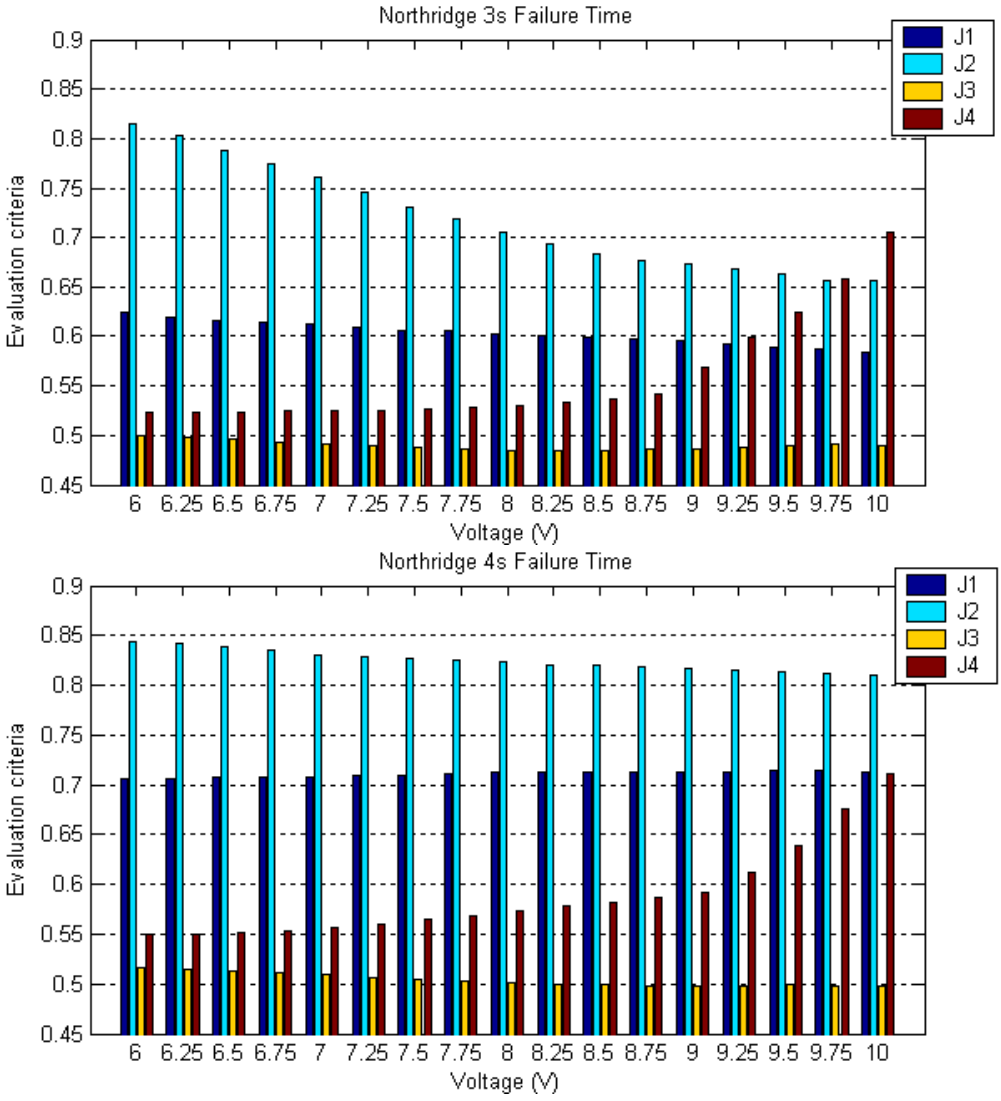

FIGURE 4-14. Evaluation criteria for the worst case time failures (0 sec and 6 sec) for the Northridge excitation at a voltage range near the optimal

For the Kobe responses, the results are nearly identical for the 0 sec and 6 sec failure times. These results are shown in Figure 4-15. The drifts drop as the voltage increases, more dramatically as it increases from 6V to 7V, but they do continue do decrease with increasing voltage until leveling out after passing 9V. The accelerations, though not as

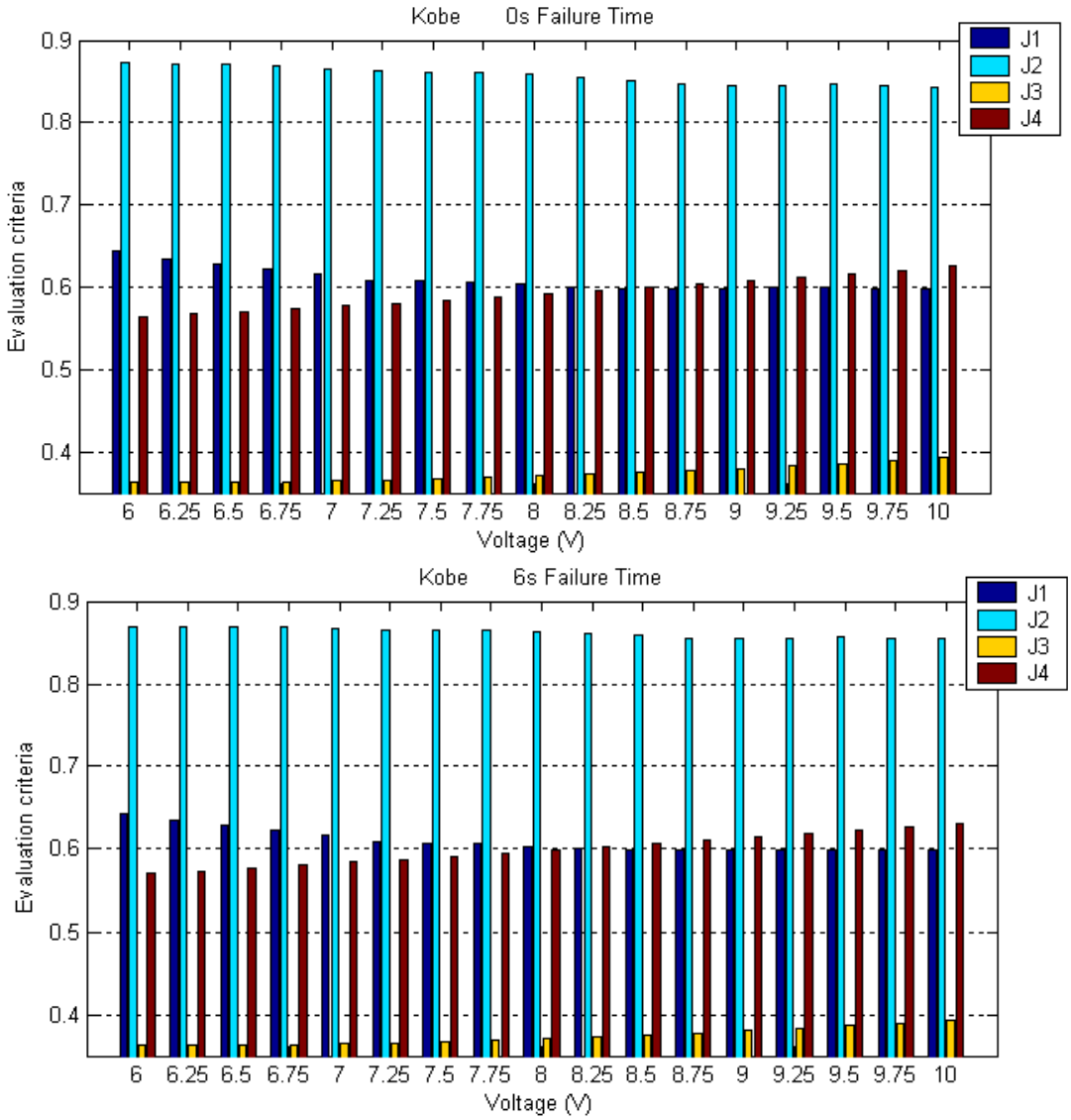

FIGURE 4-15. Evaluation criteria for the worst case time failures (0 sec and 6 sec) for the Kobe excitation at a voltage range near the optimal passive value.

pronounced, also decrease as the voltage increases from 6V to 9V where they level out. The difference between the maximum and minimum peak acceleration is small though, and the difference between the peak acceleration value at 9V and 10V is negligible. As in the Northridge case, the RMS value for acceleration grows with increasing voltage, but the difference is less noticeable, and the RMS value for drift also increases. Unlike the Northridge case though, the peak drift an acceleration level out after the 9V level,

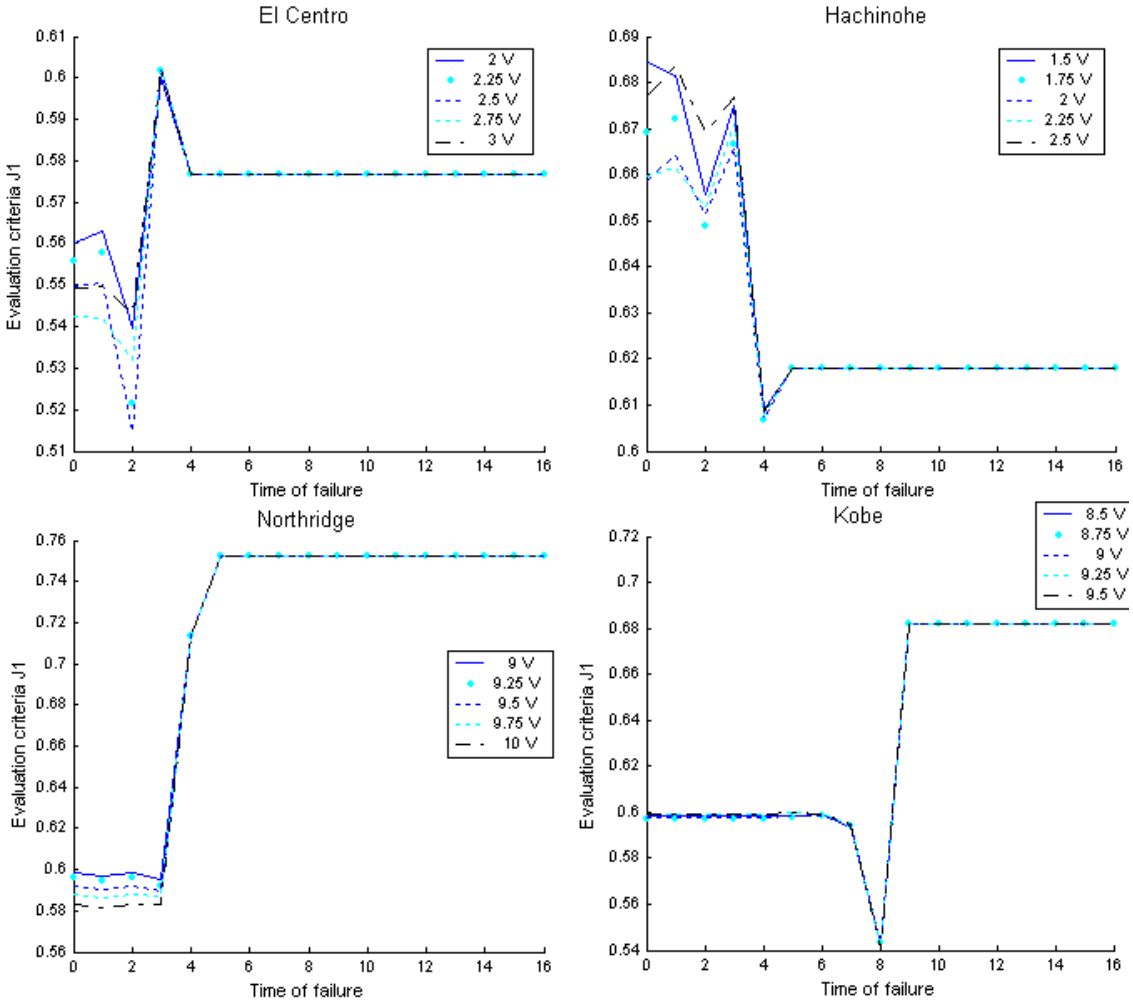

FIGURE 4-16. Evaluation criteria J_1 for the optimal passive voltage range for each earthquake versus failure time.

and it is reasonable to account for evaluation criteria J_3 and J_4. This leads to choosing 9V as the design voltage for the Kobe earthquake ground excitation.

To verify that the voltages chosen will perform adequately, voltages ranging 0.5V above and below the optimal voltage by earthquake are applied to the structure and the sequence of failure time simulations is run for each earthquake. In each of these cases, the design voltage returns the best peak drift performance, or the difference is negligible.

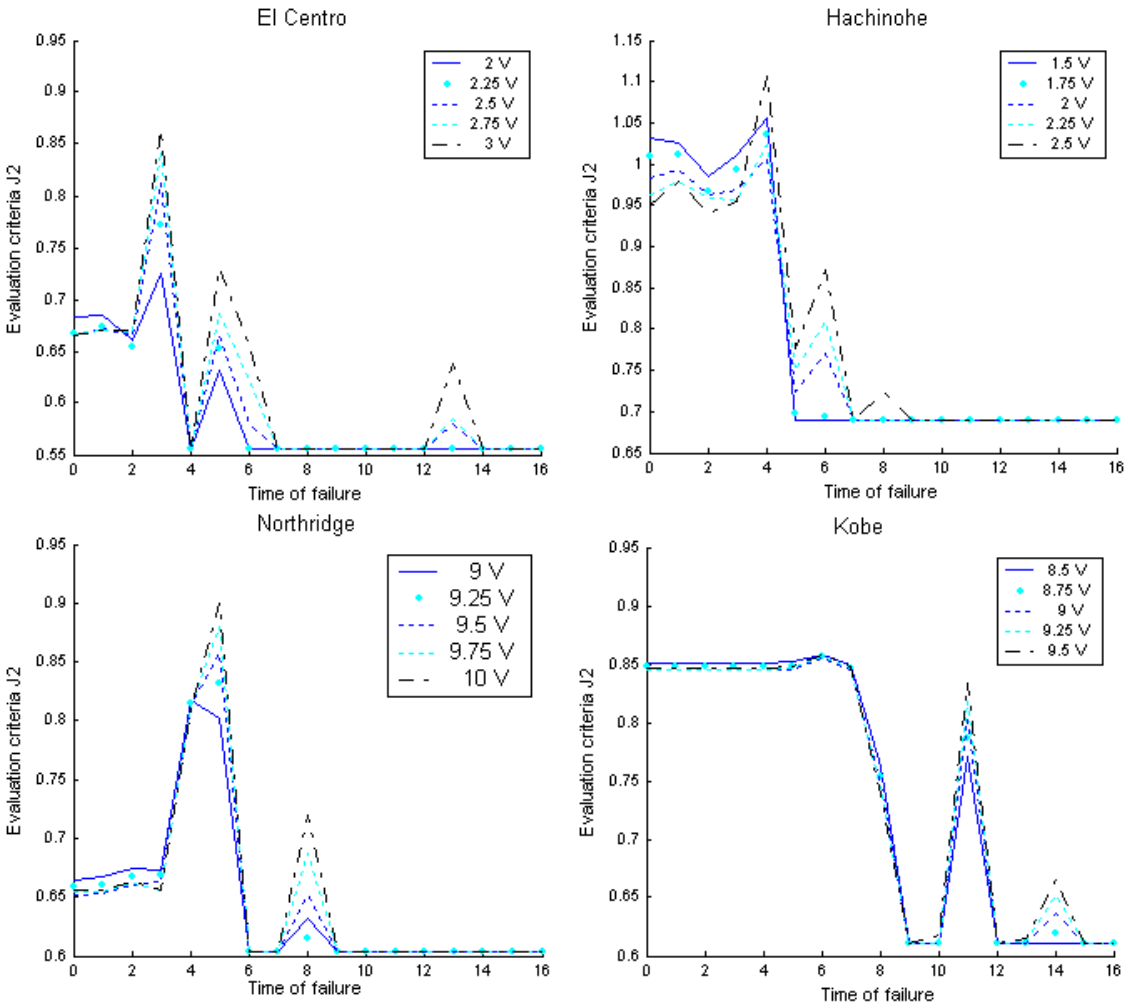

FIGURE 4-17. Evaluation criteria J_2 for the optimal passive voltage range for each earthquake versus failure time.

Notice that the peak accelerations are high for all earthquakes, and actually have the potential to be slightly worse than the uncontrolled case in the Hachinohe excitation. The design voltage, though returns the lowest worst-case J_2 value. For each of the other excitations, the lowest voltage returns the best acceleration, but the largest gain is around 7%. That gain is in the Northridge excitation, and looking at the drift criteria, there is a 2% gain in using the design voltage over the one returning the best acceleration. The small gain made in acceleration does not warrant a switch in the design.

In all cases excepting the Hachinohe excitation, peak drifts are lower in the passive case than in clipped-optimal, but the gain in performance is outweighed by the loss in acceleration performance, leaving clipped-optimal the best control option. Also, the fact that in the Hachinohe excitation, both peak drifts and peak accelerations are greater in passive than in the semiactive state indicate that using clipped-optimal a more robust control strategy in reference to an unknown ground motion. As a passive fail-safe, though, the optimum voltages are an effective means by which the structure is guaranteed to have better performance during a seismic event than if it were uncontrolled when the main control strategy cannot be applied. The chances of this occurring may be rare, but the fail-safe is there in case that small possibility becomes reality.

Running the simulations for the voltage range near the optimum voltage of the passive case yields the result that the passive design voltage maintains the best performance in the presence of failures at various times. For all earthquake excitations run, the trend for the time failures versus the 0s failures explored previously agree, indicating that the passive fail-safe design can be based upon the strictly passive case. This simplifies the process of choosing a voltage, as the time of failure does not need to be considered.

4.3.4 Effects of voltage distribution

In the previous chapter, with only two device locations to deal with, sending different voltages to each device was not considered. With the multiple device locations to chose from in the nine-story simulations, the possibility of improved performance with different distributions exists. Five methods were devised to determine the best distribution of voltages for the asymmetric nine-story building. These are, as they will be referred to in this thesis, the RMS, mean, stiffness, inverse stiffness, and intuitive methods. In this context, the optimum force refers to that force which is commanded by the H_2 LQG controller before entering the clipped-optimal control block.

- The RMS method consists of taking the RMS value over time of the optimum force for each device separately, (f_{opt_i}). This value is then multiplied by the maximum voltage, V_{ult}, and divided by the maximum RMS value of all the devices, y_{max}, as shown in Equations 4-17 and 4-18

$$y_i = \text{RMS}(f_{opt_i}) \tag{4-17}$$

$$v_{rms} = y\frac{V_{ult}}{y_{max}} \tag{4-18}$$

where the index *i* indicates the device number, and v_{rms} is the vector of voltages for the devices calculated by this method.

- The mean method takes the mean value over time of the absolute value of the optimum force commanded for each device. These values are converted to voltages in the same manner as those of the RMS method. Equations 4-19 and 4-20 show this relationship.

$$y_i = \frac{\sum_t |f_{opt_i}|}{\text{length}(f_{opt})} \tag{4-19}$$

$$v_{mean} = y\frac{V_{ult}}{y_{max}} \tag{4-20}$$

- The stiffness method takes the stiffness matrix in the x-direction (direction of excitation) and picks out the stiffness at the location of each device.

$$y_i = \text{K}_\text{x}(j, k) \tag{4-21}$$

where the indices *j* and *k* indicate the floor level and bay, respectively, of the device. This stiffness value is then converted to the voltage

$$v_{stiff} = y\frac{V_{ult}}{y_{max}} \tag{4-22}$$

- The inverse stiffness method takes the values of the stiffness method and inverts the floors, so that the larger voltages are applied at the lower floors, and the lower voltages at the upper floors. The re-arrangement does not follow the exact inverse of the stiffness method, though. Equations 4-23 show the distribution.

$$v_{inv}(1) = v_{stiff}(9),\ v_{inv}(2) = v_{stiff}(7),\ v_{inv}(3) = v_{stiff}(5),\ v_{inv}(4) = v_{stiff}(8),$$
$$v_{inv}(5) = v_{stiff}(3),\ v_{inv}(6) = v_{stiff}(6),\ v_{inv}(7) = v_{stiff}(2),\ v_{inv}(8) = v_{stiff}(4),$$
$$v_{inv}(9) = v_{stiff}(1) \tag{4-23}$$

  The reason for this distribution becomes apparent when looking at the placement of the devices. The two devices on the strong side, four and eight, switch places, while the single device in the bay next to the weakest bay remains the same, and the rest of the devices are inverted according to their floor.
- The intuitive approach assigns a voltage which is based on two criteria. The first is the floor level the device is on, and the voltage decreases as the floor level increases. The second criteria is based on the stiffness of the bay the device is located in. The devices on the weak side receive a higher voltage level than those on the strong side.

These schemes were applied to the structure in fully passive mode with a maximum voltage of 3V, as the best voltage for the small magnitude earthquakes was around 3V. For the large magnitude earthquakes the maximum voltage corresponds to the best result from the passive cases of 10V. Figure 4-18 provides the results of the comparison. It is apparent that the best results overall come from a flat distribution. Only in the El Centro case do any of the calculated methods improve upon the flat distribution, and that was the intuitive approach. It is concluded that the best approach is to maintain the simpler flat distribution. It yields the best results, and is the least complicated approach.

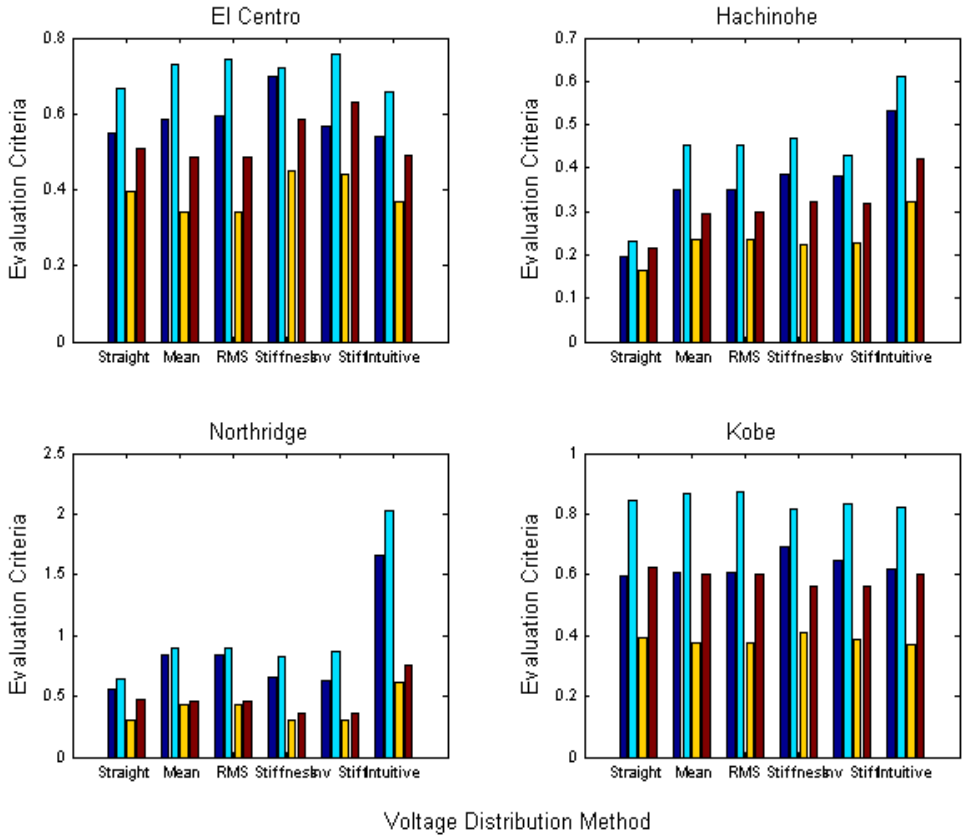

FIGURE 4-18. Results of the five different distribution schemes compared to a single voltage for all devices on leftmost bars.

4.4 Summary

In this chapter, the method developed in chapter 3 was applied and verified for a 9-story, plan-asymmetric building. The effects of passive voltage were studied to determine the value which returns the best performance. Using these values, the effects of failure time and three additional failure cases were discussed to determine the worst case scenario. The absolute worst case was found to be failure of all devices to the passive-off state during the Hachinohe earthquake excitation. The peak acceleration evaluation criteria was found to be greater than 1.0, meaning the performance was worse than the uncontrolled case for a failure time of 5 seconds. In the passive fail-safe mode, the

accelerations once again breached a J_2 level of 1.0. Because the value is slightly over 1.0 and drifts are reduced by nearly 40%, the passive fail-safe system was determined to be adequate in this case. All other cases returned evaluation criteria under 1.0, and the trends for the voltages at the worst case time failures corroborated the voltage values of the strictly passive design. In fact, the most often occurring worst case time was 0s.

The conclusions which may be drawn from this full scale study are as follows:

- The passive fail-safe system is reasonably successful in limiting the response of the structure in the presence of a failure. For all earthquakes considered, the evaluation criteria only surpassed the 1.0 threshold value one time, indicating a performance worse than the uncontrolled state. That was an acceleration value which was accompanied by a reduction in drift of nearly 40%. Also, this acceleration only occurs for one failure time in the excitation.
- The design of the optimal voltage in the passive case was corroborated in the worst case time failures, indicating that trends in system response with respect to time failure is not greatly dependent on the passive voltage applied. This means that the passive fail-safe system can be designed as if it were the sole control system of the structure.
- Comparing fail-safe results to those of clipped-optimal shows that, even though the drifts may be better contained in the passive case, accelerations are high. It is maintained in this thesis that minimization of accelerations cannot be sacrificed for a small gain in peak drift performance. The clipped-optimal control remains the better solution for control, but as a fail-safe system the passive design works well to ensure safety for the structure in the unlikely occurrence of a failure in control system.

Chapter 5

Using Passive Design Strategies to Develop Efficient Fail-Safe System Design

To remove the trial-and-error aspect of the procedure implemented in chapters 3 and 4, a methodology is adopted from typical passive design strategies. This chapter discusses the development of that design procedure, and the efficacy thereof.

Section 5.1 summarizes the passive design scheme and the adjustments made to apply this to the MR dampers. Section 5.2 discusses the Kanai-Tajimi filter, a method used here to develop a suite of earthquakes with similar frequency content. In section 5.3, the design procedure is applied to the 6 story model building and in section 5.4 it is applied to the full scale 9 story plan-asymmetric building.

5.1 Passive Design Scheme

Design of a suitable passive voltage level for a fail-safe system using MR dampers is complicated by the nonlinear nature of the devices. Their behavior is an amalgam of a friction damper and a viscous damper, but their hysteretic behavior (similar to the

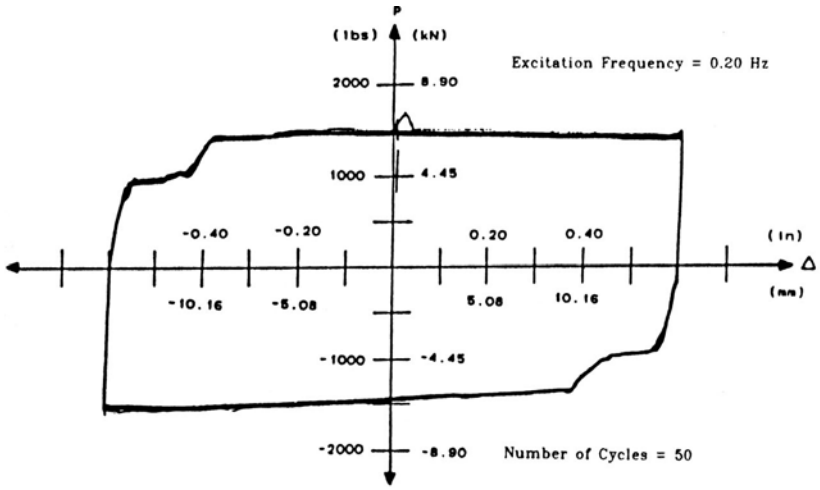

FIGURE 5-1. Force displacement loop for friction dampers (figure taken from Filiatrault and Cherry [23]).

friction devices) is the most prevalent. Figure 5-1 shows the force displacement loop for a friction damper. Comparing this loop to the force displacement loop for an MR damper (Figure 5-2), the similarities in device behavior are seen. For this reason, a design scheme developed for friction dampers is utilized to design the fail-safe passive system. Basically, the design method produces an optimal friction slip force for the devices, and that slip force is set equal to the force at which the MR damper yields and begins to move. The voltage needed to produce that force is then extracted: that is the fail-safe design voltage.

5.1.1 Design of Optimal Slip Force for a Friction Damped System

In a friction damped system, energy is dissipated through frictional resistance. It is asserted that the optimum slip load is found by maximizing the energy dissipated through the frictional device which is the product of the slip force and the distance the device slips [23]. To perform the analyses of the systems under consideration, the authors created a computer program, friction damped brace frame analysis program (FDBFAP), to simulate the different settings. Throughout their studies, the authors

discovered that the optimum slip load is not only a structural property, but is also dependent on the frequency and amplitude of the ground motion. It is therefore important to consider the site location and the properties of the soil and seismic zone. Through simulation and analysis, a design procedure is developed for these devices, and summarized below [23].

Step 1: For a new structure, design for all load combinations except those considering seismic excitation. In retrofit, verify that the unbraced moment-resisting frame is capable of carrying the load combinations, excluding seismic, safely.

Step 2: Calculate the fundamental period of the unbraced structure T_u, and choose the braces such that the natural frequency of the braced structure yields $T_b/Tu < 0.4$ if possible. Estimate the peak ground acceleration and find the period of the ground for the location of the structure.

Step 3: Verify that the non-dimensional ratios fall within the ranges:

$$0.20 \le \frac{T_b}{T_u} \le 0.80\,,\ 0.05 \le \frac{T_g}{T_u} \le 20\,, 0.005 \le \frac{a_g}{g} \le 0.4 \qquad (5\text{-}1)$$

TABLE 5-1. Table of a and b values for various NS and Tg/Tu values.

	NS = 1		NS = 2		NS = 3		NS = 4		NS = 5		NS = 6		NS = 7		NS = 8		NS = 9		NS = 10	
T_b/T_u (1)	α (2)	β (3)	α (4)	β (5)	α (6)	β (7)	α (8)	β (9)	α (10)	β (11)	α (12)	β (13)	α (14)	β (15)	α (16)	β (17)	α (18)	β (19)	α (20)	β (21)
0.20	1.15	1.22	1.94	2.01	2.73	2.80	3.52	3.60	4.31	4.39	5.10	5.18	5.89	5.97	6.68	6.76	7.47	7.55	8.26	8.35
0.25	1.08	1.16	1.80	1.90	2.53	2.64	3.26	3.38	3.99	4.11	4.72	4.85	5.44	5.59	6.17	6.33	6.90	7.07	7.63	7.80
0.30	1.00	1.10	1.67	1.79	2.33	2.47	3.00	3.16	3.66	3.84	4.33	4.52	5.00	5.21	5.66	5.89	6.33	6.58	6.99	7.26
0.35	0.92	1.04	1.53	1.67	2.13	2.31	2.73	2.94	3.34	3.57	3.94	4.20	4.55	4.83	5.15	5.46	5.76	6.09	6.36	6.72
0.40	0.85	0.99	1.39	1.56	1.93	2.14	2.47	2.72	3.01	3.29	3.56	3.87	4.10	4.45	4.64	5.02	5.18	5.60	5.72	6.18
0.45	0.77	0.93	1.25	1.45	1.73	1.97	2.21	2.50	2.69	3.02	3.17	3.54	3.65	4.07	4.13	4.59	4.61	5.11	5.09	5.64
0.50	0.69	0.87	1.11	1.34	1.53	1.81	1.95	2.28	2.36	2.75	2.78	3.22	3.20	3.68	3.62	4.15	4.04	4.62	4.46	5.09
0.55	0.61	0.81	0.97	1.22	1.33	1.64	1.68	2.06	2.04	2.47	2.40	2.89	2.75	3.30	3.11	3.72	3.47	4.14	3.82	4.55
0.60	0.54	0.75	0.83	1.11	1.13	1.47	1.42	1.84	1.71	2.20	2.01	2.56	2.30	2.92	2.60	3.29	2.89	3.65	3.19	4.01
0.65	0.46	0.69	0.69	1.00	0.92	1.31	1.16	1.62	1.39	1.93	1.62	2.23	1.86	2.54	2.09	2.85	2.32	3.16	2.55	3.47
0.70	0.38	0.63	0.55	0.89	0.72	1.14	0.89	1.40	1.07	1.65	1.24	1.91	1.41	2.16	1.58	2.42	1.75	2.67	1.92	2.93
0.75	0.30	0.57	0.41	0.78	0.52	0.98	0.63	1.18	0.74	1.38	0.85	1.58	0.96	1.78	1.07	1.98	1.18	2.18	1.29	2.38
0.80	0.23	0.52	0.27	0.66	0.32	0.81	0.37	0.96	0.42	1.10	0.46	1.25	0.51	1.40	0.56	1.55	0.60	1.69	0.65	1.84

Step 4: Determine the coefficient α_f from the Table 5-1 based on the number of stories and T_b/T_u.

The authors also develop a design criteria for the braces, which we are not concerned with as we do not use braces for these initial studies. This study only considers the force values obtained based on the design procedure which incorporates the optimum slip load for friction dampers.

Step 5: Using α_f, the total slip force V_0 can be calculated:

$$V_o = \alpha_f \frac{T_g}{T_u} m a_g \tag{5-2}$$

This optimum total slip force is then distributed equally among all of the devices. To obtain the voltage corresponding to the force calculated for each MR damper, the device parameters as well as the force per device obtained from the distribution of V_0 are used in equation 5-11.

Note that this design procedure assumes devices are placed regularly on all floors while the structures under consideration in this study have multiple floors without control

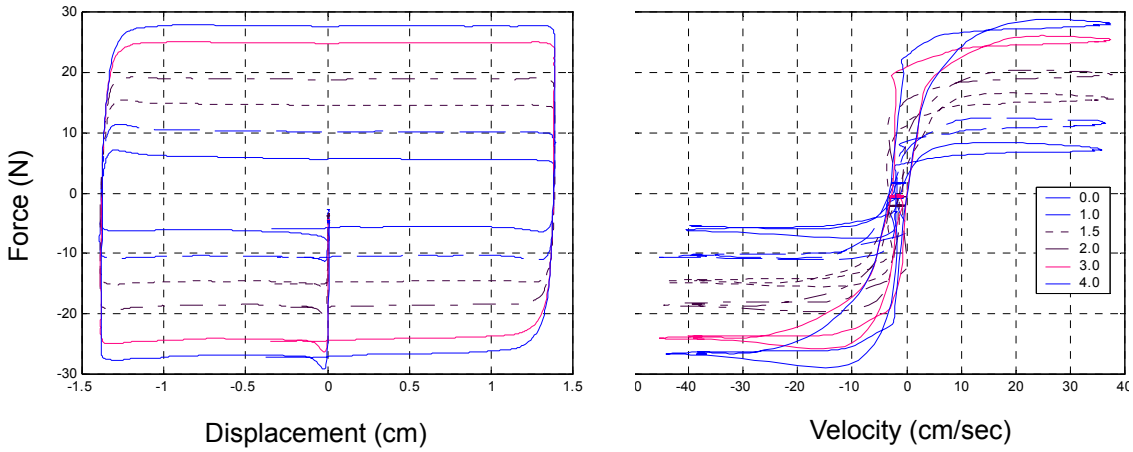

FIGURE 5-2. Force-displacement and force-velocity loops for the shear-mode MR dampers

devices. This assumption must be dealt with when designing a system for a specific building. Also, the friction damper design method attempts to maximize the energy dissipated, not to specifically limit drift or acceleration overall. The effect these assumptions have on the performance of the design are discussed in sections 5.3 and 5.4.

5.1.2 The MR Damper Yielding Force

To determine the proper voltage for command, it is helpful to return to the characteristics of the MR damper. The hysteretic behavior of the device, shown in Figure 5-2, is similar to that of the friction damper. Comparing Figures 5-1 and 5-2, it is apparent that the devices act in a similar manner. The optimum slip force found in the previous section corresponds to that is here called the corner force. The corner force refers to the point on the force-displacement loop where the force stops changing and the displacement begin changing. This essentially forms the corners of the force-displacement loops.

The equation describing the force in an MR dampers given by $f = \alpha z + c_0 \dot{x}$ [43]. Because yielding begins in a state of zero velocity, it is useful to consider the c_0 term to

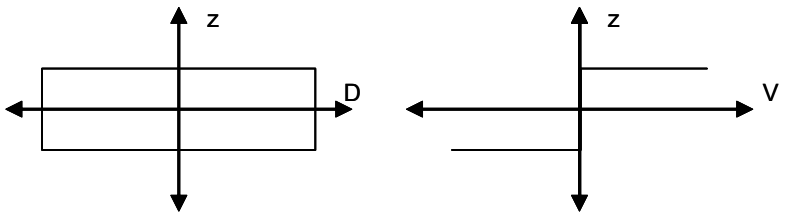

FIGURE 5-3. Displacement and velocity dependence of z with simplifying assumptions.

be zero when determining the force at which the devices yield. This step removes the dynamics and the relationship to the velocity yielding the following relation:

$$f = \alpha z \tag{5-3}$$

where

$$\dot{z} = -\gamma|\dot{x}|z|z|^{n-1} - \beta\dot{x}|z|^{n} + A\dot{x}. \tag{5-4}$$

Because the force of interest is the yielding force, it is assumed that there is no slope to the force displacement and force velocity loops. The force-displacement and force-velocity relationships are reduced to relationships between z versus x and z versus $\dot{x}$ shown in Figure 5-3. These relationships hold because of the assumption that there is no velocity dependence in the force, which leads to the direct relationship between the force and the variable z. When $\dot{z}$ is equal to zero, we have

$$\gamma|\dot{x}|z|z|^{n-1} = (-\beta|z|^{n} + A)\dot{x}. \tag{5-5}$$

Rearranging, we obtain

$$\frac{|\dot{x}|}{\dot{x}} = \frac{A - \beta|z|^n}{\gamma z|z|^{n-1}}. \tag{5-6}$$

The left side of equation 5-6 is simply the sign of the velocity. Note from Figure 5-3 that for positive velocity z is positive, and for negative velocity z is negative. It follows that, because the values of $\dot{x}$ and z are of the same sign, the equation may be written as

$$1 = \frac{A - \beta|z|^n}{\gamma z^n}, \text{ or } -1 = \frac{A - \beta|z|^n}{\gamma z^n(-1)} \tag{5-7}$$

which can be rearranged or condensed into one equation as

$$(-1)^n z^n = \frac{A}{\gamma + \beta}. \tag{5-8}$$

We know $n = 2$, and focus on the positive square root of this term which is plugged back into equation 5-3 to yield

$$f = \alpha\sqrt{\frac{A}{\gamma + \beta}} \tag{5-9}$$

where

$$\alpha = \alpha_a + \alpha_b v \tag{5-10}$$

so that the voltage v is computed by

$$v = \frac{f\sqrt{\frac{\gamma + \beta}{A}} - \alpha_a}{\alpha_b}. \tag{5-11}$$

This equation produces, when inserting the MR parameters A, γ, β, α_a, and α_b the voltage required to achieve the desired passive slip force f attained from the design procedure of section 5.1.1.

5.2 Development of an Earthquake Suite for Verification

Because of the complexity of an earthquake, and the random quality of the excitation it is necessary to test the design with a suite of earthquakes with similar characteristics. This is representative of considering an actual site location with seismic properties. An earthquake can never be duplicated in real life, but a site in a seismic zone may experience earthquakes with similar properties. A suite of ten earthquakes is designed to verify the design for specific site conditions.

To test the design method, ten earthquakes are created using a Kanai-Tajimi filter [35], a standard technique used to develop a suite of earthquakes with similar frequency content and time characteristics. Kanai and Tajimi theorized that the ground motion generated during an earthquake can be represented by the absolute acceleration of a simple oscillator consisting of a concentrated mass with a linear spring and dashpot, which is subjected to a white noise excitation of spectral density S_o [35]. The earthquakes designed via the Kanai-Tajimi filter are stationary processes which closely mimic the random quality of an earthquake within a region having a natural soil frequency of ω_g, damping ratio of ζ_g, and wave intensity of S_o. The resulting earthquakes are designed to have the same frequency content with varying magnitudes and peak acceleration times. To represent the ground motion the Kanai-Tajimi filter is presented as the power spectral density function

$$S_g(\omega) = \frac{\omega_g^4 + 4\zeta_g^2\omega_g^2\omega^2}{(\omega_g^2 - \omega^2)^2 + 4\zeta_g^2\omega_g^2\omega^2} S_o . \tag{5-12}$$

Ten earthquakes are designed for a site with a natural ground frequency ω_g of 2π rad/sec or 1 Hz, a damping coefficient ζ_g of 0.65 and a spectral density S_o of 10. The design procedure is carried out and tested using these ten earthquakes. Doing this will test the robustness of the design procedure which is based on the natural frequency and damping of the ground, as well as the expected magnitude of the seismic excitations.

5.3 Design for the 6 story model building

Because of the relative simplicity of the six story model, it is the first structure the design procedure is applied to. The optimum slip force is calculated for the structure, and then distributed among the devices. Taking the force required for each device and the MR damper parameters for the structure and plugging them into equation 5-11. The resulting voltage per device is 3.4V.

Because this structure has control devices on floors one and two only, the period T_b is obtained by considering the bottom two floors locked in place. Essentially this approach represents the period of the four story structure consisting of the top four floors of the six story model building. This yields a ratio $\frac{T_b}{T_u} = 0.69$ and an α of 1.24, making the optimum total slip force 210.06 N.

Because Filiatrault and Cherry assumed devices on all floors, the total slip force is divided by 6. Because there are two devices on each of the floors with devices, that number is divided again by 2 giving an optimum slip force per device of 17.5 N. Plugging this force and the MR parameters into equation 5-11, a voltage of 3.4V is obtained.

To validate the applicability of the design procedure for the simple six story structure, the earthquakes are simulated with a range of voltages from 0V to 5V by steps of 0.5V. Trends for each earthquake are apparent for the maximum drift and acceleration values,

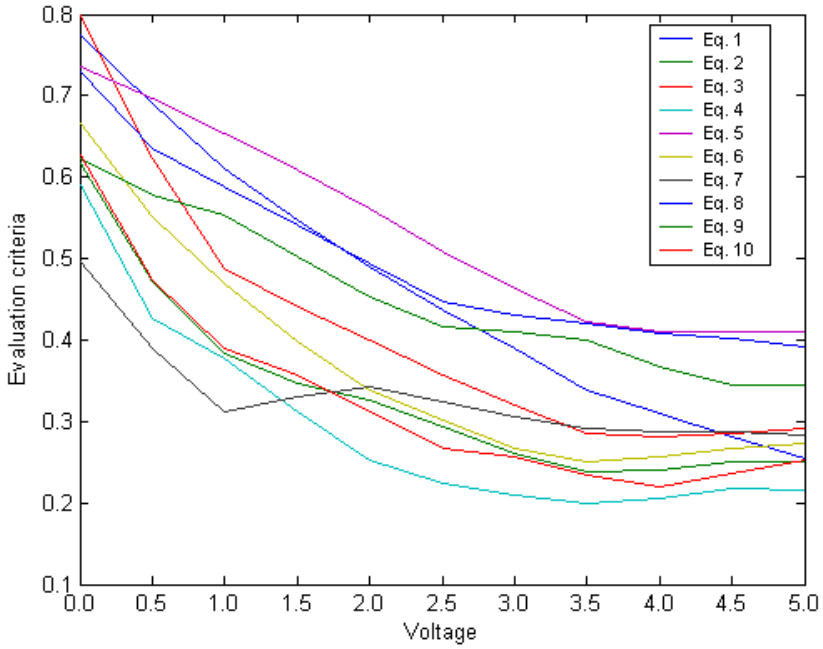

FIGURE 5-4. Trend for evaluation criteria J_1 versus voltage for each of the 10 designed earthquakes.

indicated by J_1 and J_2, respectively. These trends are shown in Figures 5-4 and 5-5. The trend for evaluation criteria J_1 shows that as the voltage increases toward 5V, the maximum drift decreases. In fact, most of the earthquake responses show that J_1 begins to level out after 4 volts, and sometimes increases. As for the trend in the maximum accelerations, Figure 5-5 shows that there is generally a dip in the middle of the voltage range around 3V. These two trends indicate that a voltage near the upper end of the allowed range is best suited for the passive fail-safe voltage.

It is also useful to study the average of the evaluation criteria over the suite of similar earthquakes, for an overall feel of the performance of the MR devices over the specific

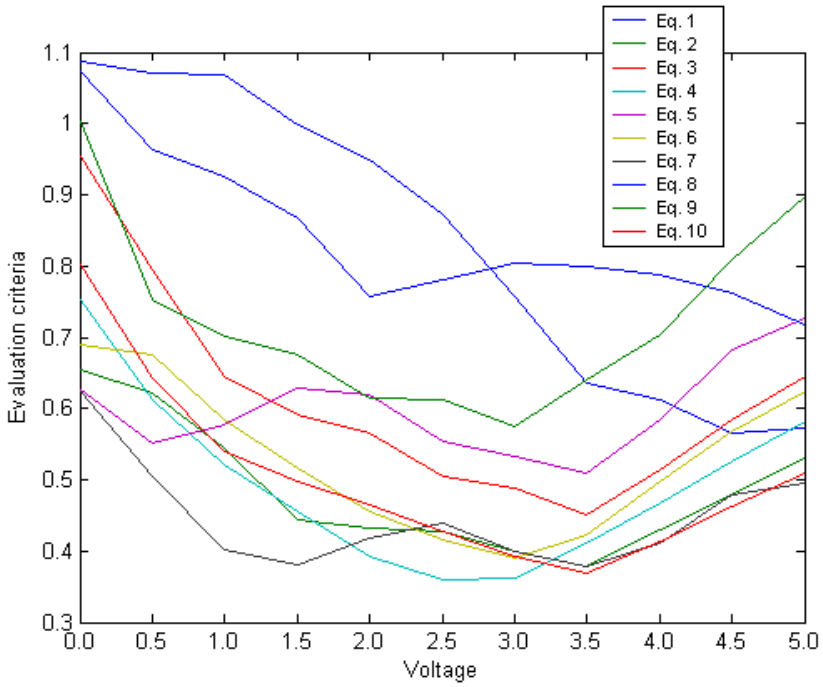

FIGURE 5-5. Trend for evaluation criteria J_2 versus voltage for each of the 10 designed earthquakes.

voltage range of interest. The averaged results are presented in Figure 5-6. Considering all of the evaluation criteria, the values between 3 and 4V should be evaluated on a smaller voltage interval. Therefore, a simulation considering the values between 3 and 4V spaced at a 0.1V interval is performed. Once again, the results indicate two trends, maximum drift and acceleration criteria values, as well as the averaged evaluation criteria over all earthquakes. The trend shown in Figure 5-7 depicts the interstory drifts for

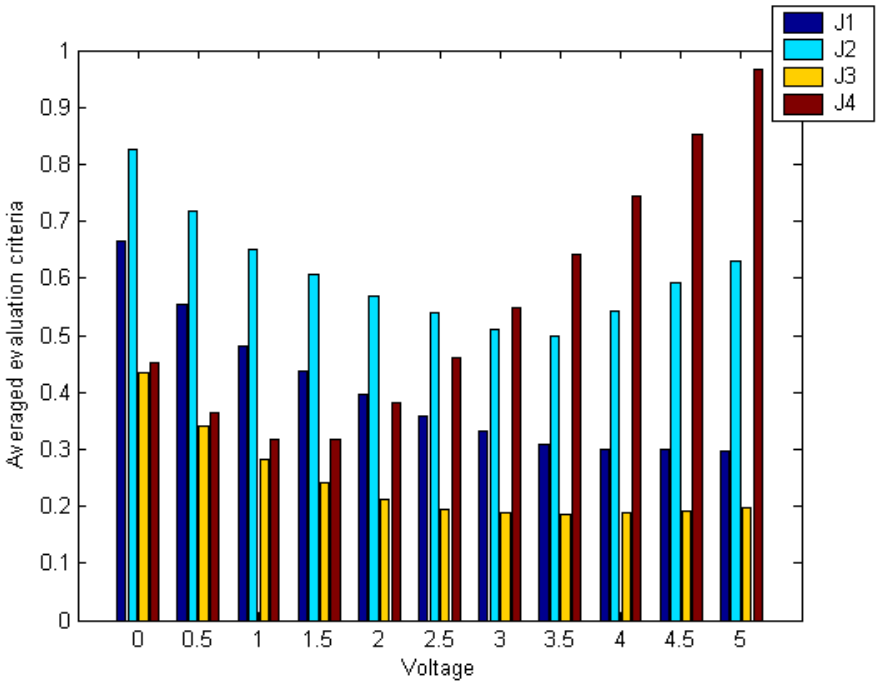

FIGURE 5-6. Evaluation criteria averaged over all earthquakes versus voltage.

most earthquakes drops slightly as the voltage increases from 3V to 4V. The trend shown for J_2 indicates that, for most earthquakes, a voltage around 3.4V is best but the

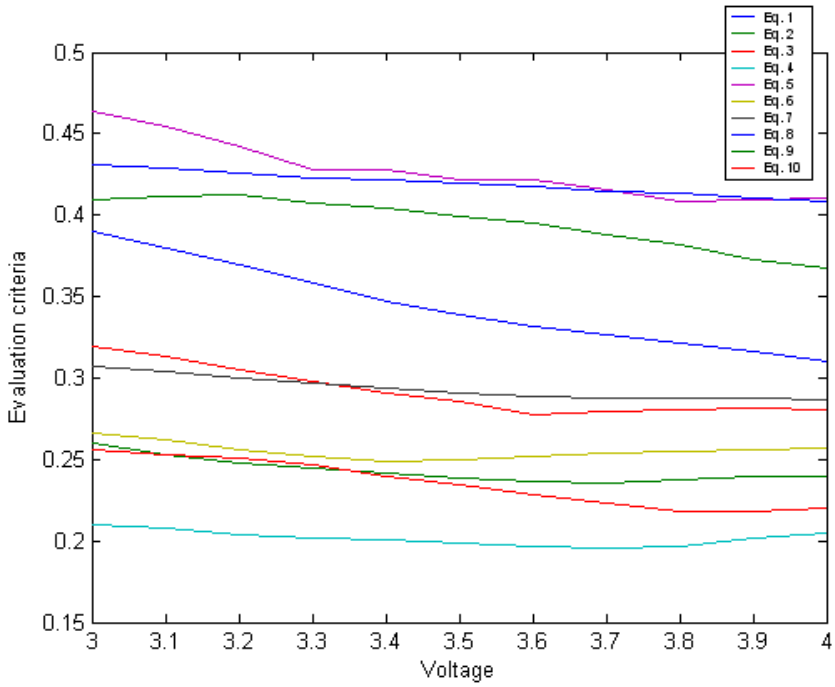

FIGURE 5-7. Trend in evaluation criteria J_1 versus voltage between 3 and 4V for all designed earthquakes.

variation between 3V and 4V is slight for most earthquakes. The averaged results are presented in Figure 5-9. Notice that, from Table 5-2, the standard deviation over all the earthquakes of evaluation criteria J_1 is around 8% for all of the voltages. The results actually become more consistent as the voltage increases, noted by the dropping standard deviation of the earthquakes. Also, note that the standard deviation for the accelerations ranges from 13 to 16%. The average for the drifts, with a standard deviation of 8%, is fairly consistent with the results, and will show a good representative trend. The accelerations are less consistent with a standard deviation around 15%. This indicates that the trend is less accurate than that of the drifts. Looking back at the individual plots,

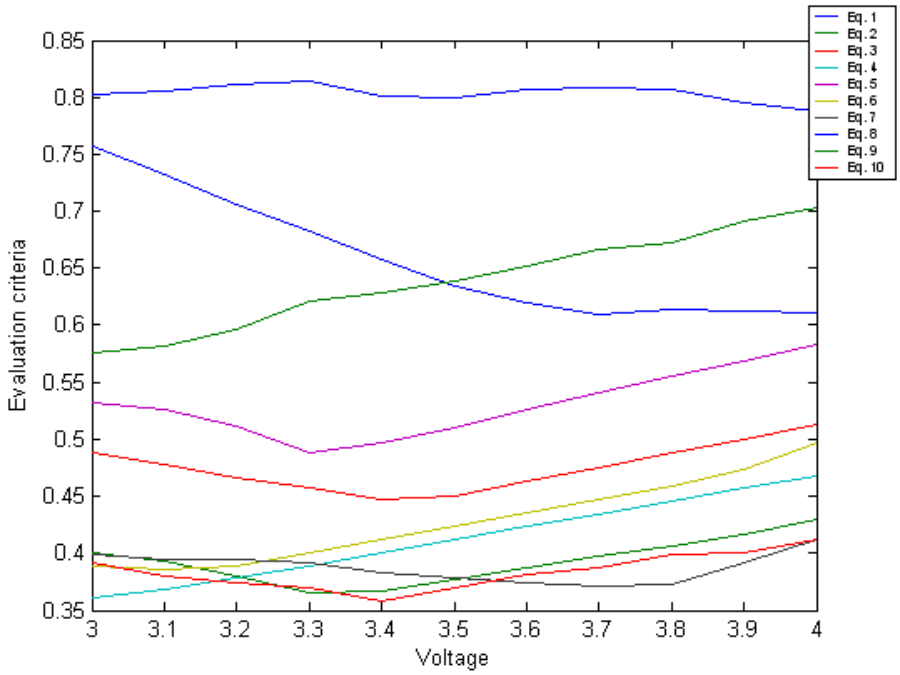

FIGURE 5-8. Trend in evaluation criteria J_2 versus voltage between 3 and 4V for all designed earthquakes.

though, using the averaged acceleration results seems reasonable, as that voltage returns reasonable results for all of the earthquakes considered.

TABLE 5-2. Standard deviations by voltage over each of the designed earthquakes.

Voltage	Standard Deviation	
	J1	J2
0V	0.0867	0.1589
0.5V	0.0862	0.1572
1V	0.0852	0.1559
1.5V	0.083	0.1553
2V	0.0834	0.1505
2.5V	0.0824	0.1453
3V	0.0826	0.1436
3.5V	0.0806	0.1425
4V	0.0788	0.1395
4.5V	0.0763	0.1345
5V	0.0745	0.1279

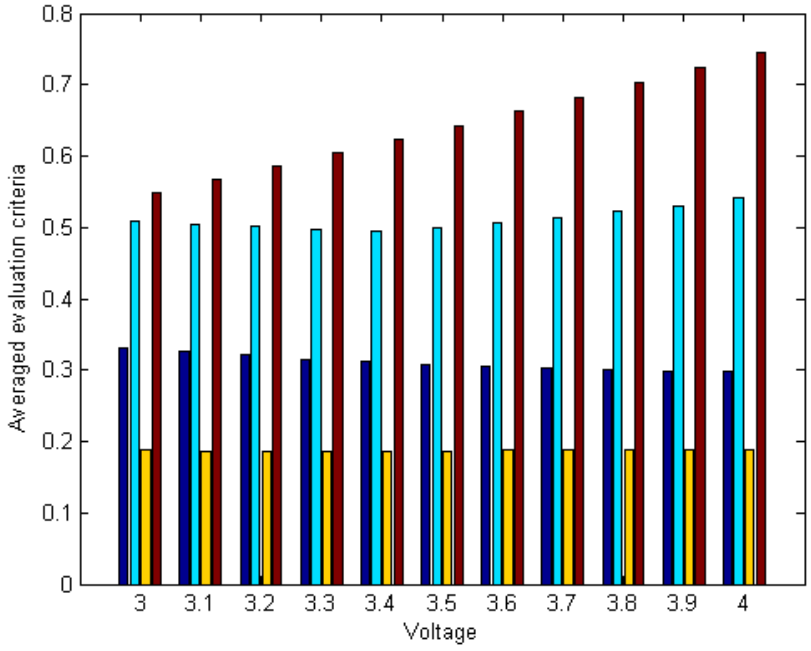

FIGURE 5-9. Evaluation criteria averaged over all earthquakes versus voltages between 3 and 4V.

It is apparent from Figure 5-9 that the RMS value of the acceleration grows rapidly as the voltage increases from 3V to 4V, while the RMS value for drifts stays roughly the

TABLE 5-3. Evaluation criteria averaged over all earthquakes versus voltages between 3 and 4V.

Voltage	J1	J2	J3	J4
3V	0.3312	0.5099	0.1878	**0.5484**
3.1V	0.3268	0.5046	0.1871	0.5674
3.2V	0.3214	0.5008	**0.1868**	0.5862
3.3V	0.3157	0.498	**0.1868**	0.6046
3.4V	0.3117	**0.4951**	0.187	0.6238
3.5V	0.3076	0.4995	0.1871	0.643
3.6V	0.3045	0.5069	0.1872	0.6629
3.7V	0.3021	0.5138	0.1877	0.6821
3.8V	0.2999	0.5221	0.1882	0.7023
3.9V	0.2991	0.5309	0.1887	0.724
4V	**0.2984**	0.5417	0.1893	0.7445

same. To determine the best voltage for this design, the peak drifts and accelerations must be weighed first, and the RMS acceleration values considered as a secondary measure. The drifts seem to drop steadily as the voltage increases towards 4V, but the peak accelerations show a local minima around 3.4V, which is the value obtained from design based on the procedure laid out in section 5.1. It is reasonable to accept 3.4 V as the design voltage as both the peak drifts and accelerations are near their minimum, and the RMS accelerations are near the middle of the values obtained for this voltage range. The design procedure developed in section 5.1 was effective in providing an efficient design of the fail-safe voltage. Looking at the averaged results, using the calculated voltage appears to deliver the best performance. Looking at the trends of all the earthquakes, the design voltage appears to be a valid and efficient choice in designing a passive fail-safe voltage. The evaluation criteria versus voltage for most quakes follow the same trend, and for those that do not the 3.4V value returns reasonable values. It should be noted, once again, that this procedure is only as good as the assumptions made in its application. The main assumption in question is that of the distribution of forces to the devices. Remember that Filiatrault and Cherry based their design on structures with friction dampers located on all floors in structures without torsional modes.

5.4 Design for the full scale 9 story plan-asymmetric building

Application to a full scale structure is necessary to verify the robustness of the design procedure. The 9-story full scale structure is considered in this design effort, but the procedure is found lacking. Using the largest possible value for α_f found in the Table 5-1, the total slip force required for the structure is 37056 N. This value must be distributed to all floors, according to the design procedure. Herein lies the problem: the full scale devices have a minimum force of 20 kN and a maximum force of 100 kN. The maximum total slip force for the structure would require a small voltage, on the order of 1V. That is, for one device to produce the required total force, a small voltage must be applied. There are 9 devices in the structure under consideration, and the total slip force must be divided by at least 9, meaning that the slip force per device is below the minimum force for the full scale damper. In Chapter 4, the voltage that produced the best results when exposed to the small peak ground acceleration earthquakes was found to be in the 2 to 3 Volt range per device. Also note that the large peak acceleration records required near the maximum force that the device could provide. The designed earthquakes averaged a peak acceleration of 0.5 g's whereas the peak in the El Centro record is about 0.34 g's and the Kobe earthquake has a peak at 0.83 g's. It is expected that the voltage per device should be somewhere between 3 and 9 Volts, yet the design procedure produced a force for the entire structure that corresponds to the force developed when 1V is applied to just one device. Thus, using the design criteria set out by Filiatrault and Cherry [23] for the 9-story plan-asymmetric building is ineffective. Moreover, those design criteria are inapplicable based on the bounds of the design parameters. To design a passive fail-safe system for a full scale structure using MR dampers, it is apparent that a new design methodology must be developed.

5.5 Summary and Discussion

In this chapter a design procedure, previously designed for friction-damped systems, is modified to provide a passive fail-safe voltage for the MR dampers in this study. When

applied to the six story model building using the ten earthquakes which were designed to have similar characteristics, it appeared to be effective. However, this approach was found to be ineffective for the nine story, plan-asymmetric, full scale structure. This may be the result of several sources. First, in the control studies, device placement is not uniform throughout the building, which is one assumption Filiatrault and Cherry made. Also, this full scale structure exhibits strong torsional modes, which are not considered in the frictional damper design procedure. Future work in this area should include a study of a wider variety of structures and placement schemes to overcome the limitation in the method. The main conclusions drawn from this design study are as follows.

- The design procedure was implemented and verified on the six story model building. It produced an efficient fail-safe voltage for the ten designed earthquakes.
- Using the friction damper methodology to find the optimum force in the full scale nine story plan-asymmetric building was found ineffective. The optimum slip force calculated for the entire building was barely above the minimum force of one MR device.
- To avoid the use of trial and error, the design procedure needs to consider a broader sampling of full scale structures, including structures which exhibit strong torsional modes.

Chapter 6

Fault Tolerance in Decentralized Control Systems

Decentralized control systems with local devices have been said to posses advantages over global control systems due to less wiring. Additionally, they are considered to be more robust due to the fact that their control strategy is dependent only on local measurements [1,4,5,30]. That is to say, sensor failure may have a less severe effect on the control strategy. If one device becomes ineffective, the other devices will not be affected. However, if the sensor corresponding to a control device on a particular floor fails, the device cannot function properly and the other devices in the structure will not be able to adjust their performance accordingly. A global system, on the other hand, has the capability of monitoring the entire plant and adjusting to accommodate the changes in the system. The goal of this chapter, therefore, is to compare a local semi-active control strategy versus the global semiactive clipped-optimal controller used in this thesis in terms of the robustness in the case of device failures.

Section 6.1 discusses one commonly used decentralized control system and the control law which governs its actions. In section 6.2 the devices are applied to the 6 story model building and in section 6.3 the decentralized devices are applied to the full scale 9 story plan asymmetric building.

6.1 The Device and Decentralized Control Law

The device considered here is a reset-able spring damper. Decentralized devices have been advocated for control due to their simple and autonomous nature, their independence of extensive cable networking to a central computer, and their claimed robust control [1,4,5,8,12,24,29,30]. Described essentially as a spring element, the equilibrium position for this device can be instantaneously changed to maximize energy dissipation in the system. To achieve this, resetting must occur when energy storage is stationary. This occurs when there is no excitation, or when the device changes direction of motion. The first scenario is interesting only because the devices will reset to their original zero position after an excitation. The second scenario is the point at which the energy storage is stationary at a local maximum, and the device can be reset for maximum energy dissipation. This occurs when the relative velocity of the device is zero. Thus, the reset criteria is determined to be the point of zero velocity. Device dynamics are assumed to be negligible as their reset times have been found to be approximately 20ms, indicating that structures with a frequency response of up to 20 Hz can be controlled effectively [5].

The reason these devices are considered to be local devices is the control law which is often implemented. Resetting of the spring is performed based on the relative velocity between the floors where the device is located. For a structure with multiple devices, each device is independent and the actions of one device are not known by other devices. The control law relies only on local measurements between the floors with control devices. To outline the control law utilized in these simulations, a single degree of

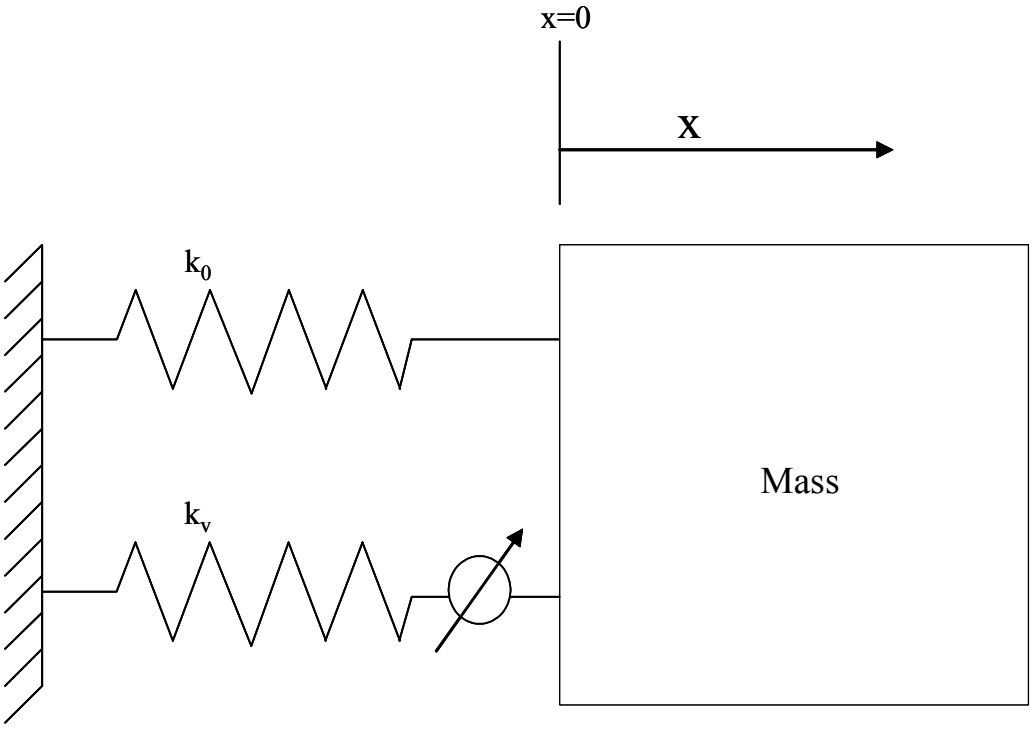

FIGURE 6-1. SDOF model with a reset-able spring

freedom model is demonstrated in Figures 6-1 and 6-2. Figure 6-1 represents a SDOF system with a reset-able spring at rest. The equilibrium position of the reset-able spring is the same as the permanent spring which is 0. The forces in this situation are described by equation 6-1

$$\Sigma F = -k_0 x - k_v x \tag{6-1}$$

where k_0 is the stiffness coefficient for the columns of the structure and k_v is the stiffness of the local device.

As the mass moves to the right, both springs stretch and work together against the motion of the mass. When the mass reaches the its greatest displacement, the velocity is zero and the device resets, releasing the energy stored within its fluid, and comes to a state of equilibrium. This position is denoted by x_v and it is equal to the position of the mass when the device resets. This means that the equilibrium positions of the two springs are no longer the same. From this point on, the two springs do not necessarily work together, and the forces in the system are described by equation 6-2

$$\Sigma F = (-k_0)x - k_v(x - x_v)\,. \tag{6-2}$$

Because the two springs are acting independently on the mass, the forces they impart can be considered separately. This means that the force of the local reset-able device can be expressed as in equation 6-3

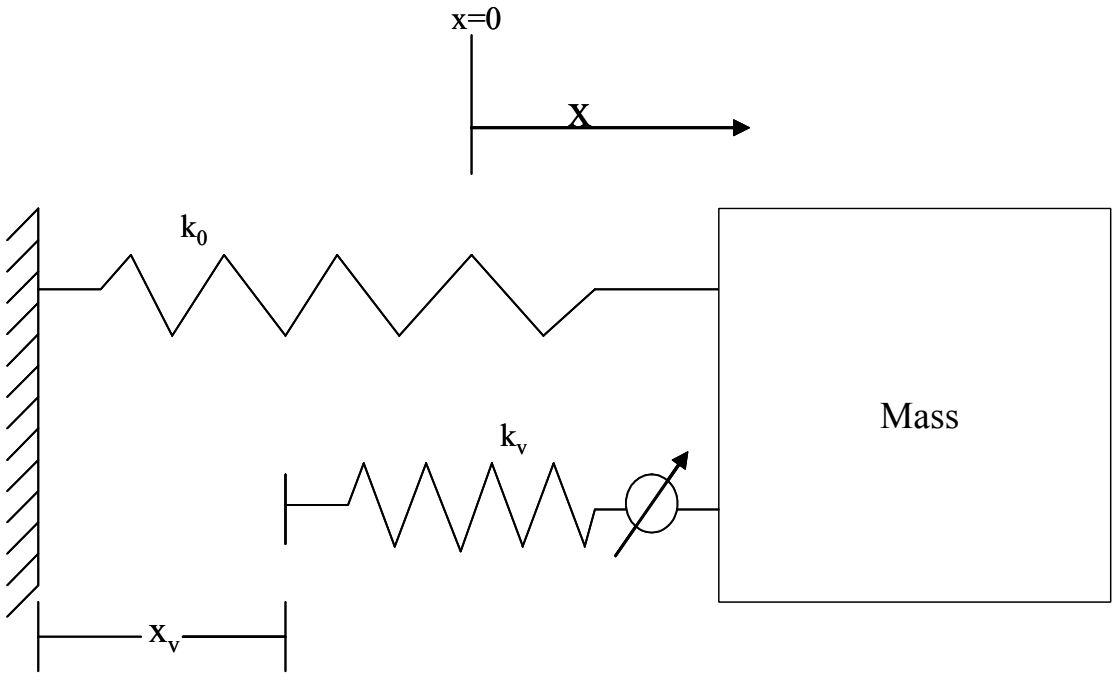

FIGURE 6-2. SDOF model with reset-able spring at the instant of reset.

$$F_{reset} = -k_v(x - x_v). \tag{6-3}$$

Equation 6-3 is used to determine the force produced by the control device in the SIMULINK model. The equilibrium position of the reset-able device x_v is determined by monitoring the sign of the relative velocity of each floor in which devices are located, as advocated by Barroso et al [5]. To do this, the signal is split and one branch is held one time step, while the other is not. The sign of each of these branches is then taken and added. When the sum is zero, the relative velocity has changed signs and the device resets, making the new equilibrium position of the device equal to the drift at the point of reset. At each time step, the forces in the reset-able devices are calculated with their corresponding equilibrium position and input back into the plant as the control forces. Figure 6-3 shows the SIMULINK model of the SDOF plant. The memory blocks serve the purpose of holding the signal one time step, which is necessary because the signals are inputs to the system and must have initial values. The SIMULINK model for the reset-able devices shows how the interstory drift and relative velocity are utilized in the

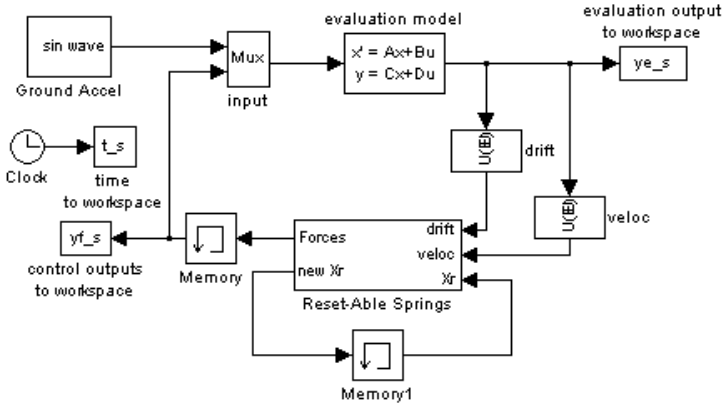

FIGURE 6-3. SIMULINK model of the SDOF system.

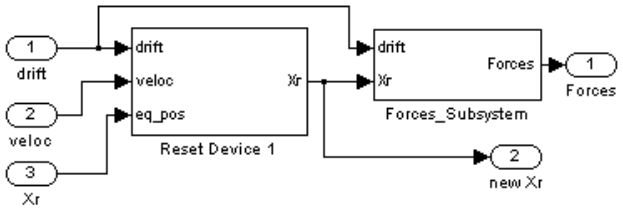

FIGURE 6-4. SIMULINK model of the resetting scheme for the SDOF system.

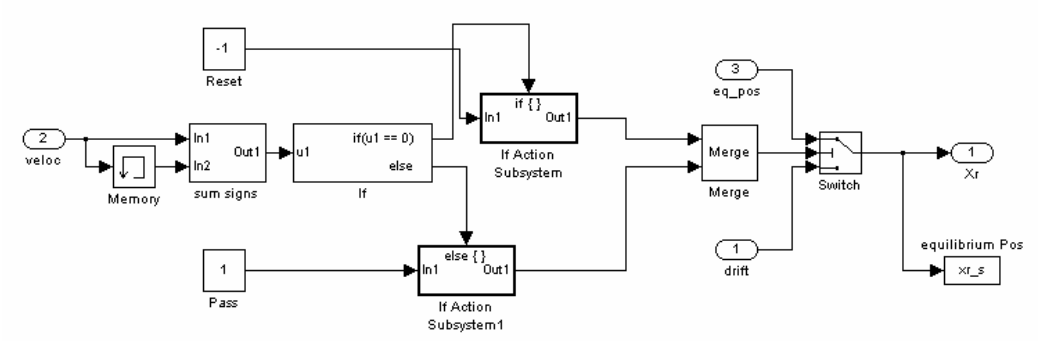

FIGURE 6-5. Device resetting SIMULINK block for the SDOF system.

decentralized control law. Figure 6-4 presents this model. The three inputs are drift, relative velocity, and device equilibrium position. Taking these inputs, the *device reset* block calculates the new equilibrium position, which is sent to the *forces* block as well as fed back to input 3 after being held one time step (see Figure 6-3). As shown in Figure 6-5, the resetting algorithm takes the velocity and splits it into two branches, holding one of the branches one time step. Those signals are then input into the *sign change* block where their signs are taken and summed. The output from that block will either be 2, 0, or -2; that signal is sent to the *if* block where, if the sum is zero, the signal is sent to the switch to reset the equilibrium position. Otherwise the previous equilibrium position is passed through unchanged. The sole output from that block is the equilibrium position

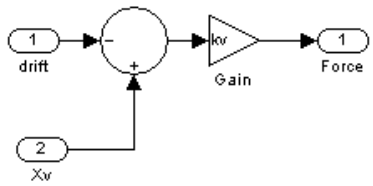

FIGURE 6-6. Forces subsystem SIMULINK block for the SDOF system.

of the device, which is input into the *forces* block along with the drift. As shown in Figure 6-6, the drift is subtracted from the equilibrium position, and multiplied by the gain k_v to attain the force of equation 6-3. This force is then fed into the plant as the control force.

A SDOF system is used for verification of the model, using a sinusoidal excitation to confirm that the simulation is accurately reproducing the device behavior. Looking at the force-velocity loop, the sudden jumps at zero velocity indicate that the device is resetting as the velocity changes sign. Also, the force displacement loop shows that the force grows linearly with displacement until the maximum displacement is reached. At this point, the force drops indicating that the device has reset. The force then decreases linearly with decreasing displacement until the minimum is reached at which the force

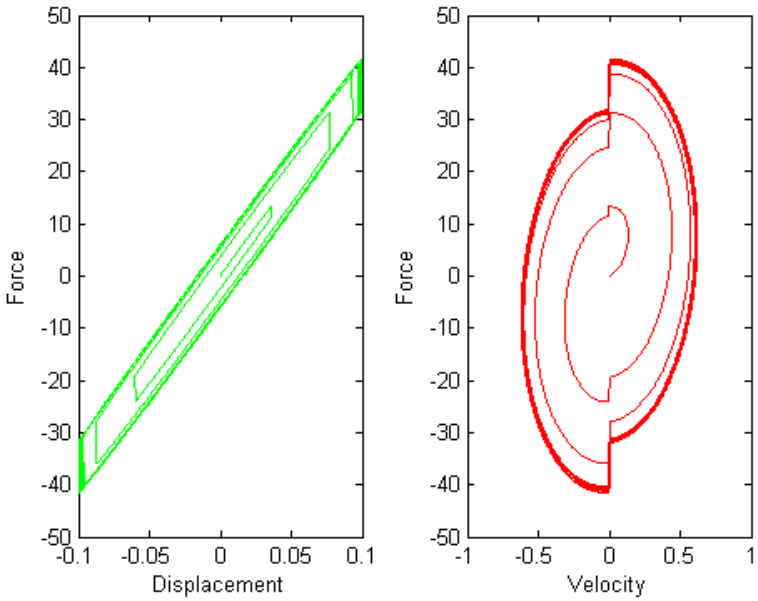

FIGURE 6-7. Force displacement and force velocity loops for the reset-able spring of the SDOF system.

(now negative) jumps up showing that the device has once again reset. These devices are tested on both the six story and nine story buildings. As these buildings have exceedingly different properties and stiffnesses, the device properties are radically different.

TABLE 6-1. Device stiffness values for each model.

Device Stiffness	
Structure	kv (N/cm)
6-Story	88.93
9-Story	44480

The values were chosen to reflect the percentage of column stiffness used by Barrosso et al. [5], which yields a device stiffness at 13.8% of that of the columns. In the nine story structure, to achieve forces comparable to those achieved in the clipped-optimal control scheme, the decentralized device stiffness had to be reduced by a factor of 2.5. Table 6-1 shows the stiffnesses used in simulation for each structure. Table 6-2 shows the two stiffnesses used to achieve comparable forces to clipped-optimal for both strong and weak ground motions. The smaller stiffness is 1/5 that of the larger stiffness. From past experiences, it is reasonable to assume that, with lower device stiffness, the accelerations may come down while drifts increase. It is apparent that these devices must be designed separately for different ground motions. Nominal control responses are shown and discussed for both stiffnesses in section 6.3.

TABLE 6-2. Relative maximum forces of the decentralized scheme as compared to the maximum forces of the clipped-optimal controller.

Maximum Forces (resettable/clipped-optimal)		
Earthquake	Stiffness (N/cm)	Relative Force
El Centro	222400	2.0131
	44480	0.5993
Hachinohe	222400	1.5988
	44480	0.5114
Northridge	222400	4.3139
	44480	2.0882
Kobe	222400	5.3666
	44480	2.0165

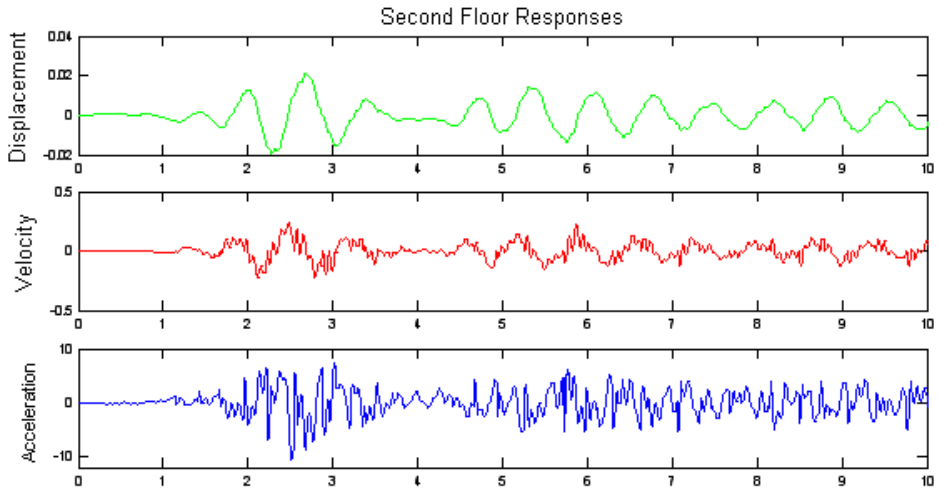

FIGURE 6-8. First ten seconds of the response of the second floor due to the El Centro excitation.

6.2 Six story MDOF model

To consider the ability of this reset-able damper to reduce earthquake responses in the six story structure, the El Centro ground excitation is run for this control scheme, and the evaluation criteria used throughout this thesis applied to the responses. The results of the simulations are shown in Figures 6-8 to 6-9. Notice in Figure 6-8, both the velocity and

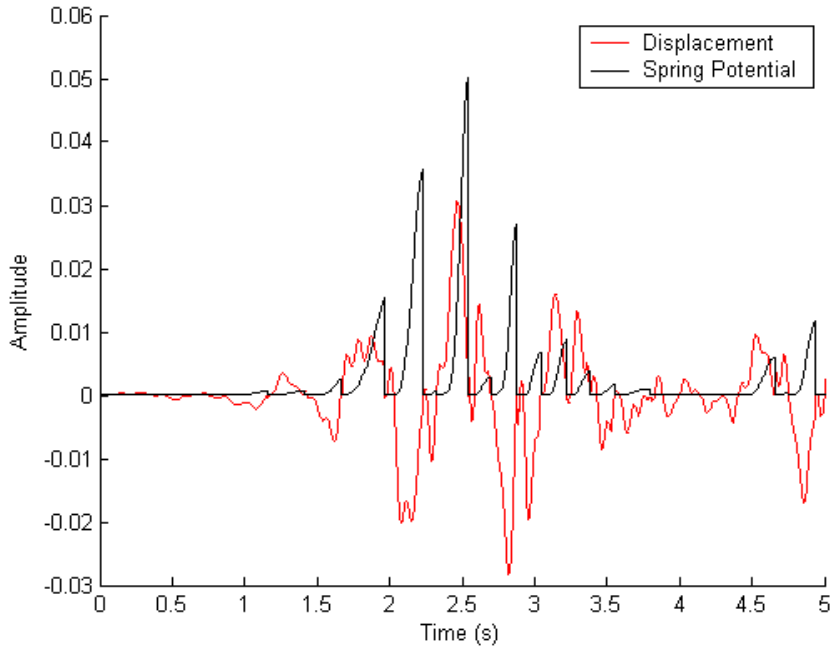

FIGURE 6-9. Spring potential and relative velocity plotted versus time for the first floor device for the El Centro ground excitation.

acceleration of the second floor are very choppy. Table 6-3 compares the evaluation criteria of the clipped-optimal controller to those of the local control scheme for the El Centro earthquake. The results indicate that in nominal operation, the clipped-optimal scheme is more effective in minimizing the responses of the structure than the decentralized controller. The reset-able devices achieve only a 27% reduction in peak drift and a 9.6% reduction in peak acceleration. The clipped-optimal scheme, however, achieves about a 37% reduction in both peak drift and peak acceleration.

TABLE 6-3. Evaluation criteria of the clipped-optimal and reset-able controllers for the El Centro excitation.

	Evaluation Criteria			
Control Scheme	**J1**	**J2**	**J3**	**J4**
Clipped Optimal	0.6396	0.636	0.295	0.4067
Resettable	0.7253	0.9043	0.4583	0.579

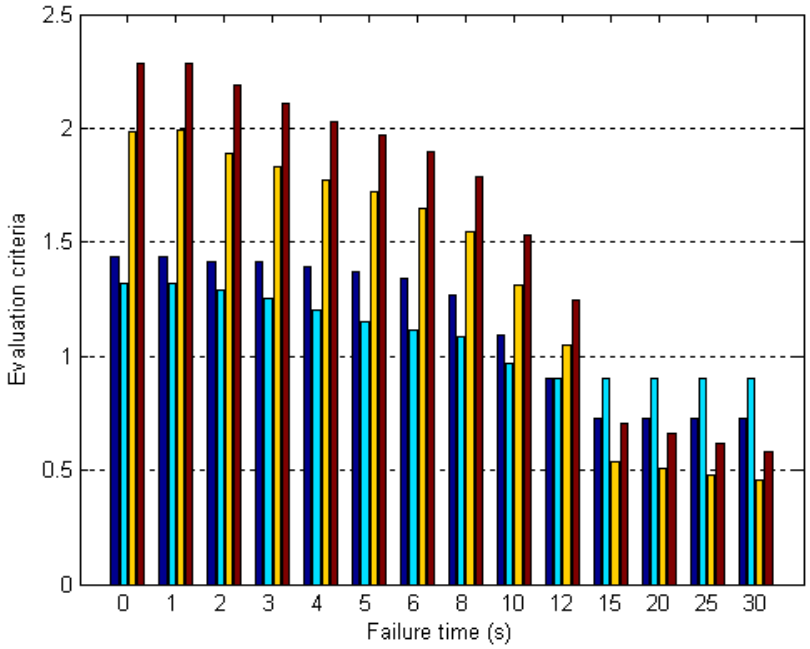

FIGURE 6-10. Evaluation criteria for the reset-able devices failing at the specified time in the six story building.

The goal of this study, though, is to test local devices in the presence of a device failure. The failure to be considered will involve a power failure scenario, with the device being stuck in a passive state. Considering a power failure, it is assumed that the devices can no longer reset. When the failure occurs, the equilibrium position of the device remains where it is when the failure occurs and then no longer resets. The failure times considered include failure times in the preliminary time failure simulations for the six story building with the MR dampers. The results are shown in Figure 6-10. From these results, it is apparent that a time failure at either 0 sec or 1 sec yields the worst performance, but for failures after 1 sec, the criteria drop as the time of failure increases. When the time of failure is 12 sec or later, then the peak evaluation criteria drop back below the 1.0 threshold, indicating that the responses are no longer worse than the uncontrolled case. This means that, with this ground excitation, a failure during the simulation will cause the system response to grow larger than the uncontrolled case 1/3 of the time. The drifts

reach a value of 1.4 times the uncontrolled case, indicating that a failure is likely to cause structural damage. The local control law is not robust in application to this six story model structure.

6.3 Full Scale 9 Story MDOF Model

For a complete picture of the performance of these reset-able devices, they are applied to the 9-story plan-asymmetric building studied in Chapter 4. The size of the structure and torsional response will be good test for the local control scheme as to whether or not it is adequate. Under nominal control conditions (no failures), the maximum forces developed in the devices range from 1 to 2 times the maximum forces developed in the MR devices using the clipped-optimal controller depending on the strength of the ground motion. Considering two stiffnesses values is necessary to obtain comparable forces for the weak and strong ground motions.

Before failures are introduced to the system, the local devices of both stiffnesses are tested at their full capacity for energy dissipation. As shown in Figure 6-11, the large stiffness devices perform reasonably well in lowering the drift of the structure, but increase the peak acceleration by about 1.8 times the uncontrolled value in the Hachinohe simulation. The lowest peak acceleration response is for the Northridge simulation,

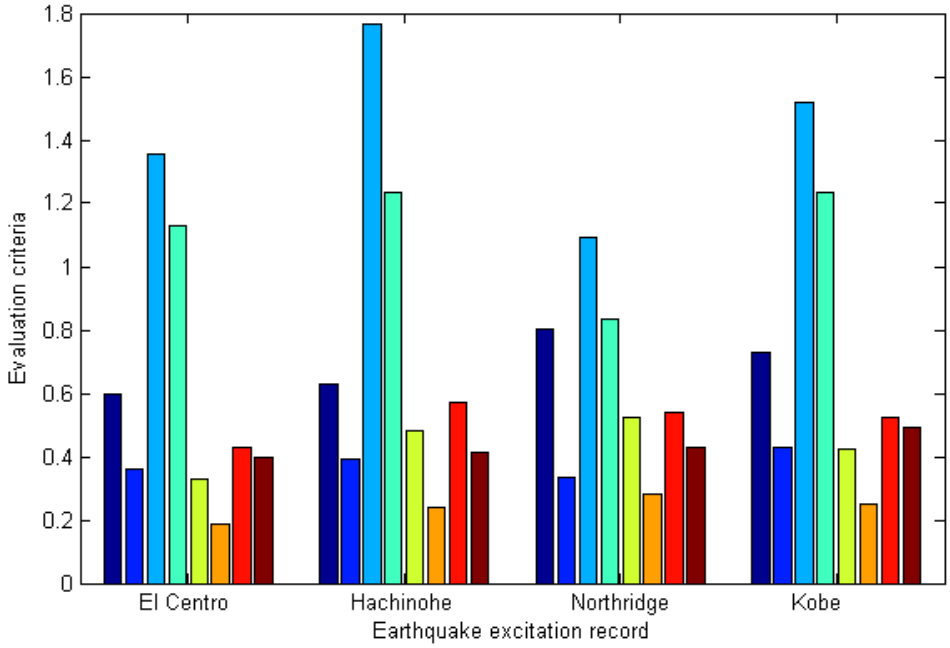

FIGURE 6-11. Evaluation criteria for the reset-able devices without failure in the nine story building (kv = 222400).

with a J_2 of about 1.1. Not surprisingly, it is the weak side of the structure which performs the poorest in nearly all cases. These results suggest that the local device control strategy is not as effective as a global strategy in minimizing the overall response of the structure. Comparing these results to the clipped-optimal performance, it is noted that the decentralized scheme achieves similar reductions in the peak drift. However, while the clipped optimal controller achieves 30-45% reductions in accelerations, the decentralized control law generally degrades the acceleration responses to a state worse than uncontrolled. While the local strategy does protect the structure from structural damage due to interstory drift, life safety and non-structural damage demand that accelerations be controlled. Therefore, the stiffness is reduced by a factor of 5 and the simulations run again.

Figure 6-12 shows, through the results of these simulations, that by using the lower stiffness, all of the responses are brought down below the 1.0 uncontrolled threshold. By

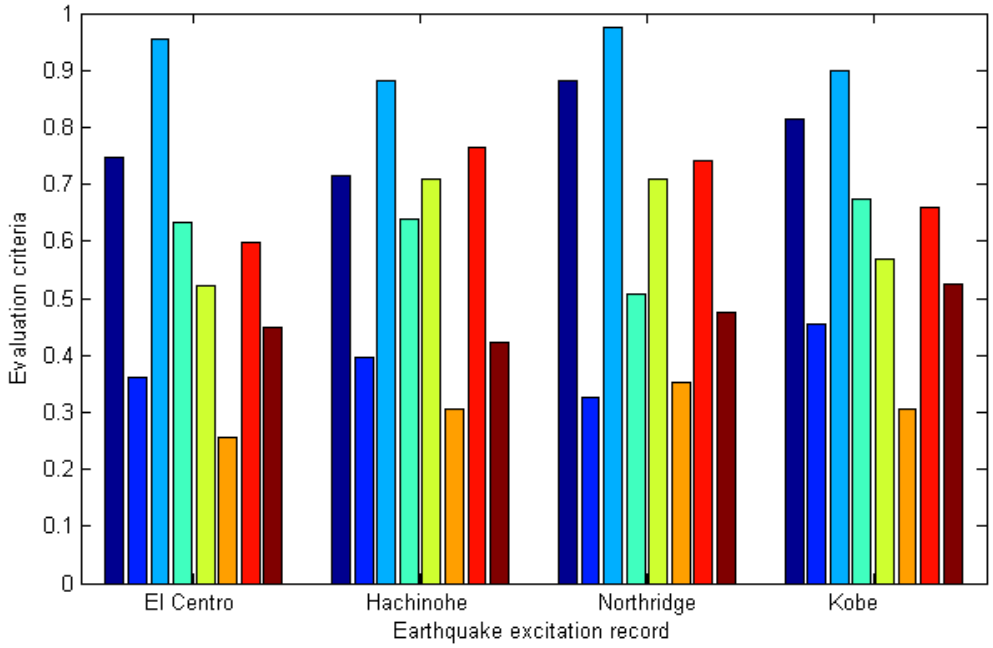

FIGURE 6-12. Evaluation criteria for the reset-able devices without failure in the nine story building (kv = 44480).

reducing the device stiffness the accelerations are reduced to an acceptable level, though interstory drifts increase by 5-10% (compared to uncontrolled) across the board. Once again, though, the clipped-optimal out-performs the decentralized scheme. This time both drift and acceleration are better controlled in the global scheme. It is still necessary, however to test the robustness of these devices in the presence of failures. These failures are tested using the lower stiffness value of 44480 N/cm.

Device failure is simulated in the same failure distribution schemes as in Chapter 4 where all devices fail, weak side devices fail, strong side devices fail, and devices on floors two and three fail. The devices are tested to fail at the same time failure points as the six story structure as a starting point. Through trial and error, it is found that these

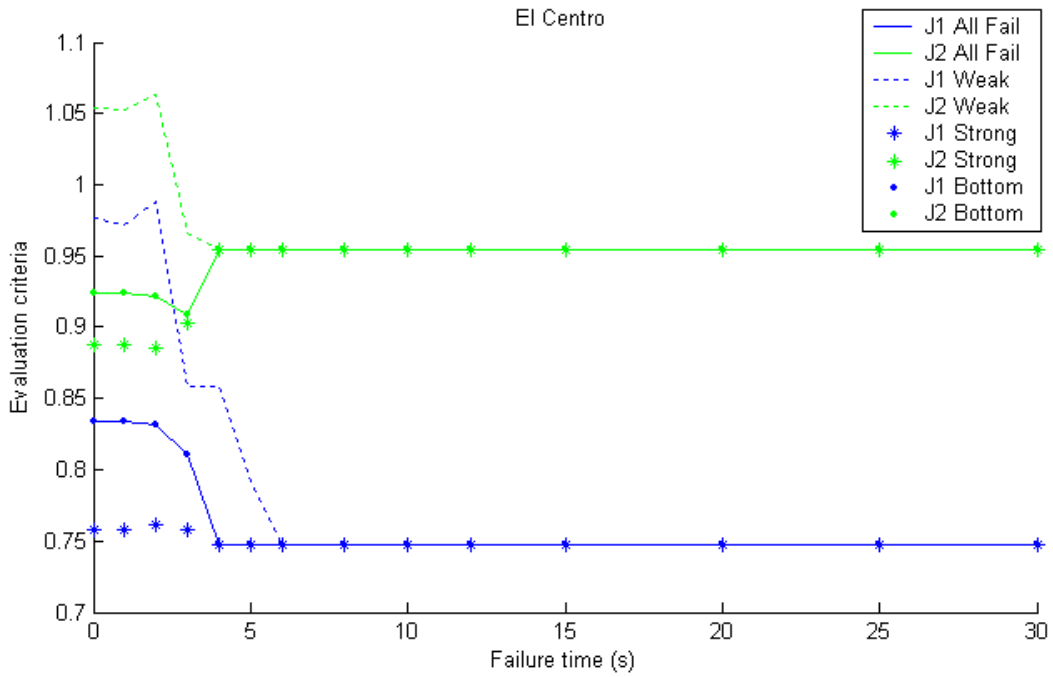

FIGURE 6-13. Evaluation criteria for the reset-able devices for all failure scenarios in the nine story building subjected to the El Centro earthquake excitation.

values are adequate in finding the worst-case scenario. As shown in Figure 6-13, the accelerations and drifts for the El Centro excitation both start out with different values for the different failure schemes, but then converge to a single value after approximately 6 sec. Weak side failure is the worst case scenario, degrading accelerations to a state worse than uncontrolled. The drifts are also high for weak side failures, starting with a J_1 of nearly 1.0 and converging to a final value near 0.75 with a consistent overall tendency to lower as the failure time increases.

The results from the Hachinohe excitation are similar to those of the El Centro in the fact that weak side failure provides the worst case scenario for both acceleration and drift. Accelerations start out greater than 1.0 for weak side failure. Weak side failure can cause a degradation in interstory drifts shown by a J_1 value of about 0.87. All responses except the weak side settle after 5 sec, while the weak side responses show that performance is

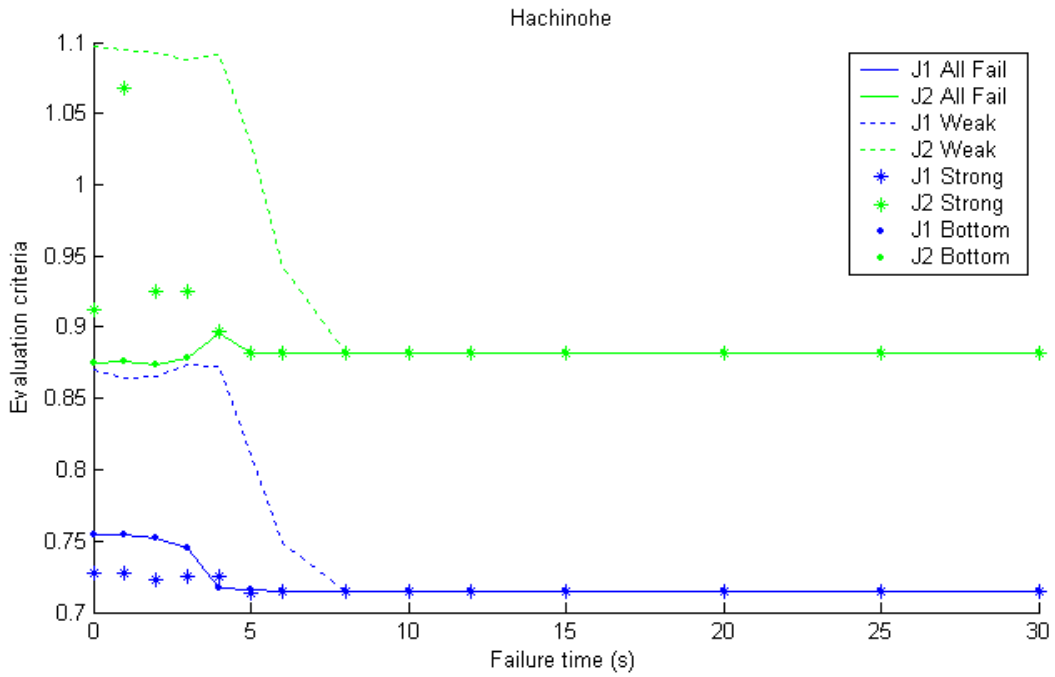

FIGURE 6-14. Evaluation criteria for the reset-able devices for all failure scenarios in the nine story building subjected to the Hachinohe earthquake excitation.

degraded up to 7 sec where the drifts reach their final resting point with J_1 near 0.72. Hachinohe excitation responses are presented in Figure 6-14.

In response to the Northridge excitation, failure in multiple schemes degrades performance past the 1.0 uncontrolled barrier. The drifts are not greatly affected though, except for the failure of weak side devices. Weak side failure takes the J_1 value to about 0.94 before settling back down to the nominal control value of 0.87, which is fairly high.

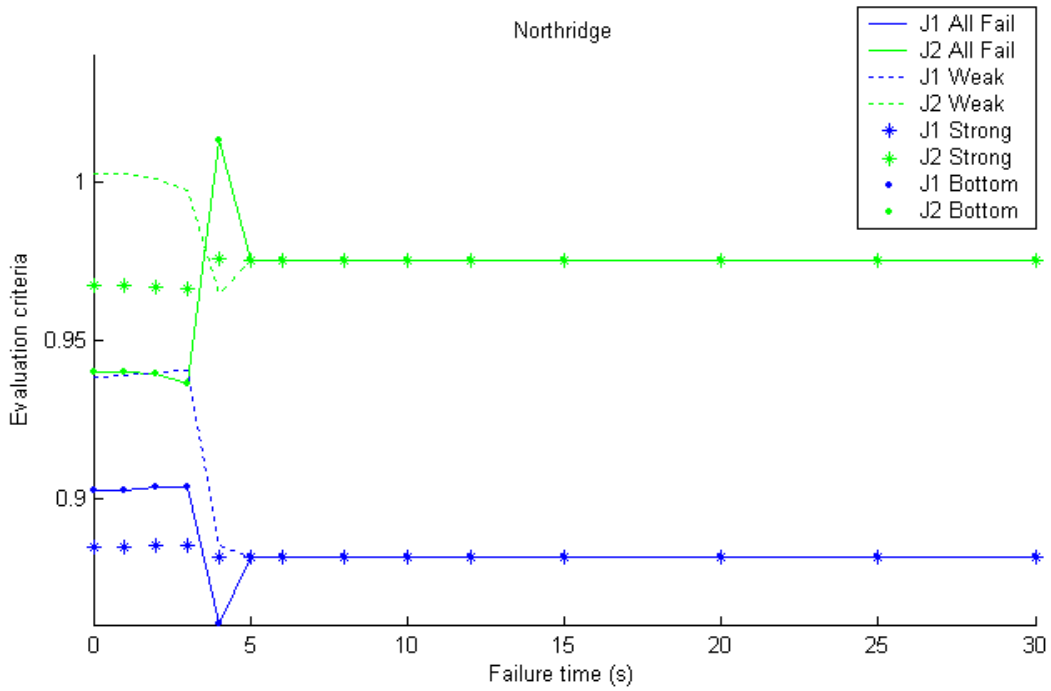

FIGURE 6-15. Evaluation criteria for the reset-able devices for all failure scenarios in the nine story building subjected to the Northridge earthquake excitation.

The accelerations as well settle to a fairly high, though less than 1.0, J_2 value. These results are shown in Figure 6-15.

Concluding this portion of this study are the responses to the Kobe excitation. Drifts have the overall tendency to decrease as the time of failure increases toward the time of convergence at J_1 near 0.82 while accelerations mimic the pattern until they eventually

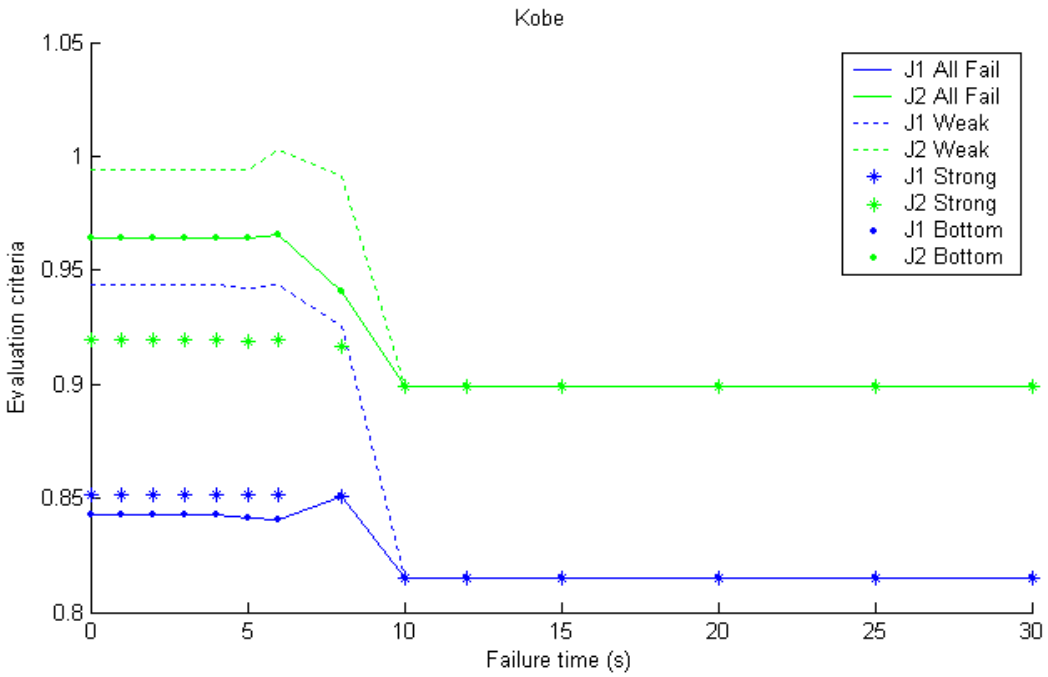

FIGURE 6-16. Evaluation criteria for the reset-able devices for all failure scenarios in the nine story building subjected to the Kobe earthquake excitation.

meet at a J_2 near 0.9. The worst-case scenario is failure of the weak side devices at 6 seconds for a J_2 which breaches the 1.0 level. These results are shown in Figure 6-16.

In all earthquakes, when subjected to failure, the are overall trend is for peak acceleration to be minimally controlled at best, and for weak side failures to be able to degrade responses to a state worse than uncontrolled. Effects of failure on the peak drift performance are also negative, sometimes nearing the uncontrolled response level. Comparing these results to the passive fail-safe system explored in Chapter 4, it is evident that the MR fail-safe system is the better choice for a robust system because it achieved at least mild control gain in both drift and acceleration in the presence of failures at all times whereas the reset-able devices tended to degrade the acceleration performance of the building to a state worse than uncontrolled.

The overall performance of the decentralized control strategy can be summarized as follows: in nominal operation drifts are limited reasonably well and therefore the strategy is effective in reducing the most serious risk of structural damage in this situation. As maintained in this study, non-structural damage can be costly, and should be avoided if possible. This local control strategy does not limit the performance of the structure in regards to the accelerations of the floors by any margin greater than 13%. Larger accelerations can cause life safety issues and lead to non-structural damage.

In terms of the robustness of these devices to a failure such as loss of power, not only are accelerations pushed beyond the responses of the uncontrolled structure, but the drift evaluation criteria approach the 1.0 uncontrolled barrier in the weak side failure case. The time of failure generally degrades the structure response for failure times between zero and 5 seconds, the severity of which is dependent on the case. This is especially evident looking at the trends of the accelerations of the floors with failure time. Before implementing these types of devices on any structure, more research must be done to verify whether a passive fail-safe mode may exist in which the devices can dissipate energy in the event of device failure. It is concluded from the studies performed in this chapter, that the reset-able devices, while reducing interstory drift reasonably well under nominal working conditions, may not be the best choice for the control of a structure. The global semiactive control scheme utilized in this study is able to limit the accelerations as well as the drifts in both nominal conditions and in the presence of device failure. The ability to design a passive fail-safe scheme for the MR dampers makes them an economical and practical choice in structural control.

6.4 Summary and Conclusions

Structural control is a rising field, and robust control is highly sought. There are many theories concerning the most reliable controller, and some have advocated decentralized control. In this chapter, a local controller has been developed and verified. This local

control scheme has been tested in the presence of faults, and found not to be robust in the presence of failures. Power failure caused these devices to degrade the performance of the building to a state worse than uncontrolled, meaning the control strategy could actually be harmful to the structure, leading to structural damage. Not only were accelerations greater than the uncontrolled case, but interstory drifts were degraded to less than 10% gain in most cases. From a practical and economic standpoint for both the six and nine story buildings, in terms of life safety as well as structural and non-structural damage, the more robust global system is the best choice. Any advantages the local scheme may have over a the global scheme considered are outweighed by the lack of robustness and ability to control accelerations.

Chapter 7

Conclusions and Future Work

This thesis presented a look at possible failures in a structural control system and developed a procedure by which these failures may be dealt with. Chapter 1 presented a literature review of work done in fault detection and accommodation in various fields. Detecting a fault in a control system is the first step in dealing with failures. This thesis focuses on fault-accommodation using a passive fail-safe system. It was shown in chapters 3 and 4 that switching to an entirely passive fail-safe control scheme is still effective in reducing structural response. Chapter 5 presented a procedure based on an friction damped design scheme, modified to apply to MR dampers. It was found that the procedure was inadequate for the full-scale building whereas it found an efficient voltage for the six story building. Decentralized control is compared to the clipped-optimal controller in Chapter 6, where it is discovered that clipped-optimal control, in conjunction with the passive fail-safe system, is both more robust and the better nominal controller.

7.1 Conclusions

Conclusions were drawn throughout the thesis at the ends of the chapters. They are summarized herein.

7.1.1 Device Failure Investigation and Development of a Procedure

- Fail-safe Response: In both cases studied, the fail-safe passive voltage which was found to be optimal returned reasonable responses for the structure. The peak drifts were reduced as well as the peak accelerations in most cases. The ability to

design a passive fail-safe system such as this makes the control system much more robust. The fact that this fail-safe system involves using permanent magnets to apply the optimum passive conditions makes it inexpensive as well.

- Failure Time: Both cases studied indicate that failure time, while usually having an adverse effect on the performance of the structure, does not strongly affect the voltage which yields optimum performance. This means that the passive fail-safe system can be designed without considering the time of failure.
- Passive versus Clipped-optimal: In many instances, the passive modes of control achieve better control of drift than does the clipped-optimal control. This, however, is accompanied by larger peak accelerations. The passive system cannot achieve the same level of control of a building as a semiactive system. The semiactive controller provides more overall control gain and is therefore better suited to maintain safety in the event of a seismic excitation. Also, as the ground motion cannot be known a priori, the semiactive system is more robust because it is able to adapt to the ground motion.

7.1.2 Passive Design and Decentralized Control

- Passive Design: Currently, the best design procedure is to follow the procedure used in chapters 3 and 4. This involves a trial and error method of selecting the best passive voltage. Another approach, based on friction-damped design modified to give a voltage level for the MR dampers, was used to design the passive fail-safe voltage level. This was found to be efficient in the case of the six story regular structure, but not for the full scale irregular building. A new design procedure must be developed for full scale and torsional buildings.
- Decentralized Control: The decentralized control scheme based on reset-able spring devices was effective in limiting drift under nominal conditions. Accelerations, in the full scale structure, were found to be less adequately controlled. This indicates that clipped-optimal control performs better in nominal conditions. When subjected to failure, the decentralized controller allowed the peak drifts for

the weak side faiulres to approach the 1.0 uncontrolled value. Also, the peak accelerations for weak side failure in all excitations are allowed to exceed those of the uncontrolled case, whereas the fail-safe system of the MR dampers did not. The studies performed suggest that clipped-optimal outperforms the decentralized controller in nominal control as well as in the presence of failures.

7.2 Future Work

While this thesis addresses many topics and presents methods for dealing with failures in a semiactive control system, there is further work to be done.

- An effective passive design method for MR dampers needs to be developed. Basing the design on a friction-damper-based design worked for the regular model structure (six story), but was inapplicable to the full-scale nine story irregular building which exhibits strong torsional modes.
- The fault-accommodation system needs a fault-detection and identification system before it can truly become effective. Developing a FDI is the next step in implementing a fault-accommodation system.
- The passive fail-safe system is effective and gains respectable performance over the uncontrolled case, however, there may be a more efficient fault-accommodation system. This system could account for sensor failure as well as device failure, and consider switching algorithms to account for the failures which occur instead of shutting completely down to a passive system, leaving that option as a last resort.

References

[1] Agrawal, A.K., Yang, J.N., and He, W.L., (2003). "Application of Some Semiactive Control Systems to Benchmark Cable-Stayed Bridge." Journal of Structural Engineering, ASCE, Vol 129, No. 7, pp. 884-894.

[2] Ankireddi, S., and Yang, H.T.Y., (1999). "*Neural Networks for Sensor Fault Correction in Structural Control*" Journal of Structural Engineering, ASCE, Vol 125m, No. 9, pp. 1056-1064.

[3] Bajpai, G., Chang, B. C., 2001. "Decoupling of Failed Actuators in Flight Control Systems" *Proc. of the American Control Conference.*

[4] Bakule, L., Paulet-Crainiceanu, F., Rodellar, J., and Rossel, J., 2003. "Decentralized overlapping control design for a cable-stayed bridge benchmark." *Proc. of the 3rd World Conference in Structural Control*.

[5] Barroso, L.R., Chase, J.G., and Hunt, S., (2003). "Resettable smart dampers for multi-level seismic hazard mitigation of steel moment frames" Journal of Structural Control, Vol 10, pp. 41-58.

[6] Battaini, M., Dyke, S. J., 1998. "Fault Tolerant Structural Control Systems for Civil Engineering Applications" *Journal of Strucural Control* Vol 5, No 1, pp. 5-26.

[7] Blanke, M., Staroswiecki, M., and Wu, N.E., 2001. "Concepts and Methods in Fault-Tolerant Control" *Proc. of the American Control Conference.*

[8] Bobrow, J.E., Jabbari, R., Thai, K., 2000. "A new approach to shock isolation and vibration supression using a resettable device" *ASME Transactions on Dynamic Systems, Measurement and Control* Vol. 122, pp. 570-573.

[9] Borner, M., Zele, M., Isermann, R., 2001. "Comparison of different fault detecion algorithms for active body control components: automotive suspension system" *Proc. of the American Control Conference.*

[10] Boskovic, J.D., Li, S., and Mehra, R.K. 2001. "On-Line Failure Detection and Identification (FDI) and Adaptive Reconfigurable Control (ARD) in Aerospace Applications" *Proc. of the American Control Conference*.

[11] Boskovic, J. D., Li, S., Mehra, R. K., 2001. "Robust Supervisory Fault-Tolerant Flight Control System" *Proc. of the American Control Conference.*

[12] Chase, J.G., Barroso, L.R., Hunt, S., 2003. “Impact of decentralized semiactive control on the stability of tall structures under seismic loading” *Proc. of the 2003 Pacivfic Earthquake Engineering Conference*.

[13] Chen, S., Tao, G., Joshi, S. M., 2001. “Adaptive Actuator Failure Compensation for a Transport Aircraft Model” *Proc. of the American Control Conference.*

[14] Demetriou, M.A., and Hou, Z., (2003). “On-line fault/damage detection schemes for mechanical and structural systems” Journal of Structural Control, Vol. 10, No. 1, pp. 1-23.

[15] Ding, S. X., Maiying, Z., Bingyong, T., Zhang, P., “An LMI Approach to the Design of Fault Detection Filter for Time-delay LTI Systems with Unknown Inputs” *Proc. of the American Control Conference.*

[16] Doraiswami, R., Diduch, C. P., Kuehner, J., 2001. “Failure Detection and Isolation: A New Paradigm” *Proc. of the American Control Conference.*

[17] Dyke, S.J., Spencer, B.F.Jr., Sain, M.K., and Carlson, J.D., (1998). “An experimental study of MR dampers for seismic protection.” *Smart Mat. and Struct.: Spec. Issue on Large Civ. Struct.,* 7, 396-703.

[18] Dyke, S.J., Spencer, B.F., Jr., Quast, P., Kaspari, D.C., Jr., and Sain, M.K., (1996a). “Implementation of an AMD using acceleration feedback control.” *Micro-computers in Civ. Engrg*., 11, 305-323.

[19] Dyke, S.J., Spencer, B.F.,Jr., Quast, P., Sain, M.K., Kaspari, D.C., Jr., and Soong, T.T., (1996b). “Acceleration Feedback Control of MDOF Structures.” *Journal of Engineering Mechanics*, ASCE, Vol. 122, No. 9, pp. 907-918.

[20] Dyke, S.J., Spencer, B.F., Jr., Sain, M.<., and Carlson, J.D. (1996c). “Modeling and control of magnetorheological dampers for seismic response reduction.” *Smart Materials and Structures*, 5, 565-575.

[21] Elgersama, M., Glavaski, S., 2001. “Reconfigurable Control for Active Management of Aircraft System Failures” *Proc. of the American Control Conference.*

[22] Fadali, S. M., Gummuluri, Satya 2001. “Robust Observer-based Fault Detection for Periodic Systems” *Proc. of the American Control Conference*.

[23] Filiatrault, A., and Chery, S., (1990). "Seismic Design Spectra for Friction-Damped Structures" *Journal of Structural Engineering*, ASCE, Vol 116, No 5, pp 1334-1355.

[24] Hunt, S., 2002. "Semiactive smart dampers and resettable devices for mulitilevel swismic hazard mitigation of steel moment resisting frames" Masters Thesis in Mechanical Engineering, University of Canterbury.

[25] Jakubek, S., and Jörgl, H.P., 2001. "Sensor-Fault-Diagnosis Using Inverse Dynamic Systems" *Proc. of the American Control Conference.*

[26] Jansen, L.M., and Dyke, S.J., (2000). "Semiactive Control Strategies for MR Dampers: Comparative Study." *Journal of Engineering Mechanics*, ASCE, Vol. 126, No. 8, pp. 795-803.

[27] Kabore, P., Wang, H., 2001. "A B-Spline Neural Network Based Actuator Fault Diagnosis in Nonlinear Systems" *Proc. of the American Control Conference.*

[28] Kurata, N., Kobori, T., (2003). "Reliability of Applied Semiactive Structural control System." Journal of Structural Engineering, ASCE, Vol. 129, No. 7, pp. 914-921.

[29] Leitmann, G. (1994). "Semiactive control for vibration attenuation." Journal of Intelligent Mat. Sys. and Struct., (September), 841-846.

[30] Lynch, J.P. and Kincho, J.L., (2002). "Decentralized control techniques for large-scale civil structural systems." *Proc. of the 20th International Modal Analysis Conference.*

[31] Mahmoud, M., Jiang, J., Zhang, Y., 2001. "Effects of Fault Detection and Isolation to the Stability of Fault Tolerant Control Systems" *Proc. of the American Control Conference.*

[32] Ramallo, J.C., Johnson, E.A., and Spencer, B.F. Jr., 2000. "'Smart' Base Isolation Systems." *Proceedings of ASCE Structures Congress: Advanced Technology in Structural Engineering*.

[33] Shafai, B., Pi, C.T., Bas, O., Nork, S., Linder, L.P., 2001. "A General Purpose Observer Architecture with Application to Failure Detection and Isolation" *Proc. of the American Control Conference.*

[34] Song, B., Hedrick, J.K., and Howell, A., (2003). "Fault tolerant control and classification for longitudinal vehicle control" *Journal of Dynamic Systems, Measurement and Control*, Vol. 125, pp. 320-329.

[35] Soong, T.T., and Grigoriu, M., (1993). *Random Vibration of Structural and Mechanical Systems*, Prentice Hall, Englewood Cliffs, New Jersey.

[36] Spencer, B.F.Jr., Dyke, S.J., Sain, M.K., and Carlson, J.D., (1997a). "Phenomenological Model for Magnetorheological Dampers" *Journal of Engineering Mechanics,* Vol. 123, No. 3, pp. 230-38.

[37] Spencer, B.F.Jr., Carlson, J.D., Sain, M.K., Yank, G. (1997b). "On the current status of magnetorheological dampers: Seismic protection of full-scale structures." *Proc. of the Amer. Contr. Conf.*, pp. 458-62.

[38] Stoorvogel, A. A., Niemann, H., Saberi, A., 2001. "Delays in fault detection and isolation" *Proc. of the American Control Conference.*

[39] Tao, G., Tang, X., Joshi, S. M., 2001. "Output Tracking Actuator Filure Compensation Control" *Proc. of the American Control Conference.*

[40] Wang, H., 2001. "Detecting Faults in Dynamic and Bounded Stochastic Distributioins: An Observer Based Techniques" *Proc. of the American Control Conference.*

[41] Wiess, K.DE., Carlson, J.D., and Nixon, D.A. (1994). "Viscoelastic properties of magneto- and electro-rehelogical fluids." *Journal of Intelligent Matrial Systems and Structures*., 5, 772-775.

[42] Xing, L., Datta, A., 2001. "Adaptive Model Algorithmic Control" *Proc. of the American Control Conference.*

[43] Yi, F., Dyke, S.J., Caicedo, J.M., and Carlson, J.D., (2001). "Experimental Verification of Multiinput Seismic Control Stategies for Smart Dampers" *Journal of Engineering Mechanics*, ASCE, Vol 127, No. 11, pp. 1152-1164.

[44] Yoshida, O., (2002). "Torsionally Coupled Response Control of Earthquake Excited Asymmetric Buildings: Development and Application of Effective Control Systems Using Smart Dampers." *Ph.D. Dissertation,* Department of Civil Engineering, Washington University in St. Louis, Missouri.

Vita

Steve Williams

EDUCATION

- Washington University, St. Louis, MO, M.S: Civil Engineering, 2004
- Lake Forest College, Lake Forest, IL, B.A: Physics, 2001

PROFESSIONAL HISTORY

- *Graduate Research Assistant* – Washington University Structural Control & Earthquake Engineering Laboratory, St. Louis, Missouri (January 2002–present)
- *Undergraduate Research Assistant* – Lake Forest College Physics Department, Lake Forest, Illinois (Summers 1999, 2000)
- *Tutor (Physics)* - Lake Forest College, Lake Forest, Illinois (August 1999 - May 2001).
- *Pier Teacher (Physics)* - Lake Forest College, Lake Forest, Illinois (August 1998 - May 1999).
- *Construction Laborer* - Excel Constructors, Kansas City, Kansas (May - August 1997 and May -August 1998)

AFFILIATIONS

- Earthquake Engineering Research Institute
- Mid America Earthquake Center
- American Society of Civil Engineers

May 2004

Short Title: Fault-Tolerant Smart Damping, Williams, May 2004